WATER FLOW AND SOLUTE TRANSPORT ACROSS THE SURFACE-SUBSURFACE INTERFACE IN FULLY INTEGRATED HYDROLOGICAL MODELS

Submitted by:

Jessica Erin Liggett, B.Sc. (Hons.), M.Sc.

As a requirement in full for the degree of Doctor of Philosophy in the

School of the Environment,

Faculty of Science,

Flinders University, South Australia

November 2014

Summary

Modelling studies often separate surface water and groundwater, despite the known connection between the two. Physically based, fully integrated hydrological codes that simulate both surface and subsurface processes have proved useful for capturing the complex dynamics of entire catchments in a single model. While the coupling of surface and subsurface hydrologic processes in these codes is a major advantage, few studies address the impacts of the coupling method on dynamic catchment processes such as overland flow, streamflow generation and solute transport. This thesis examines the implementation of surface-subsurface coupling approaches in fully integrated codes, evaluates their controls on simulating integrated flow and solute transport, and provides guidance for model users.

The influence of a commonly used approach to couple surface and subsurface flows (first-order exchange coefficient; FOEC) is systematically explored in the first half of this thesis using different hydrological scenarios of overland flow generation, infiltration, and exfiltration. In a mesh-centred code (HydroGeoShpere), results converge on the more accurate, but more computationally intensive, continuity of pressure coupling approach as the coupling length parameter (l_e) within the FOEC is decreased. Lower l_e values are required for infiltration under Hortonian conditions, in lower permeability soils, and to capture the initiation of overland flow. A threshold value of l_e is found to be equal to rill storage, above which inaccurate simulations can occur.

The FOEC approach is explored further with an analysis of its numerical implementation in a block-centred code (MODHMS), where a half-cell distance

separates the surface and uppermost subsurface nodes. Defining the FOEC based on the uppermost grid size inhibits accurate prediction of infiltration and the time to initiate overland flow under Hortonian conditions. Increasing the FOEC independently of the grid allows for accurate simulation of infiltration, but not the timing of overland flow. The addition of a thin layer at the surface improves model accuracy substantially.

In the second half of the thesis, the effects of solute dispersion across the surface-subsurface interface, versus within the subsurface, on integrated solute transport and tracer hydrograph separation are evaluated. In 2D hypothetical hillslopes, the pre-event water contribution from the tracer-based separation agrees well with the hydraulically determined value of pre-event water, despite dispersion occurring in the subsurface. In this case, subsurface dispersion parameters have little impact on the tracer-based separation results. The pre-event water contribution from the tracer-based separation is larger when dispersion across the surface-subsurface interface is considered. In a 3D catchment model, solute discharge is compared to field measurements during a rainfall event. Adding solute transport into a fully integrated 3D flow model can improve the assessment of internal model dynamics, but transport results are highly sensitive to model parameters and must be interpreted with caution.

The results of this thesis show that although fully integrated codes do not require an explicit boundary condition between the surface and subsurface, the coupling parameters can highly influence both the integrated and distributed response of flow and solute transport. As such, it is important that these parameters are carefully chosen and sensitivity analyses be performed to ensure robust model performance.

Declaration

I certify that this thesis does not incorporate, without acknowledgment, any material previously submitted for a degree or diploma in any other university; and that to the best of my knowledge and belief it does not contain any material previously published or written by another person except where due reference is made in the text.

Jessica E. Liggett

Co-Authorship

Jessica E. Liggett is the primary author of this thesis, including the published documents. Co-supervisors Assoc. Prof. Adrian Werner and Prof. Craig Simmons provided intellectual supervision and editorial comments on this thesis and the associated published manuscripts. Preliminary work for Chapter 3 was undertaken by Matthew Knowling for his B.Sc. Honours thesis "Partitioning Infiltration and Overland Flow Using a Block-Centred Coupled Surface-Subsurface Code (MODHMS)" (2010, Flinders University, School of the Environment), under supervision from Ms. Liggett and Assoc. Prof. Werner. This work was subsequently re-modelled, re-interpreted, and re-written by Ms. Liggett for this thesis. Dr. Brian Smerdon provided intellectual discussion and editorial help with Chapter 4. Dr. Dan Partington provided code support and intellectual discussion for Chapters 4 and 5. And finally, Dr. Sven Frei provided intellectual discussion and background data for Chapter 5.

Acknowledgements

A great many people have been part of this PhD journey and have contributed to who I am today, both personally and professionally. Firstly, I would like to thank my supervisors, Professors Adrian Werner and Craig Simmons, for providing stimulating discussions, guidance, and encouragement throughout my PhD. I admire Adrian's attention to detail and ability to focus in on the very essence of a research question, and Craig's wonderful perspective to frame research questions within the big picture. My PhD experience benefited from these complimentary supervisory styles.

Being part of the National Centre for Groundwater Research and Training (NCGRT) has been an amazing opportunity. I am grateful to have been able to attend numerous short courses and workshops, to have interacted with many top-class researchers from around the world, and to have the opportunity to share my research at numerous conferences. The NCGRT has been a place to thrive, both academically and personally, and I thank all the staff, students, and post-docs/researchers for making the time so wonderful.

I also gratefully acknowledge funding from an Australian Postgraduate Award, the Goyder Institute for Water Research, and the NCGRT. The Goyder Institute also provided me with numerous opportunities to connect with state government and industry stakeholders to present and discuss my research.

Thank you to Dan Partington for great discussions about fully integrated modelling, support with HGS, and using the HMC method. I enjoyed the opportunity to work with Matthew Knowling and Megan Sebben on their honours' projects, and thank them for their patience and collaboration. Thank you to Ed Sudicky and René Therrien for the use of HydroGeoSphere, Rob McLaren, Young-Jin Park, and Jon Paul Jones for support.

The last part of this thesis would not have been possible without the contributions by Sven Frei and Jan Fleckenstien, who generously let me work with the Lehstenbach catchment, provided field data collected by others, contributed their knowledge of the catchment functioning, and brought a new perspective into the work.

I strive to maintain a balanced life, and this would not be possible without family and friends. Thanks to my fellow Tuesday morning Cake Clubbers for delicious conversation and treats each week, and to my office-mates (especially Tariq). Thank you to the "Adelaide Family" – the Gardners, the Smiths, the Harringtons, Chani, Lieke, and Jordi – for support both inside and outside the university walls, and for providing so many wonderful escapes from what can sometimes be an all-consuming task. Of course, there's the unending support from my actual family: my parents, sister, husband, and daughter. Words cannot describe the gratitude for my husband Brian, who dealt with everything from post-dinner paper discussions and edits, to actually making dinner in the first place. Finally, thank you to my daughter Orla, who came along in the middle of all this, and as is totally cliché but totally true, put all of it into perspective.

Table of Contents

List of Figures

List of Tables

1. Introduction

1.1 Research overview

Penman (1961) defined the study of hydrology as determining “what happens to the rain”, which encompasses a wide range of processes from the short-term generation of overland flow during a rainfall event, to the long-term movement of groundwater in geologic basins. It has long been known that surface water and groundwater interact with one another in the hydrological cycle (e.g. Theis, 1941), and indeed are part of the same interconnected resource that should be managed accordingly (Winter et al., 1998; Sophocleous, 2002; Fleckenstein et al., 2010). Traditional hydrological and hydrogeological modelling studies typically separate surface and subsurface flow and solute transport, using the results of one domain as a boundary condition for the other (Fleckenstein et al., 2010, Guay et al., 2013). However, Guay et al. (2013) showed that the traditional “uncoupled” modelling approach is unable to capture the complex surface-subsurface dynamics in streams and near-stream (riparian) environments, where hydrological links between the surface and subsurface are strong. In this thesis I refer to surface-subsurface interactions, which includes hillslope processes that link the surface and subsurface (e.g. overland flow, infiltration, unsaturated flow, discharge, etc.) in addition to direct connections between surface water bodies (e.g. lakes, rivers, etc.) and groundwater.

In 1969 Freeze and Harlan put forth a “Blueprint for a physically-based, digitally-simulated hydrologic response model”, which connected precipitation, evapotranspiration, overland flow, channel flow, and groundwater flow in a single numerical modelling framework. Since then, many different codes have been developed to achieve this vision. Fully integrated codes such as HydroGeoSphere

(HGS, Therrien et al., 2009), MODHMS (Panday and Huyakorn, 2004), ParFlow (Kollet and Maxwell, 2006), and Integrated Hydrology Model (InHM, VanderKwaak and Loague, 2001), are capable of simulating distributed, physically based, variably saturated flow and transport. These codes numerically solve the solutions for the surface and subsurface domains in a single set of equations (Furman, 2008). This is in contrast to iteratively coupled codes, where the surface and subsurface domains are solved sequentially, but with feedback between the domains within a single time step until a set of convergence criteria is reached (Furman, 2008; e.g. GSFLOW – Markstrom et al., 2008). The use of fully integrated codes has been gaining in popularity and they have been used to simulate surface-subsurface interactions including streamflow generation mechanisms (e.g. VanderKwaak and Loague, 2001; Partington et al., 2013), interactions with surface water bodies (e.g. Smerdon et al., 2007; Brookfield et al., 2009), and hillslope and catchment dynamics (e.g. Li et al., 2008; Mirus et al., 2011; Guay et al., 2013).

Despite the gaining popularity of fully integrated codes, effectively coupling the surface and the subsurface is still a significant conceptual challenge (Ebel et al., 2009) and verifying the numerical solutions is difficult due to a lack of analytical solutions for complex surface-subsurface processes (Sebben et al., 2013). Whilst a number of methods for surface-subsurface coupling have been identified (Morita and Yen, 2000; Furman, 2008), two coupling methods are most frequently used in fully integrated codes: the continuity of pressure (COP) approach and the first-order exchange coefficient (FOEC) approach (Ebel et al., 2009). The COP approach enforces a direct connection between the surface and subsurface by ensuring that the surface and uppermost subsurface pressure heads and concentrations are the same. The FOEC, or "conductance", approach assumes flow (and transport) across the surface-subsurface interface is proportional to the head (or concentration) difference across the interface. The FOEC approach requires additional parameters to be specified by the model user, although it is usually seen as less computationally intensive than the COP approach. Previous studies have identified that the surface-subsurface coupling approach can affect modelled catchment behaviour by influencing infiltration, overland flow, exfiltration, and connection of groundwater to surface water bodies (e.g. VanderKwaak, 1999; Delfs et al., 2009; Ebel et al., 2009; Gaukroger and Werner, 2011).

1.2 Aim and Objectives

This thesis examines the implementation of surface-subsurface coupling approaches in fully integrated codes and evaluates their controls on simulating integrated flow and solute transport. It expands on previous studies by evaluating the influence of the coupling approach on numerous types of rainfall-runoff conditions (e.g. Hortonian overland flow, Dunne overland flow, exfiltration, etc.), including surface-subsurface solute transport, and providing guidance for model users on the parameterisation and use and of such approaches.

The objectives are to:

1. assess the sensitivity of simulated hillslope processes of infiltration, exfiltration, and overland flow generation to the parameterisation of the FOEC coupling approach;

2. compare the numerical implementation of the FOEC coupling approach in mesh-centred and block-centred codes;

3. evaluate the effects of solute dispersion across the surface-subsurface interface, versus within the subsurface, on integrated solute transport and tracer hydrograph separation; and,

4. investigate the integrated and distributed impact of solute dispersion across the surface-subsurface interface on solute transport in a 3D catchment model.

This thesis follows a journal paper based format, with four distinct bodies of work (Chapters 2-5) that contribute to the overall objectives. Each chapter is summarised below, and Chapter 6 presents unifying conclusions of this work.

Chapter 2 - Influence of the first-order exchange coefficient on simulation of coupled surface-subsurface flow

In physically based catchment hydrology models, dynamic surface-subsurface interactions are often represented using the FOEC coupling approach. Chapter 2 systematically explores the relationship between the FOEC and surface-subsurface exchange flux, subsurface-surface head difference and time to initiate overland flow by using 1D soil column simulations with the fully integrated code HydroGeoSphere. Numerical experiments adopt five different hydrological scenarios and nine different soil profiles. Results converge on the more accurate, but sometimes more computationally intensive, COP coupling approach as the coupling length (l_e) parameter within the FOEC is decreased (i.e. FOEC increased). Threshold l_e values that produce results converged on the COP approach vary considerably with hydrological scenario, soil type and total obstruction height (H_s; accounting for sub-grid depression storage), with most threshold l_e values $\leq 10^{-2}$ m. Lower l_e values are required for infiltration under Hortonian conditions, under non-Hortonian conditions in lower permeability soils, and to capture timing of initiation of overland flow. The condition $l_e > H_s$ precludes top-down saturation under Hortonian conditions. Steady-state exchange flux and time to initiate overland flow are within 0.05% and 24%, respectively, of COP results when $l_e = H_s = 1$ mm. 3D simulation of a hypothetical catchment demonstrates that the general FOEC sensitivities obtained through 1D simulation are transferrable to the 3D case. Chapter 2 shows that a value of $l_e = H_s$ provides an appropriate initial value for modelling applications. A FOEC parameter sensitivity assessment is suggested on a case-by-case basis to ensure adequately converged results and to avoid unrealistic model behaviour.

Chapter 3 – On the implementation of the first order exchange coefficient approach using a block-centred surface-subsurface hydrology model

Guidance on FOEC parameterisation within block-centred codes is limited, and common practice is to express the FOEC as the quotient of the vertical saturated hydraulic conductivity and the half-cell thickness of the uppermost layer. Chapter 3 evaluates the implementation of the FOEC approach utilising a popular block-centred, surface-subsurface hydrology code (MODHMS) to simulate one-dimensional infiltration experiments under Hortonian conditions. Results show that defining the FOEC based on a half-cell thickness of the uppermost subsurface cell inhibits accurate prediction of infiltration rates (q_{ex}) and the time to initiate overland flow (t_{OLF}) for the adopted rainfall-runoff scenario. Increasing the FOEC independently of the grid allows for accurate simulation of q_{ex}, but not t_{OLF}. The addition of a thin layer at the surface is shown to improve model accuracy substantially, such that q_{ex} and t_{OLF} approach those obtained using an equivalent mesh-centred model (i.e. where the surface and upper subsurface nodes are coincident). Whilst the addition of a single thin layer in block-centred codes allows improved prediction of surface-subsurface interaction, it does not provide a surrogate for fine discretisation throughout the subsurface that is necessary for accurate simulation of unsaturated zone flow. Chapter 3 offers guidance on the implementation of the FOEC approach in a block-centred code and demonstrates the importance of systematic testing of parameters (that are otherwise calibrated) in physically based surface-subsurface hydrology models.

Chapter 4 – Fully integrated modelling of surface-subsurface solute transport and the effect of dispersion in tracer hydrograph separation

Tracer hydrograph separation has been widely applied to identify streamflow components, often indicating that pre-event water comprises a large proportion of stream water. Previous work using numerical modelling suggests that hydrodynamic mixing in the subsurface inflates the pre-event water contribution to streamflow when derived from tracer-based hydrograph separation. Chapter 4 compares the effects of hydrodynamic dispersion, both within the subsurface and across the surface-subsurface interface, on the tracer-based pre-event water contribution to streamflow. Using a fully integrated surface-subsurface code, I simulate two hypothetical 2D hillslopes with surface-subsurface solute exchange determined under a range of advective and dispersive conditions. Results show that when surface-subsurface solute transport occurs via advection only, the pre-event water contribution from the tracer-based separation agrees well with the hydraulically determined value of pre-event water from the numerical model, despite dispersion occurring within the subsurface. In this case, subsurface dispersion parameters have little impact on the tracer-based separation results. However, the pre-event water contribution from the tracer-based separation is larger when dispersion across the surface-subsurface interface is considered. This chapter demonstrates that dispersion within the subsurface may not always be a significant factor in apparently large pre-event water fluxes over a single rainfall event. Instead, dispersion across the surface-subsurface interface may increase estimates of pre-event water contribution. This work also shows that solute transport in numerical models is highly sensitive to the representation of the surface-subsurface interface. Hence, models of catchment-scale solute dynamics require careful treatment and sensitivity testing of the surface-subsurface interface to avoid misinterpretation of real-world physical processes.

Chapter 5 – Surface-subsurface solute transport in a fully integrated catchment model

Previous studies on fully integrated solute transport focus on small scales, simple geometric domains, and have not utilised many different field data sources. The objective of Chapter 5 is to include both flow and solute transport in a 3D, fully integrated catchment model, utilising high resolution observations of dissolved organic carbon (DOC) export from a wetland complex during a rainfall event. The inclusion of both flow and solute transport is examined in relation to guiding the understanding of the internal dynamics of the catchment. A sensitivity analysis consisting of 12 simulations is performed to span a range of transport conditions, including the surface-subsurface interface condition (e.g. advective exchange only, advection plus diffusion, advection plus full mechanical dispersion) and subsurface dispersivities. The catchment model compares well to observed solute discharge at the catchment outlet, and reproduces the observed trend of an increasing proportion of discharge from the wetlands in total stream flow, with increased stream discharge.

Additionally, the model captures the hysteretic relationship between DOC export and field observations, although the characteristics of the model's hysteresis loops are quite different than the observed results. The results show that the model is sensitive to dispersion across the surface-subsurface interface, which differs in its influence on modelled solute mass flux relative to the effects of subsurface dispersion. The addition of solutes to the fully integrated catchment model can help identify where the model may differ from actual catchment processes, however the model results are highly non-unique and produce different internal distributions of solute transport. Chapter 5 highlights the importance of obtaining field data when modelling surface-subsurface solute transport in fully integrated codes to help constrain the solute transport solution.

2. Influence of the first-order exchange coefficient on simulation of coupled surface–subsurface flow

A version of this chapter is published as:

Liggett, J.E., Werner, A.D., Simmons, C.T., 2012. Influence of the first-order exchange coefficient on simulation of coupled surface–subsurface flow. J. Hydrol. 414-415, 503–515. doi: 10.1016/j.jhydrol.2011.11.028

2.1 Introduction

The development of fully integrated hydrological codes which enable the catchment-scale simulation of water movement both within and between the surface and subsurface has helped fulfil Freeze and Harlan's (1969) blueprint for physically based, hydrological response modelling (Loague et al., 2006). Fully integrated codes are defined here as those which solve the surface and subsurface domains simultaneously in a single matrix of equations (Morita and Yen, 2002; Furman, 2008). Integrating surface and subsurface processes can aid studies of catchment behaviour and water management where interdependency of surface and subsurface domains is an important aspect of the spatial and temporal variability in catchment hydrological functioning (Loague and VanderKwaak, 2004).

Popular fully integrated codes include HydroGeoSphere (HGS; Therrien et al., 2009), Integrated Hydrology Model (InHM; VanderKwaak, 1999; VanderKwaak and Loague, 2001), MODHMS (Panday and Huyakorn, 2004; HydroGeoLogic Inc.,

2006) and ParFlow (Kollet and Maxwell, 2006). These types of codes have been successfully applied to a wide range of hydrological problems that include simulation of overland flow (e.g. VanderKwaak and Loague, 2001; Kollet and Maxwell, 2006; Mirus et al., 2009), surface water and groundwater interaction (Werner et al., 2006; Smerdon et al., 2007; Cardenas, 2008; Brookfield et al., 2009), diffuse recharge (Lemieux et al., 2008; Smerdon et al., 2008), and atmosphere-surface-subsurface interactions (Maxwell and Kollet, 2008a; Kollet et al., 2010).

Determining the most effective method for coupling the surface and the subsurface is one of the most significant conceptual challenges in fully integrated catchment simulation (Ebel et al., 2009). The surface-subsurface coupling approach can influence catchment rainfall-runoff behaviour by potentially imposing controls on infiltration, recharge, overland flow, groundwater exfiltration, and exchanges between surface water bodies (lakes, rivers, wetlands, etc.) and the subsurface (e.g. Ebel et al., 2009; Gaukroger and Werner, 2011). A number of methods for surface-subsurface coupling have been identified (Morita and Yen, 2000; Furman, 2008); however, the most common coupling methods in fully integrated codes are the continuity of pressure (COP) and first-order exchange coefficient (FOEC) approaches (Ebel et al., 2009).

The COP approach assumes that the surface and uppermost subsurface pressure heads are the same, enforcing a direct connection between the domains (Figure 2.1a). The surface water and porous media flow equations are solved simultaneously at a single surface-subsurface interface node. There are no additional parameters needed to define the surface-subsurface exchange processes beyond those needed for independent surface and subsurface flow simulation. This approach is arguably the

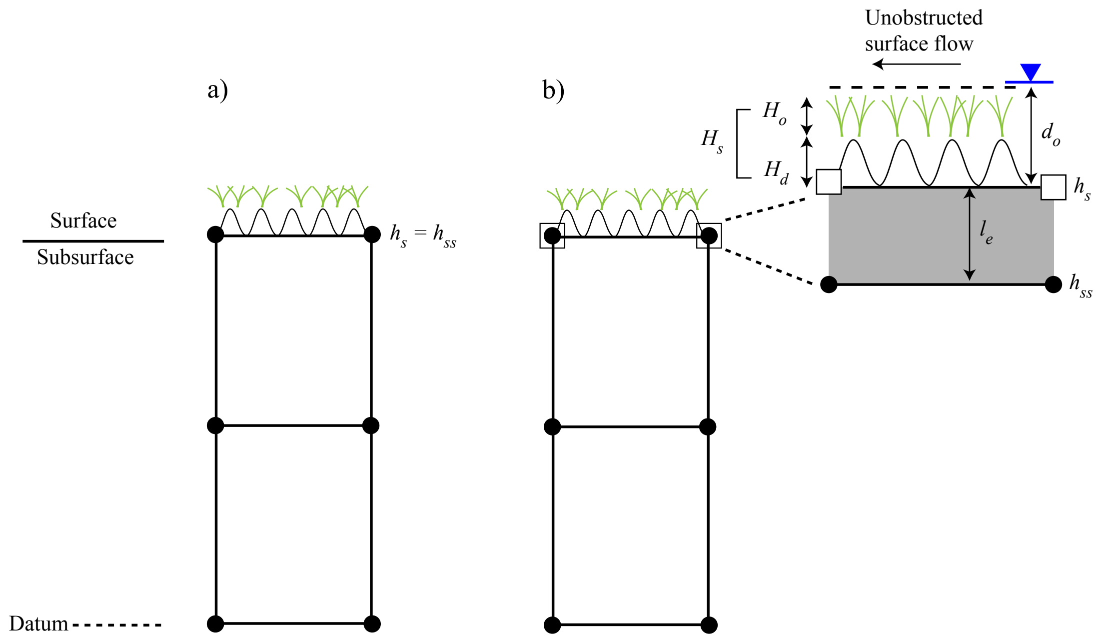

Figure 2.1 Schematic of the a) COP and b) FOEC coupling approaches for surface-subsurface exchange. The FOEC coupling approach is shown here as a conceptualisation of flow through an exchange interface, which creates a hydraulic separation between the surface and subsurface (shown in grey); however, the nodes are co-located in the model. The concept of total obstruction height (H_s) shown in b), comprised of sub-grid depression storage (H_d) and obstruction storage exclusion (H_o, e.g. grass, trees), also applies to the COP approach. h_s is the surface head, h_{ss} is the subsurface head at the uppermost node, d_o is the depth of water in the surface domain, and l_e is the coupling length.

most physically based manner for coupling the domains (Kollet and Maxwell, 2006); however, rapid changes in surface pressure can lead to numerical instabilities at the subsurface boundary, which can be overcome using small time steps, but may lead to very long simulation times (Beven, 1985; Ebel et al., 2009; Huang and Yeh, 2009).

A commonly used alternative to the COP approach is the FOEC or “conductance” approach (Ebel et al., 2009) (Figure 2.1b). Here, the surface-subsurface exchange flux is proportional to the head difference between separate surface and subsurface nodes, and the FOEC. High values of FOEC promote surface-subsurface exchange, and Huang and Yeh (2009) demonstrated that the FOEC approach can approximate the COP approach. They used an iteratively coupled scheme to assess FOEC relationships using a hypothetical 3D watershed. Ebel et al. (2009) explored relationships between the FOEC parameterisation and hydrological processes occurring within a simulated instrumented watershed (the R5 catchment). They concluded that the FOEC approach can be applied both to balance simulation run times and to minimise the head difference across the surface-subsurface interface under saturated conditions. They found that a critical threshold of FOEC parameters existed, below which consistent results were obtained in terms of both the integrated and distributed catchment responses. These were assessed using the discharge hydrograph and surface-subsurface head differences, respectively. Ebel et al. (2009) based their analysis at the catchment scale, with a heterogeneous saturated hydraulic conductivity field and variable topography and rainfall. It is our intention to consider a smaller scale than that adopted by Ebel et al. (2009) and Huang and Yeh (2009) in order to isolate the effects of the FOEC on specific hydrological scenarios, rather than on the whole catchment response.

Delfs et al. (2009) used 1D simulations to explore relationships between FOEC parameterisation and the prediction of hydrological processes associated with Hortonian overland flow (i.e. driven by infiltration excess or top-down saturation; Horton, 1933). Their results also show that infiltration becomes relatively insensitive to FOEC, as FOEC increases. The Delfs et al. (2009) analysis was constrained to sensitivities associated with Hortonian conditions, and further testing is needed to extend the analysis to other surface-subsurface interactions. Additionally, neither Delfs et al. (2009) nor Ebel et al. (2009) compared the FOEC approach directly to the COP approach.

While Ebel et al. (2009) found a critical value for the FOEC parameter to accurately simulate their catchment-scale model, they point out that this critical value may vary depending on the specific runoff generation mechanism, soil hydraulic properties, mesh discretization, surface flow properties and topography. The primary aim of Chapter 2 is to extend the work of Ebel et al. (2009), Delfs et al. (2009) and Huang and Yeh (2009) by analysing the sensitivity of overland flow generation mechanisms to FOEC parameters for a range of simple physical conditions and basic hydrological scenarios, using homogeneous 1D soil column simulations. Hypothetical scenarios are used to isolate the effect of FOEC parameterization on specific surface-subsurface interactions, where aspects of the expected model behaviour are known *a priori* with simple theory and calculations.

The influence of FOEC parameters on rainfall partitioning into overland flow and infiltration, plus situations producing exfiltration is systematically explored for different hydrological scenarios. These include Hortonian overland flow, Dunne overland flow (i.e. driven by saturation excess or bottom-up saturation; Dunne, 1978) and exfiltration. FOEC parameter values that produce a suitably accurate solution compared to the COP approach are determined for each of the hydrological scenarios and nine different soil columns. The findings from the 1D analysis are then compared to a hypothetical 3D catchment example, which was originally devised by Panday and Huyakorn (2004). In doing this, I explore the transferability of 1D interpretations of specific hydrological scenarios to a 3D simulation with a combination of hydrological processes, in which FOEC is known to influence the predictions of catchment hydrology (e.g. Gaukroger and Werner, 2011).

2.2 FOEC coupling approach

The surface-subsurface exchange flux (q_{ex} [LT^{-1}], positive/negative as exfiltration/infiltration) is linearly dependent on the difference between the subsurface head at the uppermost node (h_{ss} [L]) and surface head (h_s [L]), and the FOEC or "conductance" (α [T^{-1}]):

$$q_{ex} = \alpha\left(h_{ss} - h_s\right) \tag{2.1}$$

The FOEC approach has been used previously to simulate flow between different continua such as fractures/macropores and rock/soil (e.g. Barenblatt et al., 1960; van Genuchten and Wierenga, 1976; Gerke and van Genuchten, 1993; Therrien and Sudicky, 1996), and in surface water-aquifer interactions through streambeds (e.g. in the MODFLOW code, McDonald and Harbaugh, 1988; Rushton, 2007). For these applications, α has been perceived as either a lumped fitting (i.e. calibration) parameter with no physical meaning (e.g. Bencala, 1984; Kollet and Zlotnik, 2003; Rushton, 2007; Mehl and Hill, 2010), or as a function of geometry and characteristic length scales of an exchange interface (e.g. Warren and Root, 1963; Gerke and van Genuchten, 1993).

The conceptualisation of the FOEC approach for surface-subsurface interaction in fully integrated codes (e.g. InHM, MODHMS, HGS) is generally based on Darcy's Law for flow through an exchange interface (e.g. Gerke and van Genuchten, 1993; VanderKwaak, 1999). The parameterisation of α varies slightly between codes. For example, in HGS (the code used in this chapter), α is defined as:

$$\alpha = k_r \frac{K_{sat}}{l_e} \tag{2.2}$$

where k_r is a scaling factor related to the interface relative permeability [-], and l_e is a user specified parameter termed the "coupling length" [L] (Therrien et al., 2009). α increases as l_e decreases, producing higher surface-subsurface fluxes for a given head difference (h_{ss}-h_s), and promoting continuity of pressure between the surface and subsurface as l_e approaches zero. Note that l_e must be larger than zero otherwise Equation 2.2 becomes undefined. MODHMS (HydroGeoLogic Inc., 2006) adopts a similar parameterisation of α, except that K_{sat}/l_e is user-specified as a whole. InHM (VanderKwaak, 1999) uses a similar approach to HGS, where the l_e parameter in Equation 2.2 is termed the "coupling length scale", but there are additional parameters to describe the permeability of the exchange interface as well as an additional scaling parameter.

Conceptually, the combination of Equations 2.1 and 2.2 can be likened to a hydraulic separation of the surface and subsurface by an exchange interface of a given thickness (i.e. l_e), as shown in Figure 2.1b, although the surface and subsurface nodes are physically co-located in the model domain. Additionally, it has been argued that a distinct exchange layer is not always present in the field (e.g. Kollet and Zlotnik, 2003). Irrespective of the conceptualisation of the FOEC approach, Ebel et al. (2009) point out that this approach is useful in modelling surface-subsurface interactions. That is, the FOEC approach can reduce model run time while preserving near-continuity of pressure heads, and can be used where disconnections between the surface and subsurface are known to occur (e.g. due to structural surface sealing by raindrop impact, agricultural cultivation, fire effects) (Ebel et al., 2009).

There is little guidance on assigning α or l_e values in simulation models, taking into account trade-offs between model stability and attempts to produce physically based surface-subsurface interaction. HydroGeoLogic Inc. (2006) suggest setting l_e as the half-cell thickness; which, considering the block-centred arrangement of the MODHMS code, assumes that the surface-subsurface exchange interface represents a half-cell of saturated subsurface material between the surface and uppermost subsurface nodes. However, Gaukroger and Werner (2011) found that this method imposed restrictions to infiltration and increased overland flow rates. Additionally, there is no separation of the surface and uppermost subsurface nodes in a mesh-centred approach (e.g. HGS), so the suggestion of setting l_e equal to the half-cell thickness is therefore not applicable.

Selection of appropriate values of α (or parameters used to define α) in codes that use the FOEC approach is confounded by inconsistent reporting of FOEC parameters in published studies – e.g. α or l_e is not reported by VanderKwaak and Loague (2001), Jones et al. (2008) or Frei et al. (2010) among others. This is possibly due to the different parameterizations of α between codes, and the change in α during a simulation due to scaling parameters such as k_r (Equation 2.2). Goderniaux et al. (2009) adopted a value for l_e of 0.01 m in their study using HGS, and stated that the results were insensitive to changes in this parameter. Various FOEC algorithms and values were adopted by Delfs et al. (2009) and Huang and Yeh (2009) covering a K_{sat}/l_e range of approximately 10^{-7} to 10^{-3} s^{-1}. Ebel et al. (2009) used values for the parameter equivalent of l_e (i.e. coupling length scale) of 10^{-5}, 10^{-4}, 0.01 and 0.1 m in their analysis and found that values $\leq$ 0.01 m produced suitably accurate results. Mirus et al. (2011) simulated four different instrumented catchments with a uniform coupling length scale value in each, ranging between 10^{-4} and 0.01 m. The verification examples contained in software documentation (e.g. VanderKwaak, 1999; HydroGeoLogic Inc., 2006; Therrien et al., 2009) also provide some indication of K_{sat}/l_e (i.e. ranging from about 10^{-6} to 3.6 s^{-1}), but without explanation of the influence of FOEC parameters on model predictions. Values for l_e in the verification examples for HGS included with the software documentation (Therrien et al., 2009) range from 0.0135 m to 1 m and the default in the code is 10^{-4} m.

2.3 Methods

2.3.1 HydroGeoSphere

HydroGeoSphere is a fully integrated code intended to produce physically based simulation of surface and variably saturated subsurface flow (and transport) with a mesh-centred, finite control-volume approach (Therrien et al., 2009). 2D surface flow is calculated with the diffusion wave approximation to the Saint Venant equations, and 3D variably saturated subsurface flow is calculated with a modified form of Richards' equation, as described in the software documentation (Therrien et al., 2009). The surface and subsurface domains can be linked by either the COP or FOEC approaches.

The COP approach in HGS is referred to as the *shared-node* approach while the FOEC approach is referred to as the *dual-node* approach (Therrien et al., 2009). Two coincident nodes, a surface node and a subsurface node, are present at the surface with the dual-node approach (Figure 2.1b). Flux between these nodes is determined via Equations 2.1 and 2.2. k_r is used to scale q_{ex} and varies from zero to unity. During exfiltration, k_r is equal to the relative permeability of the porous media (e.g. 1 for saturated flow). During infiltration, k_r varies with the depth of water in the surface domain (d_o [L]) according to (Therrien et al., 2009):

$$k_r = \begin{cases} \left(\dfrac{d_o}{H_s}\right)^{2\left(1-\frac{d_o}{H_s}\right)} & when\ d_o < H_s \\ 1 & when\ d_o > H_s \end{cases} \tag{2.3}$$

$$where,\ H_s = H_d + H_o$$

H_s [L] is the total obstruction height, comprised of the sub-grid depression storage height (H_d [L]), which must be filled before overland flow occurs, and the obstruction storage exclusion (H_o [L]), which reduces the available area for flow and storage of water due to vegetation and surface structures (Figure 2.1b). Equation 2.3 is non-linear to represent a corrugated microtopography, where the infiltration is concentrated in rills (Dunne et al., 1991; VanderKwaak, 1999).

2.3.2 Hydrological Scenarios and Model Setup

Five hydrological scenarios were selected in this chapter to represent simplified forms of common overland flow generation mechanisms. These are illustrated in Figure 2.2. Simulations produce only minimal ponding at the surface above small values of H_d, because the focus is on situations involving shallow overland flow, rather than those involving surface water bodies. Subsurface flow occurs through 1D (vertical) homogeneous soil columns, which are 2 m deep. The assumption of vertical flow only in the unsaturated zone has been adopted in previous studies (e.g. Keese et al., 2005; Delfs et al., 2009).

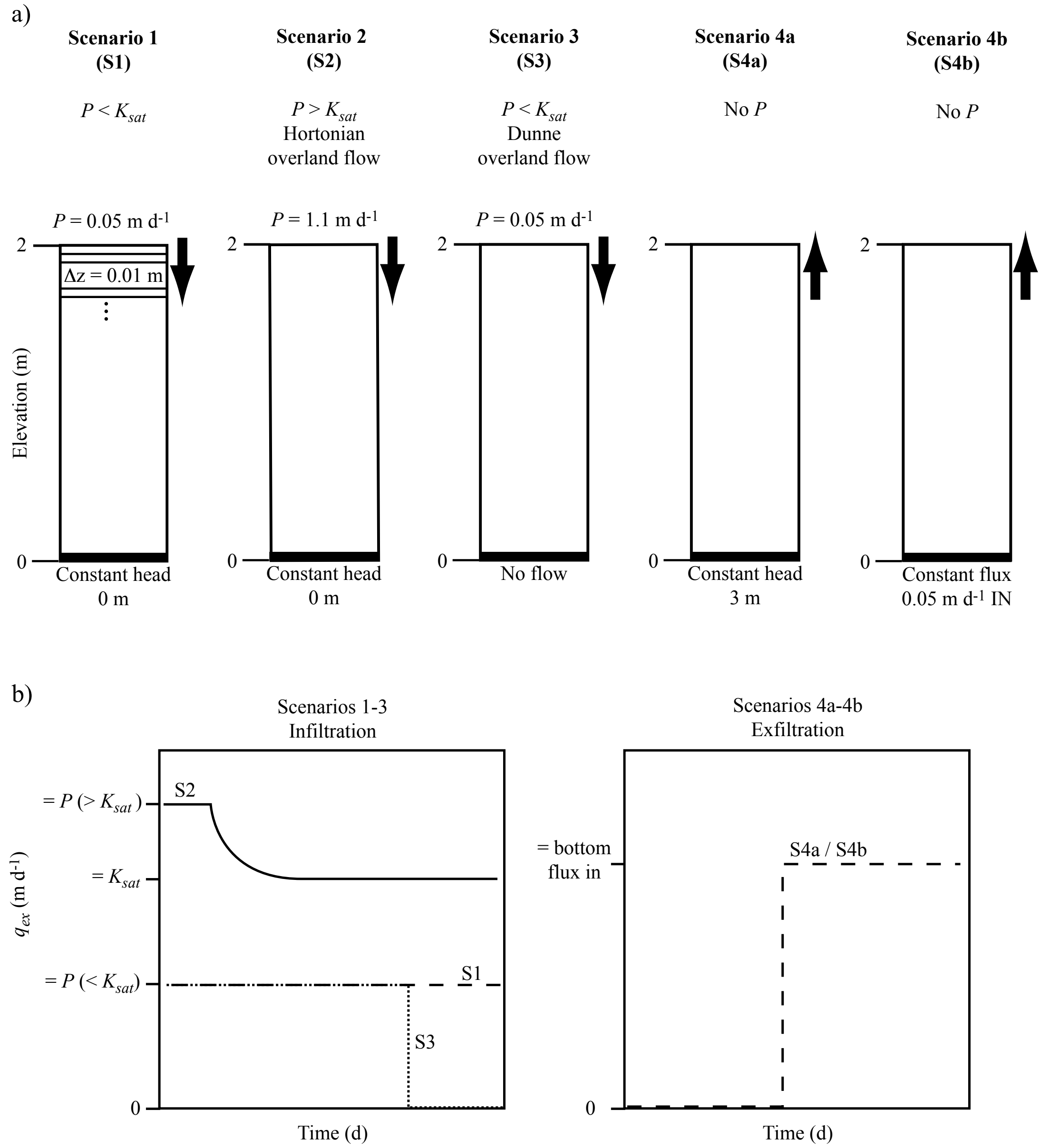

Figure 2.2 a) Hydrological scenarios and boundary conditions, and b) expected infiltration and exfiltration responses from each hydrological scenario

The first scenario (S1; Figure 2.2a) has a precipitation rate (*P*) of 0.05 m d^{-1}, which is less than the steady-state infiltration capacity of all three soil types used, thereby inducing non-Hortonian infiltration conditions. This value of *P* is slightly lower than the global mean rainfall rate of 3.47 mm h^{-1} (0.083 m d^{-1}) as determined by Dunkerley (2008). The steady-state infiltration capacity is equal to K_{sat} under conditions of minimal surface ponding (e.g. atmospheric pressure), homogeneous and isotropic soil, and free from the effects of swelling clays, macropores, and surface capping (Hillel, 1980).

As K_{sat} is higher than P in the S1 scenario, infiltration should equate to P throughout the duration of the rainfall event, inducing a flux-controlled surface condition (Figure 2.2b) (Hillel, 1980). Additionally, the column should remain unsaturated if the lower boundary condition is sufficiently free flowing. The lower boundary conditions are given in Figure 2.2a for all scenarios.

In the second scenario (S2; Figure 2.2a), P is 1.1 m d^{-1}, which is greater than the K_{sat} of all three soils and therefore produces Hortonian overland flow. A P of 1.1 m d^{-1} is high relative to average rates of rainfall, but is within common rates for high or extreme events (Dunkerley, 2008). The high rainfall rate can also be a substitute for scenarios of runon-generated Hortonian overland flow, where K_{sat} is larger than P, but smaller than the sum of P and overland flow arriving from upslope (i.e. the runon) (Maxwell and Kollet, 2008b). In this scenario, infiltration is expected to occur at P during the initial stages of the simulation when infiltration capacity is high due to the large matric potential of dry soil (Hillel, 1980). When the uppermost subsurface cell approaches saturated conditions, the infiltration capacity and therefore q_{ex} (as infiltration) drops to K_{sat}. Excess water then fills any surface storage (i.e. H_d) before becoming overland flow for the remaining duration of the rainfall event (Figure 2.2b) (Hillel, 1980). Saturation of the column should occur from the top-downwards.

The third scenario (S3; Figure 2.2a) is an extension of S1, where $P < K_{sat}$; however, the column is not allowed to drain freely. A no-flow bottom boundary condition is implemented in order to generate Dunne overland flow by bottom-up saturation of the column. Infiltration is expected to occur at P until the column becomes saturated, at which point infiltration ceases (q_{ex} = 0) and overland flow occurs at a rate of P (Figure 2.2b).

Finally, the S4a and S4b scenarios (Figure 2.2a) are included to examine situations involving exfiltration of groundwater, imposed in the 1D context using either constant head (S4a) or constant flux (S4b) boundary conditions at the bottom of the column. Rainfall is not considered. In the case of S4a, the rate of lower boundary inflow varies due to the changing head conditions of the column, whereas the rate of inflow is equal to the specified boundary flux in the S4b column (Figure 2.2). The rate of exfiltration (i.e. q_{ex}) is zero until the column saturates from the bottom-up, at which point q_{ex} equals the lower boundary inflow (Figure 2.2b).

In addition to testing the FOEC sensitivity using varying values of l_e in different hydrological scenarios, the sensitivity of l_e is also tested against various physical and numerical parameters by altering soil type, H_d and vertical grid resolution as shown in Table 2.1. Each of the soil columns shown in Table 2.1 are identified by the soil type used and a number indicating the combination of H_d and vertical grid resolution (e.g. SL-1). The five hydrological scenarios (Figure 2.2) are simulated using each of the nine soil columns (Table 2.1). The resulting 45 combinations are used for testing seven different l_e values (10 m, 1 m, 0.1 m, 0.01 m, 10^{-3} m, 10^{-4} m and 10^{-5} m) and the COP approach: a total of 360 numerical experiments.

Table 2.1 Soil column parameters. SL = sandy loam, SiL = silty loam, CL = clayey loam.

Soil Column ID	K_{sat} (m d^{-1})	H_d (m)	Vertical grid resolution (m)
SL-1	1.0608	0.001	0.01
SL-2	1.0608	0.01	0.01
SL-3	1.0608	0.001	0.2
SiL-1	0.108	0.001	0.01
SiL-2	0.108	0.01	0.01
SiL-3	0.108	0.001	0.2
CL-1	0.0624	0.001	0.01
CL-2	0.0624	0.01	0.01
CL-3	0.0624	0.001	0.2

Vertical grid resolution is varied in this chapter (Table 2.1) to explore whether the mesh resolution significantly influences the relationship between FOEC parameters and hydrological predictions. This follows studies such as Mehl and Hill (2010) who demonstrated the grid dependence of the conductance approach for stream-aquifer interactions, and Downer and Ogden (2004) and Vogel and Ippisch (2008), who showed that grid resolution plays an important role in the simulation of soil moisture dynamics. A grid convergence analysis was performed using grid resolutions of 1 mm, 1 cm, 20 cm and 50 cm for the S2 SL-1 (Figure 2.2, Table 2.1) simulation. Compared to the finest (i.e. 1 mm) grid resolution results, resolutions of 50 cm and 20 cm showed considerable variation in the head versus depth profile. There was up to an 80 cm difference in elevation between the wetting fronts of the 1 mm resolution and the 50 cm resolution results. There was no more than a 5 cm difference in the elevation of the wetting front between grid resolutions of 1 cm and 1 mm. The time to initiate overland flow decreased by 58% and 54% between grid resolutions of 50 cm to 20 cm and 20 cm to 1 cm, respectively; but only decreased by 10% between resolutions of 1 cm and 1 mm. Based on these results, a grid resolution of 1 cm was chosen for the majority of the numerical experiments (Table 2.1). Furthermore, simulations with a grid resolution of 20 cm were run for each hydrological scenario and soil type (Table 2.1, the “-3” columns, i.e. XX-3, where XX is the soil type) to examine the sensitivity of the l_e to grid resolution.

The value of H_o is zero, therefore H_s is entirely comprised of H_d (Figure 2.1) as per Table 2.1. A critical-depth boundary is applied at the surface to allow overland flow to exit at the edges of the model domain. The initial head in the subsurface is equal to the bottom of the column (0 m) in all simulations. Hydraulic properties of sandy loam (SL), silty loam (SiL) and clayey loam (CL) are adopted from Carsel and Parrish 1988 to parameterise the van Genuchten (1980) water retention curves, as listed in Table 2.2.

Table 2.2 Soil hydraulic properties.

Soil Type	**K_{sat} (m d^{-1})**	**Porosity(-)**	**van Genuchten α (1 m^{-1})**	**van Genuchten β (-)**	**Residual saturation (-)**
SL	1.0608	0.41	7.5	1.89	0.159
SiL	0.108	0.45	2	1.41	0.149
CL	0.0624	0.41	1.9	1.31	0.232

Adaptive time stepping is used with an initial time step of 1.15x10^{-4} d and a maximum time step of 1.15x10^{-3} d for all simulations. Sensitivity analyses of both the maximum time step size and convergence criteria were performed. Both were set such that lowering them further had minimal effect on the accuracy of the solution while reducing computational expense. Larger convergence criteria (up to three orders of magnitude) were required for the simulations of the S2 scenario with silty loam and clayey loam soil columns in order to maintain numerically stable and accurate results. The duration of the simulated events varied between 0.5 and 150 d. Such long durations for a constant rainfall rate are unrealistic in nature, but ensured that all simulations reached steady state regardless of l_e. Steady state was assumed to be reached when the rate of change in storage was on the order of 10^{-16} m^3 d^{-1} and when changes in q_{ex}, overland flow (q_{OLF} [LT^{-1}]), h_{ss} and h_s were insignificant (i.e. no change around the 10th decimal place). Both the steady state and transient responses of the simulations were evaluated, using the steady-state q_{ex}, steady-state h_{ss}-h_s and time to initiate overland flow (t_{OLF} [T]) to assess hydrological response.

2.3.3 Estimate of Appropriate Coupling Length for Hortonian Conditions

A maximum l_e for the S2 (Hortonian) scenario that allows for top-down saturation of the subsurface, as would be expected under Hortonian conditions, can be determined from Equations 2.1 to 2.3. To achieve saturation of the uppermost subsurface node, h_{ss} must at least be equal to its nodal elevation at the top of the column. Very soon after the subsurface node saturates, the land surface is saturated (i.e. $d_o = H_d$) by rainfall, leading to h_s = (d_o + elevation head) = (H_d + elevation head). Excess water above H_d flows out of the model domain. In order to maintain saturation of the uppermost subsurface node and produce top-down saturation, the magnitude of the steady-state q_{ex} (as infiltration) must at least equal K_{sat} – i.e. the flux condition associated with saturated gravity flow. $q_{ex} = K_{sat}$ will be achieved when both $k_r = 1$ and $l_e = h_{ss}$-h_s (Equations 2.1 to 2.3), which is equivalent to H_d under saturated conditions, as described above. Top-down saturation does not occur when $l_e = H_d$ for cases where $H_o > 0$, because this creates a condition where $k_r < 1$ (Equation 2.3) and therefore q_{ex} will be lower then K_{sat}.

In summary, setting $l_e = H_s$ (only comprised of H_d) will allow for top-down saturation of the subsurface and produce a steady-state q_{ex} very close in magnitude to

K_{sat}. With $l_e > H_s$ the steady-state q_{ex} is lower in magnitude than K_{sat} and saturation of the uppermost node does not occur. With $l_e < H_s$, the steady-state q_{ex} will approach the steady-state q_{ex} of the COP case, which will be slightly larger in magnitude than K_{sat} due to the small amount of water stored in the surface (equal to H_d). To the best of the my knowledge, this relationship between H_s and l_e for Hortonian overland flow scenarios has not been previously documented.

The relationship between l_e and H_s described above is only meaningful for the S2 scenario. For the S1 scenario, the head difference across the FOEC interface for a particular l_e is not known *a priori* due to the unsaturated conditions of the column and the associated non-linear relationships between h_{ss}, relative hydraulic conductivity, q_{ex} and d_o. The S3, S4a and S4b scenarios involve bottom-up saturation of the subsurface regardless of l_e, so the relationships between l_e, H_s and subsurface saturation are not the same as the S2 scenario. Additionally, the transient behaviour of all hydrological scenarios, such as t_{OLF}, is not readily estimable *a priori*. Numerical modelling is used to evaluate the effects of l_e on transient behaviour of the hydrological scenarios, the effects of l_e on the S1, S3, S4a and S4b scenarios, and whether the relationship between l_e and H_s described above holds for the S2 scenario.

2.3.4 Extension to a Hypothetical 3D Catchment

A brief evaluation of the effects of l_e in a 3D model is presented in order to test whether the 1D results provide insight into 3D model behaviour. The conceptual model follows the V-catchment example (without evapotranspiration) used by Panday and Huyakorn (2004) in their testing of MODHMS. This example is also included in the HGS software package (Therrien et al., 2009). For brevity, the problem is not described in detail here and the reader is referred to Panday and Huyakorn (2004) for a detailed explanation of the model set-up. In this example, it rains for 35 d at P = 3x10^{-6} m s^{-1}. The vertical K_{sat} of the soil is 5x10^{-6} m s^{-1}. Since $P < K_{sat}$ there should be no Hortonian overland flow, although Dunne overland flow and exfiltration are expected in parts of the domain. The V-catchment test case is simulated with the same l_e values as used for the soil columns, i.e. ranging from 10^{-5} to 10 m, and the COP approach. The V-catchment is also simulated with l_e = 0.5 m, which is used in the HGS verification example and produces the same value of α as the original Panday and Huyakorn (2004) example. H_d = 1 cm and H_o is zero, as in the HGS verification example. An additional set of simulations are conducted to induce Hortonian overland flow with $P > K_{sat}$ by doubling P to 6x10^{-6} m s^{-1}.

2.4 Results

In general, the 1D simulations show converging trends of FOEC results approaching COP results as l_e decreases, except for the S3 scenarios, which are discussed separately in Chapter 2.4.1. As an example, Figure 2.3 illustrates the temporal results of q_{ex}, q_{OLF}, h_{ss} and saturation of the uppermost subsurface node (S_{ss} [-]) for the S2 SL-1 scenario (Hortonian overland flow in a sandy loam). All metrics from the FOEC simulations converge on the COP case as l_e decreases, as expected. Setting $l_e > H_s$ (i.e. > 1 mm) restricts infiltration and produces a steady-state q_{ex} value significantly lower in magnitude than K_{sat} (Figure 2.3a), as expected following Chapter 2.3.3. High values of l_e (above H_s) also result in the production of overland flow without top-down saturation of the subsurface, and unsaturated conditions persist throughout the subsurface (Figure 2.3b, d), contrary to the expected behaviour under Hortonian conditions.

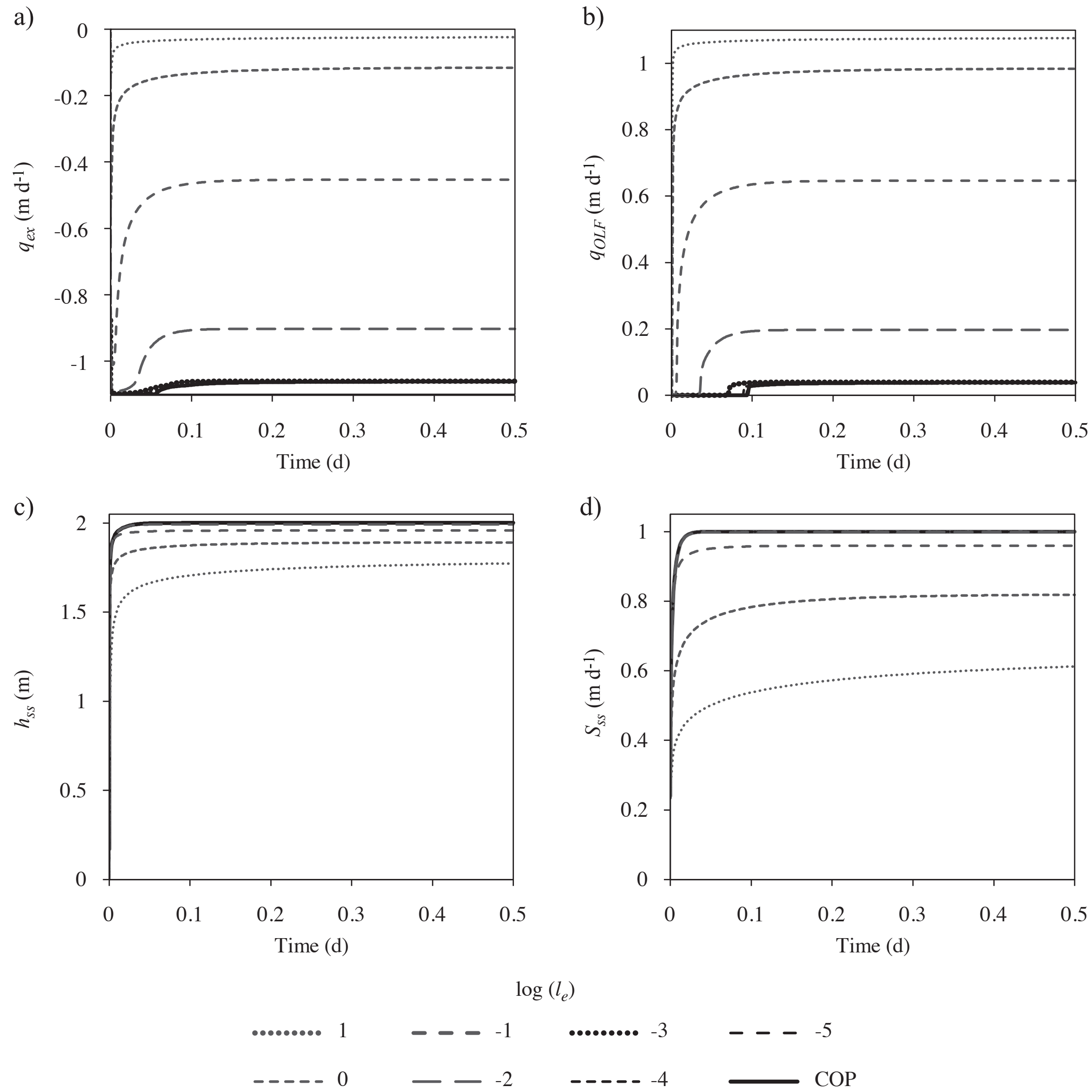

Figure 2.3 Simulated trends for the S2 SL-1 simulation for a) q_{ex}, b) q_{OLF}, c) h_{ss} and d) S_{ss} for the first 0.5 d of simulation. Results converge on the COP case as l_e decreases, and some of the lines become obscured.

Figure 2.4 illustrates the convergence of FOEC results approaching the COP results in terms of the steady-state q_{ex}, steady-state h_{ss}-h_s, steady-state S_{ss} and t_{OLF} for the SL-1, SiL-1 and CL-1 soil columns (Table 2.1), and for the S1, S2, S4a and S4b scenarios (Figure 2.2). The pattern of convergence varies between soil type and hydrological scenario. For the S2, S4a and S4b scenarios, steady-state h_{ss}-h_s tends towards zero in an asymptotic manner with reducing l_e. For the S2 and S4a scenarios,

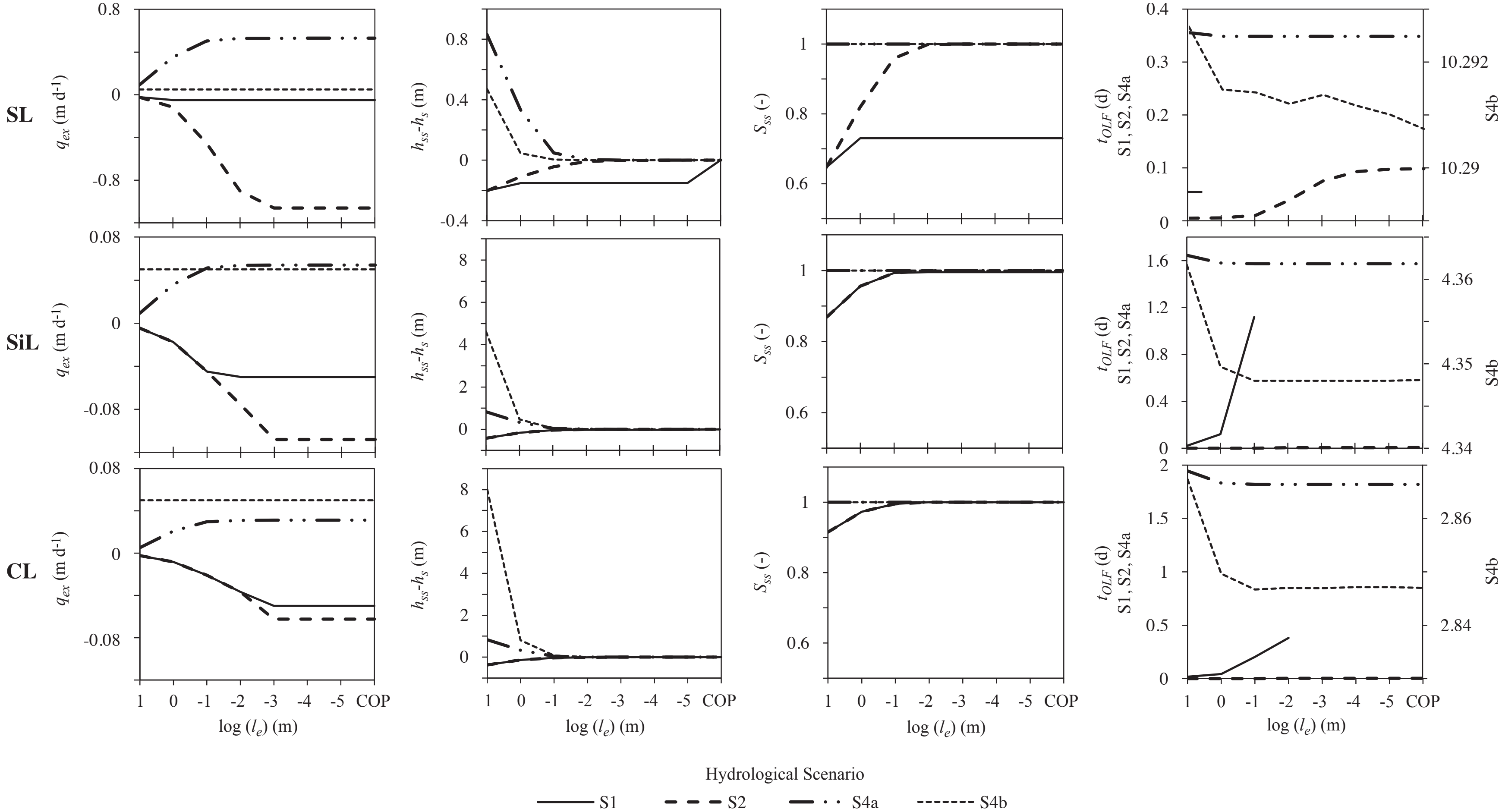

Figure 2.4 Steady-state q_{ex}, steady-state h_{ss}-h_s, steady-state S_{ss} and t_{OLF} as a function of l_e for each of the scenarios and the SL-1, SiL-1 and CL-1 soil columns. Note the different y-axes between soil types.

steady-state q_{ex} also asymptotes towards the COP result, whereas steady-state q_{ex} for the S4b scenario is equal to the specified flux at the bottom boundary condition at all values of l_e. t_{OLF} for the FOEC results approach the COP results, but do not equal the COP values for any of the scenarios. For all soil types, the S1 scenario produces overland flow for high values of l_e, despite $P < K_{sat}$. The t_{OLF} for these simulations is shown in Figure 2.4, noting that at lower values of l_e there is no overland flow produced and hence t_{OLF} is not reported.

Due to the asymptotic relationship of the simulation results (Figure 2.4), thresholds for three individual metrics were selected as a means of determining when the FOEC simulations had appropriately converged on the COP for the purposes of this chapter. These thresholds are based on the maximum l_e which produces (1) steady-state q_{ex} within 1% of the COP approach, (2) t_{OLF} within 1% of the COP approach, and (3) steady-state h_{ss}-$h_s \leq 1$ mm. Table 2.3 lists the corresponding maximum l_e values, termed the "threshold l_e" values, from the simulations of all hydrological scenarios and soil columns. A differentiation between the threshold l_e values for the three different metrics is made. The threshold l_e for the steady-state h_{ss}-h_s in the S1 scenario is not shown because h_{ss}-h_s is always above 1 mm, owing to the unsaturated conditions in the subsurface. For the FOEC simulations that produce t_{OLF} within 1% of COP (Table 2.3), the range in absolute difference from COP is < 1 min to 30 min. The largest absolute differences in t_{OLF} (up to 30 min) are for l_e values ≥ 1 m for the S4a and S4b scenarios, and the smallest absolute differences (< 1 min) are for the SiL and CL soil columns of the S2 scenarios. Depending on the purpose and scale of a particular modelling study these differences in t_{OLF} may be significant.

Table 2.3 Log of threshold l_e for each scenario and soil column. Blue shading = low threshold l_e, red shading = high threshold l_e.

Scenario	Soil Column ID		Steady-state q_{ex} ≤ 1% of COP	Steady-state h_{ss}-h_s ≤ 1 mm	t_{OLF} ≤ 1% of COP
S1	SL	-1	0	-	0
		-2	0	-	0
		-3	0	-	0
	SiL	-1	-2	-	-2
		-2	-2	-	-2
		-3	-2	-	-2
	CL	-1	-3	-	-3
		-2	-2	-	-2
		-3	-3	-	-3
S2	SL	-1	-3	-3	<-5
		-2	-2	-3	-5
		-3	-3	-3	<-5
	SiL	-1	-3	-3	<-5
		-2	-2	-3	-5
		-3	-3	-3	-5
	CL	-1	-3	-3	<-5
		-2	-2	-3	-3
		-3	-3	-3	-5
S4a	SL	-1	-2	-3	0
		-2	-2	-3	-1
		-3	-2	-3	0
	SiL	-1	-2	-3	0
		-2	-2	-3	-1
		-3	-2	-3	0
	CL	-1	-2	-3	0
		-2	-2	-3	-1
		-3	-2	-3	0
S4b	SL	-1	≥1	-2	≥1
		-2	≥1	-2	≥1
		-3	≥1	-2	≥1
	SiL	-1	≥1	-3	≥1
		-2	≥1	-3	≥1
		-3	≥1	-3	≥1
	CL	-1	≥1	-3	≥1
		-2	≥1	-3	0
		-3	≥1	-3	≥1

The threshold l_e varies depending on which metric is used to evaluate the convergence of the solution (Table 2.3). For example, capturing t_{OLF} in the S2 and S4a scenarios to the desired level of convergence requires a lower l_e than that for capturing steady-state q_{ex} (Table 2.3). The threshold l_e also differs, to varying degrees, depending on the hydrological scenario and soil column properties. With respect to hydrological scenario, accurately simulating steady-state q_{ex} and t_{OLF} requires lower values of l_e ($\leq H_s$) for the S2 scenario relative to the other scenarios (Table 2.3). The S4a and S4b scenarios (exfiltration) have higher threshold l_e values for steady-state q_{ex} and t_{OLF} compared to the S1 and S2 (infiltration) scenarios.

With respect to the soil column properties, lower permeability soils require lower threshold l_e values for accurate simulation of all metrics for the S1 scenario (Table 2.3). Increasing H_s affects the threshold l_e values differently for each hydrological scenario (Table 2.3, comparing XX-1 and XX-2 soil columns). For example, higher threshold l_e values for steady-state q_{ex} are obtained for larger H_s values for the S2 scenario and S1 CL soil column, but not for the S4a and S4b scenarios. This is because H_s is directly related to the l_e required to produce top-down saturation for the S2 scenario (Chapter 2.3.3). Threshold l_e for t_{OLF} increases or decreases as H_s is increased, depending on the hydrological scenario (Table 2.3). Finally, increasing the grid resolution to 20 cm does not affect the steady-state q_{ex} and h_{ss}-h_s values, therefore there is no change in the threshold l_e for these metrics the grid is refined (Table 2.3, comparing XX-1 and XX-3 soil columns). Grid resolution influences t_{OLF} values, although the threshold l_e for t_{OLF} is only affected for the S2 CL-3 scenario (Table 2.3).

Simulations using higher l_e values reach steady-state conditions later (Figure 2.5). The time to reach within 1% of each simulation's steady-state q_{ex} is denoted t_{qex} [T], and is used as a measure of equilibrium timing. t_{qex} values for the SL-1, SiL-1 and CL-1 soil columns (Table 2.1) for each hydrological scenario are shown in Figure 2.5. As with the other metrics, t_{qex} converges on the COP simulation as l_e decreases. The difference in t_{qex} between high and low values of l_e may be substantial; for example, t_{qex} for the S1 CL-1 scenario varies from approximately 27 d at l_e = 10 m to less than 5 s at $l_e = 10^{-5}$ m. This lag in response time may become important when simulating variable-rate rainfall events.

2.4.1 S3 Dunne Overland Flow Scenario

The S3 scenario displays slightly different behaviour than the other hydrological scenarios with respect to changes in l_e. For the S3 scenario, there is no difference in steady-state q_{OLF}, h_{ss} or h_s results when l_e is varied. t_{OLF} differences are very minor when the infiltration leading to the saturation excess is not restricted by l_e (e.g. $l_e \geq$ 10 m restricts infiltration for SL soil columns). Thus, under conditions of a no-flow bottom boundary and without restriction of the infiltration leading to bottom-up saturation subsurface, scenarios of Dunne overland flow are insensitive to l_e. However, Dunne overland flow can also occur due to heterogeneities in the soil profile, whereby low permeability layers restrict vertical fluxes and a perched water table develops (Dunne, 1978). A small amount of infiltration continues throughout the rainfall event, equal to the flux through the low permeability layer. As it was shown earlier that l_e affects infiltration (with the S1 and S2 scenarios), an additional simulation is produced to briefly examine how the presence of a low permeability layer in the subsurface alters the sensitivity of the S3 scenario to l_e. For this

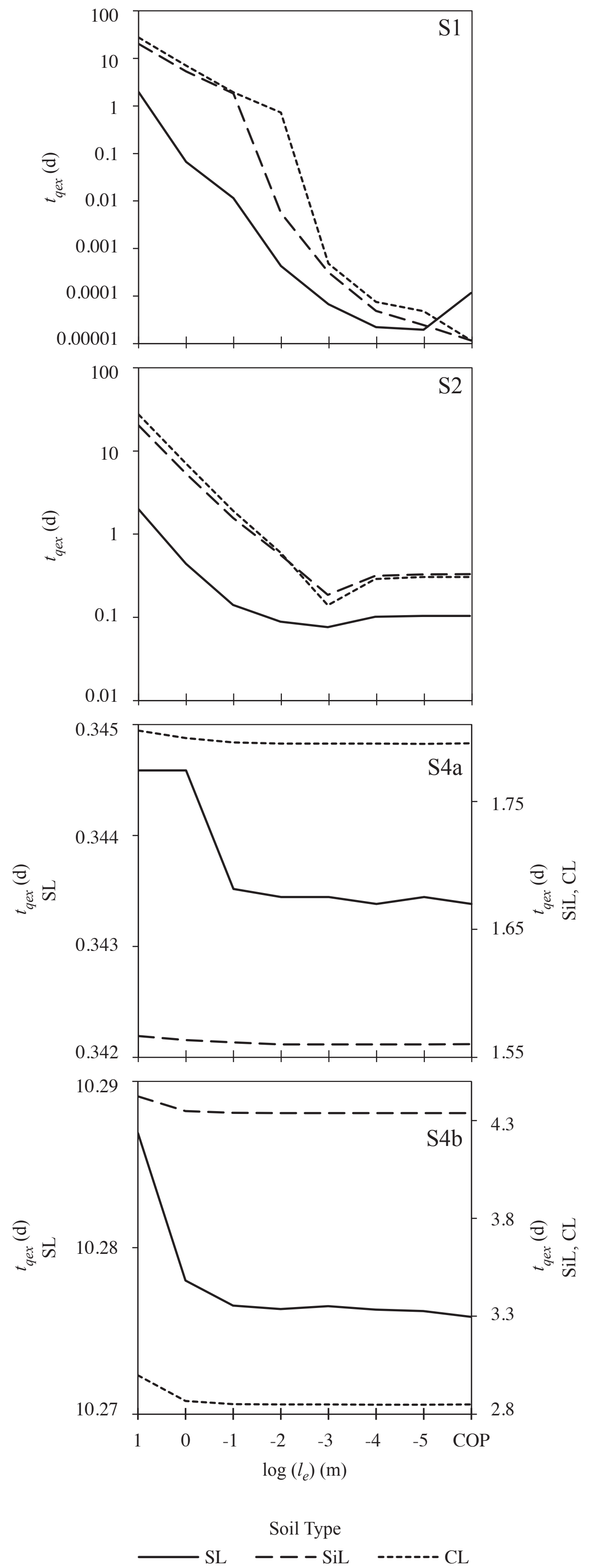

Figure 2.5 Time to reach within 1% of each simulation's steady-state q_{ex} (t_{qex}) against l_e. Note the different y-axes.

additional simulation, the S3 SL-1 soil column is modified to include a 0.25 m sandy clay layer (properties from Carsel and Parrish, 1988) at the bottom of the column with a constant head boundary of zero.

Unlike the S3 soil column with the no-flow boundary, there is a distinct difference in the t_{OLF} as l_e decreases, and results converge on the COP approach. t_{OLF} is within 1% of the COP approach for all l_e values below 10 m (infiltration was restricted at l_e = 10 m); although, there is an 18 min difference in t_{OLF} from the COP approach at l_e = 1 m. Dunne overland flow due to saturation above a leaky low permeability layer appears more sensitive to l_e than with a no-flow bottom boundary condition. This is because infiltration occurs throughout the simulation, and, as shown previously with the S1 and S2 scenarios, both q_{ex} and t_{OLF} are dependent on l_e.

2.4.2 Hypothetical 3D Catchment

Figure 2.6a shows the integrated catchment response of stream discharge for the V-catchment scenario with non-Hortonian conditions ($P = 3\text{x}10^{-6}$ m s^{-1}). With the COP approach, stream discharge initially increases slowly, as bottom-up saturation of the subsurface near the outlet of the catchment occurs and Dunne overland flow is produced. As the saturated area increases, more Dunne overland flow is produced and stream discharge increases until a steady-state is reached. Overland flow occurs only in areas where the subsurface is saturated at the land surface. Values of l_e > 0.1 m produce very different results than the COP approach, whereas values of $l_e \leq$ 0.1 m appear to produce results very close to the COP approach, as shown in the discharge hydrograph (Figure 2.6a). However, there is a noticeable difference in the h_{ss}-h_s results (Figure 2.6b, c) between the simulation with l_e = 0.1 m and those with

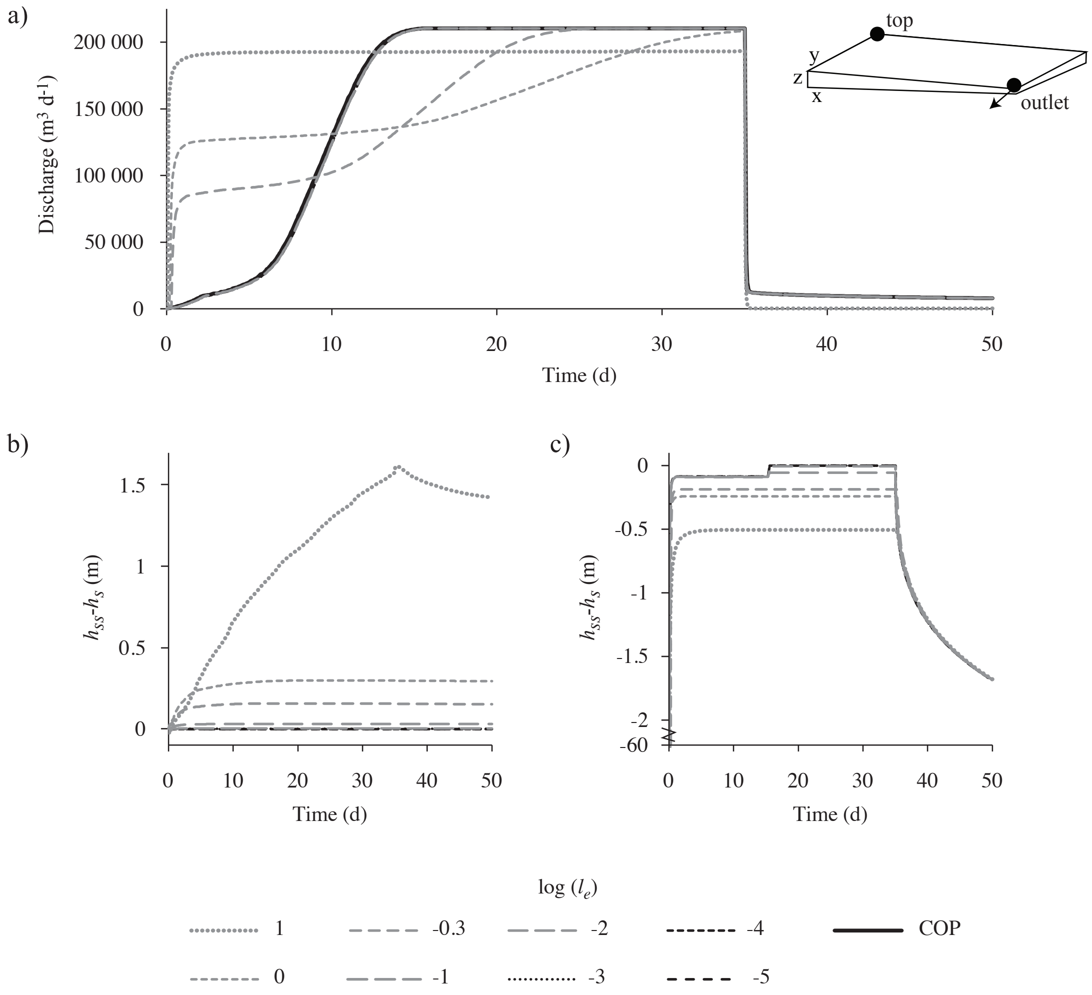

Figure 2.6 a) Integrated response of the V-catchment using the discharge hydrograph, and b) h_{ss}-h_s at the top and c) outlet of the catchment for the non-Hortonian conditions. Note the COP case is not plotted on parts b) and c) as h_{ss}-h_s is zero.

lower l_e values at the top and outlet of the catchment, where infiltration and exfiltration occur, respectively. High values of l_e (> 0.1 m) generate overland flow without top-down saturation of the subsurface, despite $P < K_{sat}$, similar to the 1D S1 scenarios. Consequently, there is rapid movement of water to the stream at the beginning of the rainfall event with high values of l_e (Figure 2.6a), and stream flow recession is quicker (by almost 5 hours) because less groundwater recharge leads to less groundwater discharge to the stream.

Figure 2.7 shows the responses of stream discharge and h_{ss}-h_s for the V-catchment scenario with Hortonian conditions (P = 6x10^{-6} m s^{-1}). With the COP approach, Figure 2.7a shows stream discharge increasing rapidly at the beginning of the simulation due to the generation of Hortonian overland flow. As the catchment saturates from the bottom-up, Dunne overland flow is also produced until a steady-state is reached. When l_e = H_s = 1 cm, top-down saturation of the catchment occurs, as seen in the 1D S2 scenarios. At this l_e, the discharge hydrograph results appear converged on the COP approach (Figure 2.7a), although there are still small h_{ss}-h_s

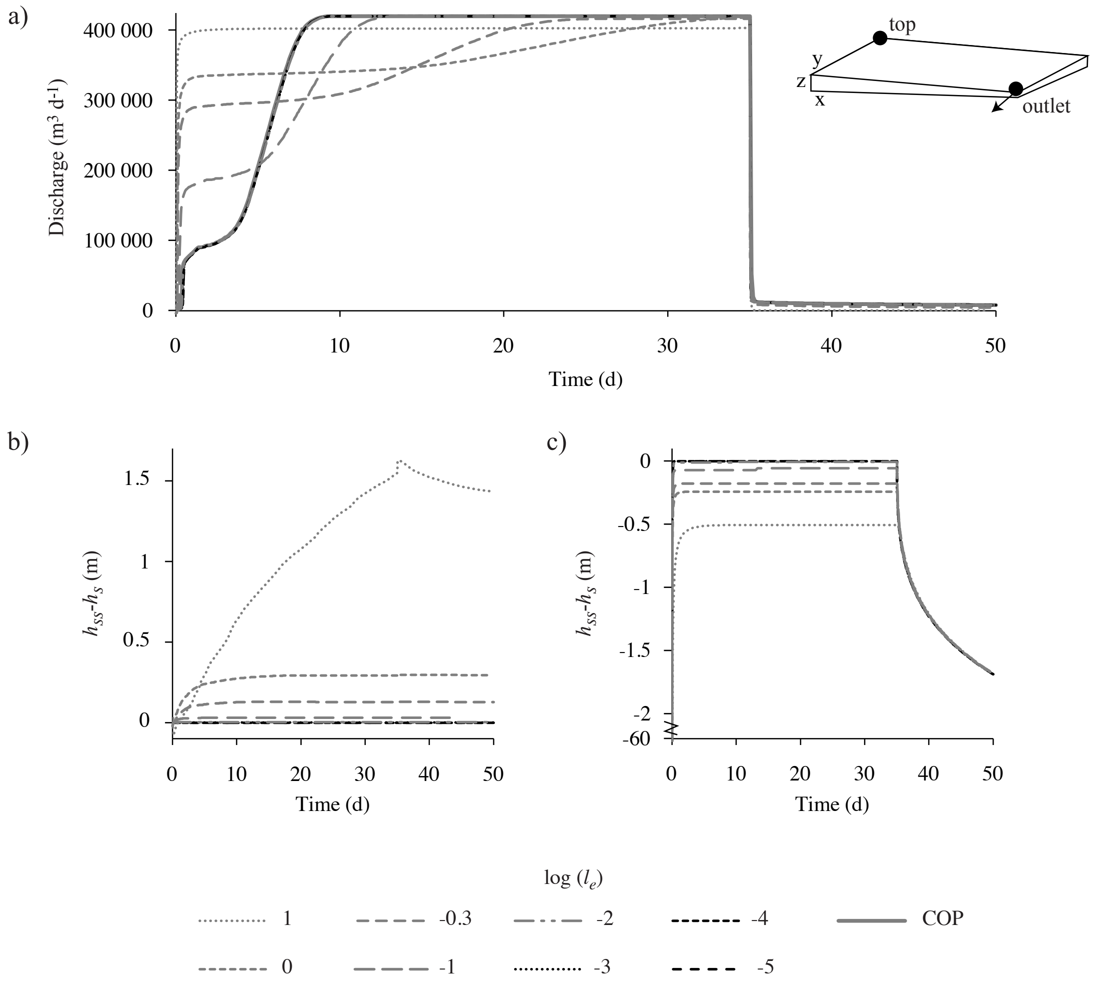

Figure 2.7 a) Integrated response of the V-catchment using the discharge hydrograph, and b) h_{ss}-h_s at the top and c) outlet of the catchment for Hortonian conditions. Note the COP case is not plotted on parts b) and c) as h_{ss}-h_s is zero.

values (< 1 cm) at the top of the catchment where infiltration occurs. Timing of the initiation of stream discharge varies from about 0.05 d (l_e = 10 m) to about 0.45 d (l_e = 10^{-5} m), although the initiation of stream discharge for the COP case occurs earlier (at 0.3 d) than the simulation with the lowest l_e. For both the non-Hortonian and Hortonian V-catchment scenarios, a value of l_e = 0.5 m, which is used in the verification example in HGS and Panday and Huyakorn (2004), produces results which are not converged with respect to the COP approach (Figure 2.6a, 2.7a).

2.4.3 Model Run Times

Ebel et al. (2009) found that model run time increases as l_e (coupling length scale in InHM) decreases, and points out that one of the advantages of the FOEC approach is that it alleviates the numerical difficulties of the COP approach. However, for the 1D simulations in the current chapter there was very little difference in model run time with low l_e values compared to high l_e values or the COP simulation. The only exception was for the low permeability soils (SiL and CL) of the S2 scenario. This lack of correlation between l_e and run time could be due to the simplified 1D approach used in this chapter. It may be the case that excessively slow run times with low values of l_e may only become an issue for models with multiple dimensions, heterogeneous soils, low permeability soils and/or Hortonian conditions, but this was not rigorously tested here. For the 3D V-catchment example, run time increased from 63 to 138 s as l_e decreased, but the COP simulation took less time to run than the simulation with the lowest l_e (126 s for the COP case) (Intel Core 2 PC, Quad, 64-bit, 3.0 GHz, 4.0 GB RAM, SATA HDD).

2.5 Discussion

The results of the 3D analysis are consistent with the 1D column analysis in that Hortonian overland flow scenarios require a smaller l_e (i.e. larger α) than non-Hortonian conditions (in higher permeability soils), and top-down saturation occurs when l_e is equal to H_s. The value of the difference between the FOEC and COP approaches for a given l_e in a 1D column model will not be the same for a 3D model of similar properties (e.g. surface-subsurface interaction, soil type, H_s). This is because topography, subsurface gradients and flow paths, surface flow, surface ponding, etc. may influence the sensitivity of the 3D model to l_e.

A value of l_e that is too high (i.e. α that is too low) in a catchment model produces errors in the integrated and distributed response of the model, as shown in Ebel et al. (2009) and the V-catchment example in this chapter (Figures 2.6 and 2.7). For example, high values of l_e may increase overland flow in the upper catchment, which can then run downhill and cause either increased ponding and infiltration in downslope areas, or increased stream flow. Also, high values of l_e which cause earlier t_{OLF} may affect the timing of stream flow response. A larger subsurface head build-up may develop in areas of exfiltration with high values of l_e, especially in lower permeability soils (Figures 2.4, 2.6b, 2.7b), which may affect up-gradient flow paths and fluxes. The transient response of the system to changes in precipitation rate may also be affected given that simulations with high l_e values show a lag in response to precipitation (Figures 2.3 and 2.5). Additionally, a value of l_e that is too high may result in the misinterpretation of dominant overland flow generation mechanisms if the internal catchment model results are not evaluated carefully, particularly if overland flow is generated for non-Hortonian conditions or without top-down saturation under Hortonian conditions.

Table 2.4 quantifies the differences between the FOEC and COP 1D column simulations when l_e = 1 mm for steady-state q_{ex} and t_{OLF}. The steady-state h_{ss}-h_s for the FOEC simulations are also shown. This value of l_e is equal to H_s for the XX-1 and XX-3 simulations, and is less than H_s for the XX-2 simulations (Table 2.1). Table 2.4 shows that setting l_e equal to H_s (composed of H_d only in this chapter) achieves results very close to the COP approach for the indicators considered and for all scenarios, except for t_{OLF} in the S2 scenario, where large differences (up to 25% and 78 min) are apparent for the sandy loam soil columns.

The relative differences between the FOEC and COP approaches for the steady-state q_{ex} are the same for all soil columns of the S2 and S4a scenarios (Table 2.4). This is because the relative differences in steady-state q_{ex} are dependent on the ratio of the hydraulic gradients across the entire column for each coupling approach. l_e is constant for these simulations and effectively lengthens the entire column for the FOEC approach, thereby decreasing the gradient (and steady-state q_{ex}) when the column is saturated. Altering soil type or vertical grid resolution has no effect on the relative differences in steady-state q_{ex} because neither soil type nor vertical grid resolution affect the hydraulic gradient once the column is saturated. Increasing H_s affects the hydraulic gradient across the entire column, and thus alters the relative differences in steady-state q_{ex} between the COP and FOEC approaches. However, the variation in the differences in steady-state q_{ex} between the coupling approaches are so minor they do not appear in Table 2.4 due to rounding of these values. For the S1 and S4b scenarios, the relative differences in steady-state q_{ex} are the same due to the

Table 2.4 Differences between the FOEC and COP approaches for steady-state q_{ex} and t_{OLF} when l_e = 1 mm for each scenario and soil column. Steady-state h_{ss}-h_s (FOEC approach only) is also shown and is > 1 mm for the S1 scenario due to unsaturated conditions at the uppermost subsurface node.

Scenario	**Soil Column ID**		**Steady-state q_{ex} (% from COP)**	**t_{OLF} (% from COP)**	**t_{OLF} (min from COP)**	**Steady-state FOEC h_{ss}-h_s (m)**
		-1	0	0	0	-1.51×10^{-1}
	SL	**-2**	0	0	0	-1.52×10^{-1}
		-3	0	0	0	-1.51×10^{-1}
		-1	0	0	0	-3.12×10^{-2}
S1	**SiL**	**-2**	0	0	0	-3.21×10^{-2}
		-3	0	0	0	-3.12×10^{-2}
		-1	0	0	0	-1.04×10^{-3}
	CL	**-2**	0	0	0	-3.63×10^{-3}
		-3	0	0	0	-1.04×10^{-3}
		-1	5.00×10^{-2}	-2.45×10^{1}	-3.34×10^{1}	-1.00×10^{-3}
	SL	**-2**	5.00×10^{-2}	-1.49×10^{1}	-7.78×10^{1}	-1.00×10^{-3}
		-3	5.00×10^{-2}	-1.40×10^{1}	-4.14×10^{1}	-1.00×10^{-3}
		-1	5.00×10^{-2}	-1.64×10^{1}	-1.49×10^{0}	-9.98×10^{-4}
S2	**SiL**	**-2**	5.00×10^{-2}	-4.23×10^{0}	-1.02×10^{0}	-1.00×10^{-3}
		-3	5.00×10^{-2}	-9.47×10^{0}	-2.90×10^{0}	-1.00×10^{-3}
		-1	5.00×10^{-2}	-1.73×10^{1}	-9.92×10^{-1}	-1.00×10^{-3}
	CL	**-2**	5.00×10^{-2}	-5.07×10^{0}	-8.97×10^{-1}	-1.00×10^{-3}
		-3	5.00×10^{-2}	-5.08×10^{-1}	-9.46×10^{-2}	-1.00×10^{-3}
		-1	5.00×10^{-2}	1.83×10^{-2}	9.10×10^{-2}	4.99×10^{-4}
	SL	**-2**	5.00×10^{-2}	9.20×10^{-2}	4.73×10^{-1}	4.95×10^{-4}
		-3	5.00×10^{-2}	-2.76×10^{-2}	-1.25×10^{-1}	4.99×10^{-4}
		-1	5.00×10^{-2}	-5.54×10^{-3}	-1.25×10^{-1}	4.99×10^{-4}
S4a	**SiL**	**-2**	5.00×10^{-2}	0	0	4.95×10^{-4}
		-3	5.00×10^{-2}	8.20×10^{-3}	-1.61×10^{-1}	4.99×10^{-4}
		-1	5.00×10^{-2}	-1.05×10^{-2}	-2.76×10^{-1}	4.99×10^{-4}
	CL	**-2**	5.00×10^{-2}	0	0	4.95×10^{-4}
		-3	5.00×10^{-2}	1.39×10^{-2}	3.18×10^{-1}	4.99×10^{-4}
		-1	0	6.27×10^{-3}	9.30×10^{-1}	4.71×10^{-5}
	SL	**-2**	0	-1.84×10^{-3}	-2.76×10^{-1}	4.71×10^{-5}
		-3	0	-2.18×10^{-3}	-3.23×10^{-1}	4.71×10^{-5}
		-1	0	-2.00×10^{-3}	-1.25×10^{-1}	4.63×10^{-4}
S4b	**SiL**	**-2**	0	0	0	4.63×10^{-4}
		-3	0	3.65×10^{-3}	-2.28×10^{-1}	4.63×10^{-4}
		-1	0	-2.67×10^{-3}	-1.10×10^{-1}	8.01×10^{-4}
	CL	**-2**	0	4.76×10^{-3}	2.05×10^{-1}	8.01×10^{-4}
		-3	0	-1.38×10^{-2}	-5.64×10^{-1}	8.01×10^{-4}

steady-state q_{ex} being equal to the COP approach for all simulations at this value of l_e.

Setting l_e = H_s provides a starting point for the selection of l_e during modelling studies, as it will ensure top-down saturation under Hortonian conditions. l_e = H_s also produces results very close to the COP case for the non-Hortonian and exfiltration conditions (Table 2.4). However, undertaking a sensitivity analysis is required to ensure convergence of the simulation using a number of metrics (e.g. t_{OLF}, h_{ss}-h_s, q_{ex}) to a desired level of accuracy, since it is shown that some metrics (particularly t_{OLF}) have smaller values of threshold l_e. The desired accuracy of the solution (i.e. convergence on the COP approach) will likely depend on the purpose and scale of the modelling study. For example, small-scale (e.g. 1D or hillslope study), detailed studies of rainfall-runoff behaviour will likely require a greater level of convergence on the COP case than large-scale (e.g. catchment) studies aimed at integrated or general catchment response. Altering the value of l_e by no less than plus and minus one order of magnitude should span a large enough range to evaluate the degree influence of l_e on the solution (Figures 2.3 to 2.7). A sensitivity analysis is also important for determining whether the threshold l_e varies according to other parameters mentioned by Ebel et al. (2009) but not examined here, such as the effects of topography, Manning's roughness coefficient, mobile water depths, specific soil hydraulic properties such as soil-moisture curves, subsurface heterogeneity, and H_o. It is likely that l_e will need to accommodate the smallest H_s and lowest permeability soil type over the entire model domain, or will need to vary spatially with H_s and soil type, since altering these properties affects threshold l_e values (Table 2.3).

Chapter 2 only tested the influence of the FOEC parameters in one code (HGS). Other mesh-centred codes will respond similarly to changes in the value of α, with solutions converging and approaching the COP case as α is increased (e.g. InHM, as in Ebel et al. 2009). However, the parameterisation of α may vary depending on the code. For example, InHM has an additional scaling parameter in α (VanderKwaak, 1999; Ebel et al., 2009), therefore top-down saturation may not occur when $l_e = H_s$, depending on the value of this additional scaling parameter. For block-centred codes such as MODHMS, the actual separation of the surface and subsurface nodes in the model grid presents some differences in the conceptualisation and implementation of the FOEC approach (See Chapter 3). Additionally, for MODHMS, including k_r (and therefore H_s) in the determination of α is optional (Equations 2.2 and 2.3), so the relationship between l_e and H_s is unlikely to hold. While the direct application of $l_e = H_s$ may not guarantee top-down saturation in all surface-subsurface codes, it is expected to provide a useful starting point for a sensitivity analysis of l_e in codes other than HGS. Additionally, this work demonstrates the relative effects of α on various surface-subsurface interactions, and highlights the importance of finding an acceptable level of convergence of the coupling parameters.

For cases where $H_s = 0$, the suggestion of setting $l_e = H_s$ will not be applicable, as $l_e = 0$ is not possible. However, it is suggested that H_s be set to a small value (e.g. $1\text{x}10^{-6}$ m, which is currently the default in HGS), such that its effects on surface ponding and the onset of overland flow are negligible. A small value of l_e can subsequently be utilised. For codes that do not require the inclusion of H_s in the determination of α (e.g. MODHMS), it is presumed that a very small l_e would be sufficient to produce top-down saturation in these cases; although, this was not explicitly tested in this chapter.

2.6 Summary and Conclusions

Both the COP and the FOEC approaches can be useful in simulating surface-subsurface interactions. The COP approach maintains a direct connection between the surface and subsurface, but can be computationally intensive. The FOEC approach can be used to reduce the computational burden, while maintaining accuracy, by preserving a close connection between the surface and subsurface domain. The FOEC approach can also account for any known disconnection between the surface and subsurface, such as surface sealing by rainfall effects, agricultural impacts, or fire effects (Ebel et al., 2009). As such, use of the FOEC approach in surface-subsurface codes is likely to continue. However, there is little guidance on how to assign appropriate FOEC values or the effects of the FOEC on catchment dynamics. In Chapter 2, 1D hypothetical scenarios were simulated to isolate the impact of the FOEC, or coupling length (l_e), on exchange flux, surface-subsurface head differences and timing of overland flow for specific hydrological scenarios and soil columns, rather than for whole catchment responses as in previous studies (e.g. Ebel et al., 2009; Huang and Yeh, 2009). The effect of l_e on a 3D V-catchment showed comparable results to the 1D simulations.

Similar to Ebel et al. (2009), numerical simulation results show converging trends of FOEC results approaching COP results as l_e decreases (i.e. FOEC increases). However, the pattern of convergence varies with hydrological scenario, soil type and total obstruction height (H_s; comprised of sub-grid depression storage only in this chapter). Vertical grid resolution has a very minor effect on the convergence of FOEC results on COP results. Hortonian overland flow conditions generally require smaller l_e values than non-Hortonian or exfiltration conditions. It is necessary to set

$l_e = H_s$ for top-down saturation to occur under Hortonian conditions. However, smaller values of l_e may be required depending on the purpose and scale of the modelling study, especially with regards to transient aspects of the simulation such as time to initiate overland flow and response to variable-rate rainfall events. Alterations to soil type have limited effects on the l_e required to obtain a converged solution, except under non-Hortonian conditions, where smaller l_e values, on the order of those needed for Hortonian conditions, are required for low permeability soils. l_e does not have a significant effect on Dunne overland flow due to a no-flow lower boundary condition, providing infiltration leading to the saturation excess is not restricted. In contrast, l_e has a greater effect on Dunne overland flow when a freely draining lower permeability layer is used as a lower boundary condition because this scenario depends on constant infiltration into the column.

As described by Ebel et al. (2009), the goal is to find "the sweet spot" for the value of l_e that balances accuracy and reduces the computational time compared to either very low values of l_e or the COP case; although in this chapter, run time was only a factor for Hortonian conditions. From the analysis of both 1D columns and the 3D hypothetical catchment, this chapter shows that a value of $l_e = H_s$ provides an acceptable starting point for the FOEC parameterization. However, it is important that a sensitivity analysis of no less than plus and minus one order of magnitude is conducted to ensure the solution is adequately converged, using a number of metrics, for the purposes of the modelling study.

Chapter 2 shows the importance of using a value of l_e (or values, if l_e is varied spatially) that accommodates all surface-subsurface interactions, soil types and values of H_s within a model. Implications of using a high value of l_e include errors in the simulated water balance and internal catchment dynamics (e.g. overland flow, infiltration, stream flow). This may lead to errors in the interpretation of simulated results, including dominant overland flow generation mechanisms, if model results are not examined carefully. Therefore, when using the FOEC approach for modelling surface-subsurface interactions, it is important that the value of l_e that gives adequately converged model results be determined for each study.

3. On the implementation of the first-order exchange coefficient approach using a block-centred surface–subsurface hydrology model

A version of this chapter is published as:

Liggett, J.E., Knowling, M.J., Werner, A.D., Simmons, C.T., 2013. On the implementation of the surface conductance approach using a block-centred surface–subsurface hydrology model. J. Hydrol. 496, 1–8. doi: 10.1016/j.jhydrol.2013.05.008

3.1 Introduction

Over the last two decades, considerable progress in hydrologic modelling techniques has led to the development of physically based, spatially distributed codes that are capable of simulating integrated surface-subsurface hydrological processes at the catchment-scale. Popular fully integrated codes (i.e. in which surface and subsurface governing equations are solved simultaneously; Furman, 2008) include Integrated Hydrology Model (InHM; VanderKwaak, 1999), MODHMS (HydroGeoLogic Inc., 2006), HydroGeoSphere (HGS; Therrien et al., 2009) and ParFlow (e.g. Kollet and Maxwell, 2006). The coupling of the surface and subsurface domains in these models is critical in the simulation of catchment-scale hydrology, given its control on dynamic surface-subsurface processes (e.g. rainfall partitioning into infiltration and overland flow) (Ebel et al., 2009; Chapter 2).

Surface-subsurface coupling in fully integrated codes is achieved typically using one of two conceptual approaches: (1) the first-order exchange coefficient (FOEC) approach (e.g. as applied in MODHMS), and (2) the continuity of pressure and flux (COP) approach (e.g. as applied in HGS and ParFlow) (Ebel et al., 2009). The FOEC approach involves a distinct exchange interface between the surface and subsurface nodes, over which hydraulic head gradients between these nodes drive surface-subsurface exchange fluxes. However, the presence of a distinct exchange interface may not be justifiable, in a physical sense, unless a known discontinuity between the surface and subsurface domains exists (e.g. due to surface sealing from raindrop impact, fire effects, cultivation, etc.) (Ebel et al., 2009). Moreover, parameters involved in the formulation of the FOEC approach are not easily measured or estimated (Kollet and Zlotnik, 2003). The COP approach arguably yields a more physical representation of surface-subsurface systems because it avoids the assignment of the FOEC (Kollet and Maxwell, 2006). Nevertheless, the FOEC approach is easier to apply and less computationally intensive in comparison to the more physically based COP method (Huang and Yeh, 2009; Kollet and Maxwell, 2006), and as such, its application in catchment hydrology modelling is common.

The formulation of the FOEC approach for simulating surface-subsurface interactions depends on the nodal arrangement in the model grid (i.e. block-centred or mesh-centred). In mesh-centred codes (e.g. HGS), the surface and uppermost subsurface nodes are coincident at the land surface (i.e. there is no physical separation between the respective nodes). Previous studies have characterised the influence of the FOEC approach on catchment flow processes using mesh-centred codes (e.g. Ebel et al., 2009; Delfs et al., 2009; Huang and Yeh, 2010; Chapter 2). However, the application of the FOEC approach in block-centred codes in the context of overland flow generation processes has received little attention to date. For block-centred codes (e.g. MODHMS), an inherent vertical separation between the surface and the uppermost subsurface nodes exists, which is expected to affect the simulation of surface-subsurface interactions. As such, the implementation of the FOEC approach needs to account for the uppermost grid cell thickness. Few block-centred codes are capable of simulating fully integrated surface-subsurface flow, although there are some (e.g. MODHMS) that are used widely in catchment modelling (e.g. Werner and Gallagher, 2006; Barr and Barron, 2009; Donn et al., 2012). It is important that the use of the FOEC approach in block-centred codes is assessed given that fully integrated codes are increasingly being used in catchment modelling (Sebben et al., 2013).

Chapter 3 explores the influence of the block-centred implementation of the FOEC approach on simulated surface-subsurface interactions using MODHMS. The mesh-centred code HGS is used as a basis for comparison against block-centred results. One-dimensional numerical infiltration experiments of Hortonian conditions are used to examine the simulation of infiltration-excess overland flow. I explore the partitioning of rainfall into infiltration and overland flow (and the associated surface-subsurface head differences) to assess the influence of FOEC parameters and the vertical separation of the surface and uppermost subsurface nodes on modelling predictions. The primary objectives are to: (1) characterise the dependence of simulated surface-subsurface interactions on coupling parameters and uppermost cell thickness, and (2) propose ways in which the FOEC approach can be applied in a block-centred code to accurately and efficiently predict rainfall partitioning. Guidance is offered for catchment modellers on FOEC parameterisation in block-centred codes.

3.2 Background

3.2.1 FOEC coupling approach

In fully integrated codes that utilise the FOEC approach, the exchange flux q_{ex} [LT^{-1}] (negative for infiltration) across the surface-subsurface exchange interface is given by:

$$q_{ex} = \alpha(h_{ss} - h_s) \tag{3.1}$$

where h_{ss} [L] is the hydraulic head at the uppermost node of the subsurface system, h_s [L] is the hydraulic head at the surface node, and α [T^{-1}] is the FOEC, which is otherwise known as the "conductance" (e.g. Mehl and Hill, 2010; Ebel et al., 2009).

Conceptually, the FOEC approach in surface-subsurface coupling takes a similar form to FOEC-based techniques that have a long history in other hydrogeologic applications (VanderKwaak, 1999). For example, FOEC-based approaches have been used to represent fracture-matrix and macropore-matrix exchange (e.g. Barenblatt et al., 1960; Gerke and van Genuchten, 1993), and stream–aquifer interaction in the application of analytical solutions (e.g. Hantush, 1965; Hunt, 1999) and numerical models (e.g. the RIV package of MODFLOW; McDonald and Harbaugh, 1988). The FOEC parameter has been described as either a function of the exchange interface geometry (e.g. Warren and Root, 1963; Hantush, 1965; Prickett and Lonnquist, 1971; Hunt, 1999) or as a lumped calibration parameter that holds no physical meaning (e.g. Bencala, 1984; Kollet and Maxwell, 2006; Doppler et al., 2007; Mehl and Hill, 2010). The conceptualisation and numerical implementation of each of these FOEC approaches vary slightly as a result of the unique assumptions associated with each application. For example, the FOEC approach adopted in the MODFLOW RIV package is designed to represent flow across a lower conductivity streambed. It is assumed that water infiltrating through the streambed is added to the saturated groundwater system instantaneously. This package is not designed to consider dynamic surface-subsurface interactions such as the initiation of overland flow. Mehl and Hill (2010) demonstrated the differences in simulated stream-aquifer exchange using three different FOEC formulations based on the block-centred grid structure in MODFLOW. They found that stream-aquifer exchange was highly dependent on the formulation of the FOEC parameter, combined with the horizontal and vertical grid discretisation. It is therefore expected that the implementation of the FOEC approach in a block-centred code will impact the simulation of infiltration and overland flow in a variably saturated soil, given Mehl and Hill's (2010) findings for stream-aquifer exchange.

In applying the FOEC approach to surface-subsurface interactions in fully integrated codes, α is represented commonly as:

$$\alpha = \frac{K_{sat}}{l_e} \tag{3.2}$$

where K_{sat} [LT^{-1}] is the vertical saturated hydraulic conductivity and l_e [L] is the thickness of the exchange interface. Additional parameters (e.g. degree of land surface saturation or inundation) may also be included in the parameterisation of α (e.g. VanderKwaak, 1999; HydroGeoLogic Inc., 2006; Therrien et al., 2009). Codes that employ the FOEC approach require the user to specify either α as a whole (e.g. MODHMS), or l_e (e.g. the "coupling length" in HGS) is specified and K_{sat} is taken from the properties of the uppermost subsurface layer. It has been shown that nonphysical hydrologic behaviour may occur in response to inappropriate parameterisation of α (e.g. Ebel et al., 2009; Gaukroger and Werner, 2011; Chapter 2). Previous studies using mesh-centred codes conclude that informed selection of α allows the model user to optimise the trade-off between model accuracy and computational efficiency, while preserving near continuity of surface and subsurface heads (Ebel et al., 2009; Chapter 2).

The nodal arrangement within the model grid (i.e. block-centred or mesh-centred) influences the conceptualisation of the FOEC approach. In a mesh-centred code, the FOEC approach represents flow through an artificial layer of thickness l_e, given that the surface and uppermost subsurface nodes are coincident at the land surface (Figure 3.1a). In this case, l_e (and therefore α) is not related to the model grid structure. Overland flow generation (which requires the saturation of the uppermost soil profile; Horton, 1933) is therefore generated as a result of saturation of the

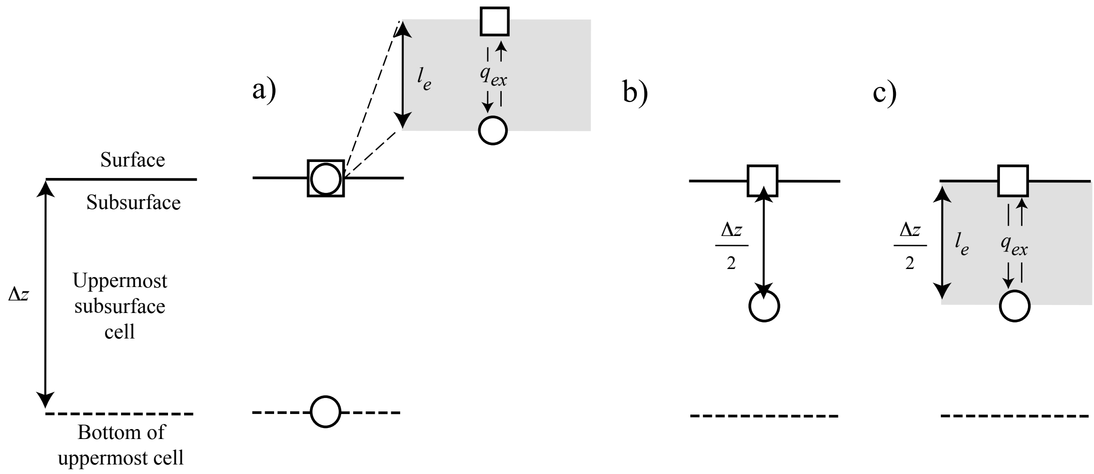

Figure 3.1 Conceptual nodal-scale representation of the FOEC approach in a) a mesh-centred code, and b) and c) a block-centred code. The squares and circles represent surface and subsurface nodes, respectively. The shaded area symbolises the surface-subsurface exchange interface.

uppermost subsurface node (i.e. when h_{ss} reaches its nodal elevation, z_{ss}) and h_{ss} intersecting the land surface concurrently. However, in a block-centred code, there is a vertical separation between the surface and uppermost subsurface nodes that is equal to the half-cell thickness ($\Delta z/2$) (Figure 3.1b). In this case, the FOEC approach represents flow through the top half of the uppermost subsurface cell (Figure 3.1c). However, saturation of the uppermost node (i.e. when h_{ss} reaches z_{ss}) is not coincident with h_{ss} reaching the land surface (Figure 3.1b, c). This combination of effects caused by the vertical separation of the surface and upper subsurface nodes is expected to affect the simulation of overland flow generation. To the best of my knowledge, this issue has not been discussed in the context of surface-subsurface interaction in fully integrated codes; therefore it is important to assess potential impacts on the simulation of overland flow processes.

3.2.2 MODHMS and HGS

MODHMS is a physically based, spatially distributed, surface-subsurface code that employs a block-centred, finite-difference solution scheme. Surface water flow is solved using the two-dimensional diffusion-wave approximation to the Saint Venant equations (HydroGeoLogic Inc., 2006). The subsurface domain is based on MODFLOW (McDonald and Harbaugh, 1988), which has been modified to solve the three-dimensional Richards equation (HydroGeoLogic Inc., 2006). A comprehensive description of the numerical framework behind MODHMS is described in the user manual (HydroGeoLogic Inc., 2006) and by Panday and Huyakorn (2004), and is therefore not repeated here. MODHMS adopts Equations 3.1 and 3.2 in applying the FOEC approach, with the option of including a relative permeability term representing the saturated/inundated fraction of the land surface due to the effects of depression or obstruction storage within the grid-block scale (Panday and Huyakorn, 2004).

Panday and Huyakorn (2004) and HydroGeoLogic Inc. (2006) suggest setting α according to Equation 3.2, whereby l_e equals the half-cell thickness of the uppermost subsurface layer (i.e. $l_e = \Delta z/2$), and K_{sat} corresponds to the uppermost soil layer. Panday and Huyakorn (2004) also suggest modifying α if a skin layer effect (i.e. a disconnection between the surface and subsurface) is desired, whereby $\alpha < K_{sat}/l_e$, to account for the reduced exchange interface permeability. The suggestion to adopt $l_e = \Delta z/2$ infers that the FOEC approach in MODHMS represents surface-subsurface exchange across a saturated interface that is comprised of the top half of the uppermost subsurface cell (Figure 3.1c). Assuming overland flow initiation occurs in response to saturation of the uppermost subsurface node, overland flow will be permitted when $h_{ss} = z_{ss}$ at a half-cell thickness below the land surface (Figure 3.1c), and hence the soil column and the uppermost cell are not truly saturated under these conditions.

In MODHMS, complete saturation of the uppermost subsurface node occurs when h_{ss} reaches the land surface (i.e. at a pressure head of $\Delta z/2$; Figure 3.2). This pressure-saturation relationship is different to the underlying cells, in which nodal saturation occurs when $h_{ss} = z_{ss}$ (Figure 3.2). The uppermost layer is treated differently to reconcile the discrepancy between saturation of the uppermost subsurface node and h_{ss} reaching the land surface. This allows overland flow to occur when the entire soil column is saturated. However, the pressure head in the uppermost cell is $\Delta z/2$ when this occurs (and $h_{ss} > z_{ss}$), which contradicts the notion of subsurface flow under gravity drainage conditions when the upper soil profile is

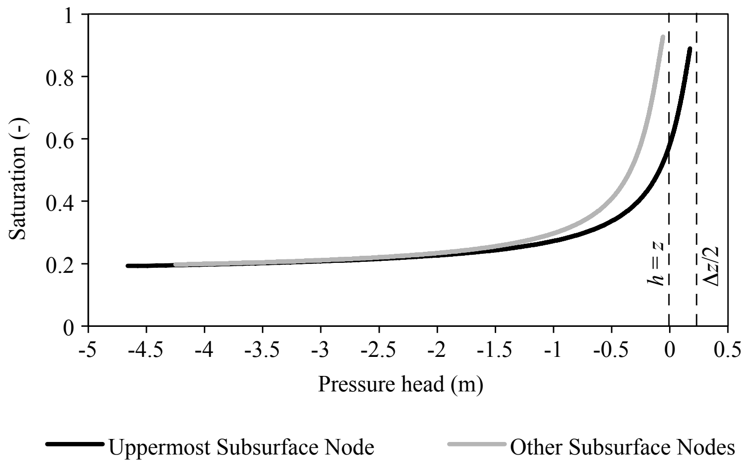

Figure 3.2 Comparison of the pressure-saturation relationship in the uppermost subsurface node (black line) and the underlying subsurface nodes in MODHMS (grey line). The simulation is for Hortonian conditions with a uniform vertical grid discretisation of 50 cm and model parameters as in Table 3.1 (i.e. the BC simulation described in Chapter 3.3). Dashed lines illustrate pressure heads of 0 m (i.e. total head equals nodal elevation) and 0.25 m (i.e. total head at top of cell), upon which saturation will reach unity.

saturated. This lack of consistency between the formulation of the pressure-saturation relationship of the uppermost cell and the conceptualisation of the FOEC approach is expected to influence the simulation of both the timing and amount of infiltration and overland flow.

The surface-subsurface flux and associated hydraulic gradients across the exchange interface can be evaluated for a Hortonian scenario from basic soil flow theory. Firstly, infiltration (i.e. negative q_{ex}) across the exchange interface will equal K_{sat} when $h_{ss} = z_{ss}$, because the hydraulic gradient across the exchange interface (i.e. $(h_{ss} - h_s)/l_e$) equals unity under these conditions of gravity flow (Equations 3.1 and 3.2; Figure 3.1c). However, the uppermost subsurface node is unsaturated when $h_{ss} = z_{ss}$ in MODHMS (Figure 3.2), and hence flow into the underlying cells is less than K_{sat}. This causes h_{ss} to rise above z_{ss}, towards the land surface. Subsequently, the hydraulic gradient across the exchange interface falls below unity (i.e. (h_{ss} - h_s) < l_e), causing q_{ex} < K_{sat}. In this case, the soil column is unable to attain top-down saturation, despite the gravity-flow conditions. It is therefore expected that the block-centred simulation will not produce entirely accurate results of q_{ex} or overland flow q_{OLF} [LT^{-1}] with MODHMS's pressure-saturation relationship in the uppermost subsurface cell (Figure 3.2), and using $l_e = \Delta z/2$ to define α. This discrepancy (and its significance) has not been explored previously. Additionally, the influence of the subsurface grid design requires further investigation for the block-centred arrangement.

HGS was used to establish a mesh-centred solution for the FOEC and COP approaches under Hortonian conditions. HGS computes flow in the surface and subsurface domains by solving similar equations to those described previously for MODHMS. HGS is capable of solving the integrated surface-subsurface flow equations by applying either finite-element or finite-difference solution schemes. The surface and subsurface flow domains can be also coupled via the COP or FOEC approaches. The reader is directed to the HGS user manual (Therrien et al., 2009) for a comprehensive code description.

Chapter 2 found that simulation results using the FOEC approach in HGS converged on the COP approach as the value of α increased (i.e. as l_e was reduced) for a number of overland flow generation scenarios, including under Hortonian conditions. Using the FOEC approach in HGS allows for a direct comparison of the mesh-centred and block-centred grid setups. The COP-based solution of HGS provides a basis for assessing the influence of the FOEC approach on the surface-subsurface response under Hortonian conditions.

3.3 Methods

3.3.1 Conceptual Model

The current chapter focuses on surface-subsurface interactions under Hortonian conditions. Hortonian overland flow occurs as a result of the precipitation rate exceeding the infiltration capacity of a soil (Horton, 1933). Overland flow generation occurs in response to saturation of the uppermost portion of the soil profile (Horton, 1933). Hortonian conditions were adopted following Chapter 2, which found that these conditions are more sensitive to α, and require higher values of α for the steady-state infiltration rate to reach within 1% of the COP approach, relative to other overland flow generation mechanisms (e.g. Dunne overland flow generation, exfiltration).

Hortonian conditions were applied to a one-dimensional soil column of 5 m depth. A homogeneous and isotropic soil was considered. Surface ponding was negligible and hence the saturated infiltration capacity will equal K_{sat} under gravity drainage conditions (Hillel, 1980). This allows the steady-state infiltration rate to be known *a priori*, ensuring that any deviations in the model results from this condition can be attributed to the implementation of the FOEC approach and/or the grid discretisation.

Soil properties are representative of a sandy loam with a K_{sat} of 1.0608 m d^{-1} and the associated van Genuchten soil parameters (van Genuchten, 1980) are from Carsel and Parish (1988). This soil type was selected in order to avoid the numerical instabilities that are often associated with fine-grained (e.g. clay) or coarse-grained (e.g. sand) soils. A rainfall rate of 1.1 m d^{-1} was applied for 5 days to induce Hortonian overland flow and steady-state conditions. This rainfall rate is considered normal for only short-lived extreme events (Dunkerley, 2008), but it was nonetheless required in order to achieve Hortonian conditions for the given soil. The model results could then be compared to the basic soil theory of infiltration under Hortonian conditions, whereby steady-state infiltration equals K_{sat} (Horton, 1933; Hillel, 1980). A summary of the model input parameters is listed in Table 3.1.

Table 3.1 Model input parameters

Parameter	**Value**
Isotropic, vertical saturated hydraulic conductivity (K_{sat})	1.0608 m d^{-1}
Porosity (n_e)	0.41
van Genuchten parameters:	
α	7.5 m^{-1}
β	1.89
Residual moisture content (θ_r)	0.1585
Rill storage height (H_d)	10^{-4} m
Simulation time	5 d
Constant time step size	10^{-4} d
Convergence criteria	10^{-5} m

For both codes, the rainfall partitioning processes were evaluated using predictions of q_{ex}, q_{OLF}, surface and subsurface hydraulic heads, and soil moisture content. In particular, the steady-state q_{ex} (as infiltration) and time to initiate overland flow (t_{OLF} [T]) were considered key measureables in comparing simulations in both codes.

3.3.2 Numerical Experiments

Numerical experiments were performed initially to illustrate the impact of the block-centred implementation of the FOEC approach (i.e. compared to the COP benchmark case). A base case (BC) was constructed to assess the differences between the results of the block-centred and mesh-centred FOEC approaches ("MODHMS BC" and "HGS BC" simulations, respectively), and the mesh-centred COP-based benchmark solution ("COP BM" simulation), using the same vertical discretisation (Table 3.2). The suggested $l_e = \Delta z/2$ by Panday and Huyakorn (2004) and HydroGeoLogic Inc. (2006) was used in setting α for both the MODHMS BC and the HGS BC simulations. The α in HGS was made equal to MODHMS by adjusting l_e. Subsequently, two methods were tested in an attempt to identify ways in which simulation of surface-subsurface interactions in MODHMS can be improved.

Table 3.2 Simulations performed in this chapter

Simulation ID	**Uppermost Layer Thickness (cm)**	**Coupling Approach**	α **(d^{-1})**
MODHMS BC	50	FOEC	4.24
HGS BC	50	FOEC	4.24
COP BM	50	COP	-
*MODHMS CS	50	FOEC	1, 10, 100, 1000, 10^4, 10^5
*HGS CS	50	FOEC	1, 10, 100, 1000, 10^4, 10^5
MODHMS TL1	1	FOEC	106.08
MODHMS TL0.01	0.01	FOEC	10608.00

* Series of simulations with a variable α

A coarse vertical grid discretisation of 50 cm was used for the BC. This represents a typical vertical discretisation for regional-scale models, where computational efficiency is an important factor in model design (e.g. Downer and Ogden, 2004). Previous studies adopt nodal spacings between 4 and 200 cm (e.g. Loague and VanderKwaak, 2002; Panday and Huyakorn, 2004; Schoups et al., 2005; Smerdon et al., 2007; Jones et al., 2008; Kollet and Maxwell, 2008; Barr and Barron, 2009; Frei et al., 2009; Kumar et al., 2009; Maneta et al., 2009; and Ebel et al., 2010). For an uppermost subsurface cell thickness of 50 cm, α was set to 4.24 d^{-1} (i.e. as $\Delta z/2 = 25$ cm) for the MODHMS BC and HGS BC simulations.

A constant-head boundary condition was assigned to the bottom node to allow for the development of gravity driven flow involving a unit hydraulic gradient under saturated subsurface conditions, presuming that top-down saturation of the column occurs. The constant head at the lower block-centred node in the MODHMS BC simulation was set to 0.5 m (elevation of the bottom of the column is 0 m). Hence, the distance between the upper and lower nodes (Δl; 4.5m) equals the head difference between the same nodes (Δh) under saturated, gravity-driven flow conditions (i.e. when h_{ss} is at the land surface; 5 m). For the mesh-centred HGS BC simulation, the elevation of the bottom of the column and the constant head boundary were both set at 0.5 m (i.e. the column length is only 4.5 m). Again, this was done to ensure a unit hydraulic gradient under saturated, gravity-driven flow conditions. Although the soil column is shorter in the HGS BC simulation, the resulting change in storage does not affect the fluxes and heads across the exchange interface under Hortonian conditions.

For the MODHMS BC, HGS BC and COP BM simulations, the initial subsurface heads (i.e. total head) were set to 0 m (i.e. the elevation of the bottom of the column), creating unsaturated and hydrostatic conditions in the subsurface. Other initial conditions were tested, and it was found that the initial conditions do not impact the results of this chapter, and only affect the time to achieve steady-state (equilibrium) heads and fluxes. A critical-depth boundary condition was used to control discharge from the surface domain, resulting in negligible ponding above the rill storage height. The surface domain had an initial water depth of 0 m.

The temporal discretisation and convergence criteria were tested and set to minimise their influence on the solution (in terms of infiltration and overland flow). Constant time steps of 10^{-4} d were used after the first 7×10^{-4} d of simulation. HGS required smaller, adaptive time steps prior to 7×10^{-4} d, whereas time stepping in MODHMS was held constant. All HGS and MODHMS simulations adopted the finite-difference solution scheme.

Following the BC simulations, a set of simulations was undertaken to evaluate the sensitivity of the simulated surface-subsurface interactions to α, and the extent to which increasing α improves simulation results when using the FOEC approach in the block-centred code. Tested α values ranged from 1 to 10^5 d^{-1}, and a grid spacing of 50 cm was adopted (see "MODHMS CS" and "HGS CS" simulations, Table 3.2). Higher α values, corresponding to a more permeable and/or thinner exchange interface, are expected to promote greater infiltration rates, as shown by Equation 3.1.

Given that smaller thicknesses of the uppermost layer reduces the separation between the surface and uppermost subsurface nodes in a block-centred code (i.e. thereby approaching a mesh-centred grid configuration), an additional set of simulations was conducted to evaluate whether the introduction of a single thin layer into the uppermost subsurface allows improved predictions of steady-state q_{ex} and t_{OLF} in the block-centred code. Two simulations with thin layers of 1 cm ("MODHMS TL1") and 0.01 cm ("MODHMS TL0.01") were constructed in MODHMS by sub-dividing the original uppermost cell from the MODHMS BC simulation (Table 3.2). The aim here was to examine the thickness of the uppermost subsurface cell required to adequately approximate the predictions of steady-state q_{ex} and t_{OLF} compared to the mesh-centred results. For these simulations, $l_e = \Delta z/2$ was adopted, which resulted in α values of 106.08 d^{-1} and 10608 d^{-1} for the MODHMS TL1 and TL0.01 simulations, respectively.

3.4 Results

Figure 3.3 shows the q_{ex} and q_{OLF} results for the coarsely discretised MODHMS BC, HGS BC, and COP BM simulations. The steady-state q_{ex} for the COP BM simulation is equal to K_{sat}, as expected given the Hortonian conditions. The results of both the MODHMS BC and HGS BC simulations deviate significantly from the COP BM.

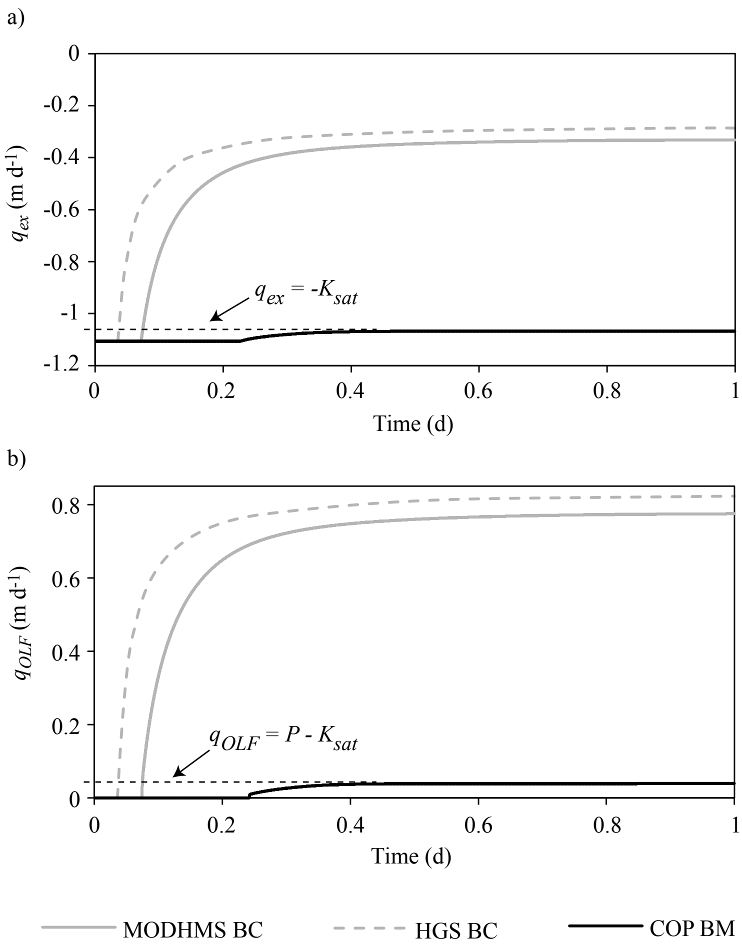

Figure 3.3 a) q_{ex} and b) q_{OLF} from the MODHMS BC and HGS BC simulations compared to the COP BM simulation for the first day of the 5-day simulation.

The steady-state q_{ex} is 70% and 74% lower than K_{sat}, and t_{OLF} is approximately 4 and 5 h (69% and 85%) earlier than the results of the COP BM, for the MODHMS BC and the HGS BC simulations, respectively. The HGS BC simulation results are consistent with the outcomes of Chapter 2, who showed that l_e must be sufficiently small (< 10^{-2} m) in order for steady-state q_{ex} and t_{OLF} to be simulated within 1% of the COP approach under Hortonian conditions. Similarly, the MODHMS BC simulation illustrates that the use of $l_e = \Delta z/2$ (Figure 3.1b) inhibits accurate simulation of rainfall partitioning for the given uppermost layer thickness (0.5 m) under Hortonian conditions.

Figure 3.4 illustrates steady-state q_{ex} and t_{OLF} for the MODHMS CS and HGS CS simulations, where α is varied (Table 3.2). The results of the COP BM are also shown as a basis for comparison. Steady-state q_{ex} and t_{OLF} converge as the value of α increases for both the MODHMS CS and HGS CS simulations, as expected from the results of Ebel et al. (2009) and in Chapter 2. The large markers in Figure 3.4 illustrate results obtained using $l_e = \Delta z/2$ to define α (i.e. the BC simulations). Note that the steady-state q_{ex} and t_{OLF} for the MODHMS BC and HGS BC simulations that adopt $l_e = \Delta z/2$ are much lower than the COP BM simulation.

For the HGS CS simulations, steady-state q_{ex} equals K_{sat} (Figure 3.4a) at high values of α, whereas t_{OLF} at high values of α is slightly later than the COP BM simulation (1.7 h or 31%; Figure 3.4b). These results are also consistent with Chapter 2, which showed that while q_{ex} may be accurate, a minor discrepancy in t_{OLF} may remain between COP-based and FOEC-based solutions. The steady-state q_{ex} for the MODHMS CS also equals K_{sat} (Figure 3.4a) at high values of α due to an increase in

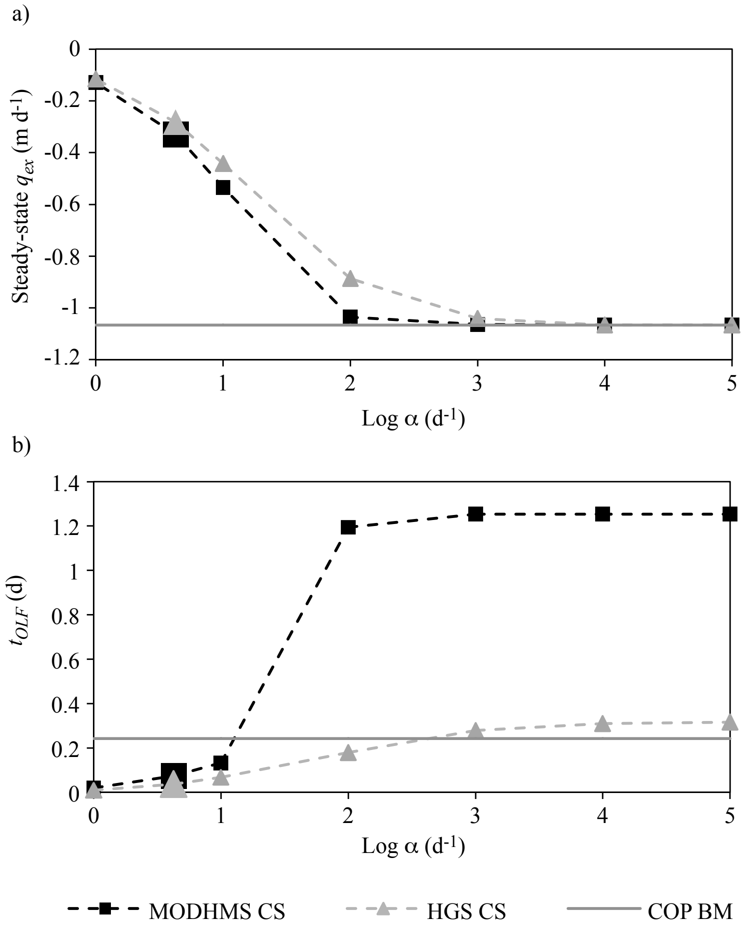

Figure 3.4 Relationship between log α and a) steady-state q_{ex}, and b) t_{OLF}. The enlarged markers show α values using $l_e = \Delta z/2$ for each of the MODHMS BC and HGS BC simulations.

the hydraulic gradient across the FOEC exchange interface – a significant improvement from the BC simulation (Figure 3.3a). However, increasing α does not allow accurate prediction of t_{OLF} in MODHMS (Figure 3.4b). The t_{OLF} at high values of α for the MODHMS CS simulations is approximately 1 d (418%) later than the mesh-centred FOEC and COP approaches. This is because h_{ss} must reach the land surface to saturate the uppermost cell, and in order for overland flow to occur. This process requires more time in block-centred codes given the distance between the uppermost subsurface node and the surface (i.e. the half-cell separation).

The q_{ex} and q_{OLF} results from the MODHMS TL1 and MODHMS TL0.01 simulations, where a single thin layer is introduced, are compared to the MODHMS BC and COP BM simulations in Figure 3.5. As the thickness of the uppermost layer is reduced in the otherwise coarsely discretised column (thereby also increasing α given that $l_e = \Delta z/2$), both the steady-state q_{ex} and t_{OLF} approach that of the COP BM. Despite the noticeable discrepancy in simulated steady-state q_{ex} and t_{OLF} with the TL1 simulation, the TL0.01 simulation approximates the COP BM very well, with an equivalent steady-state q_{ex} (= $-K_{sat}$) and a t_{OLF} 52 min (15%) later than the COP BM (Figure 3.5).

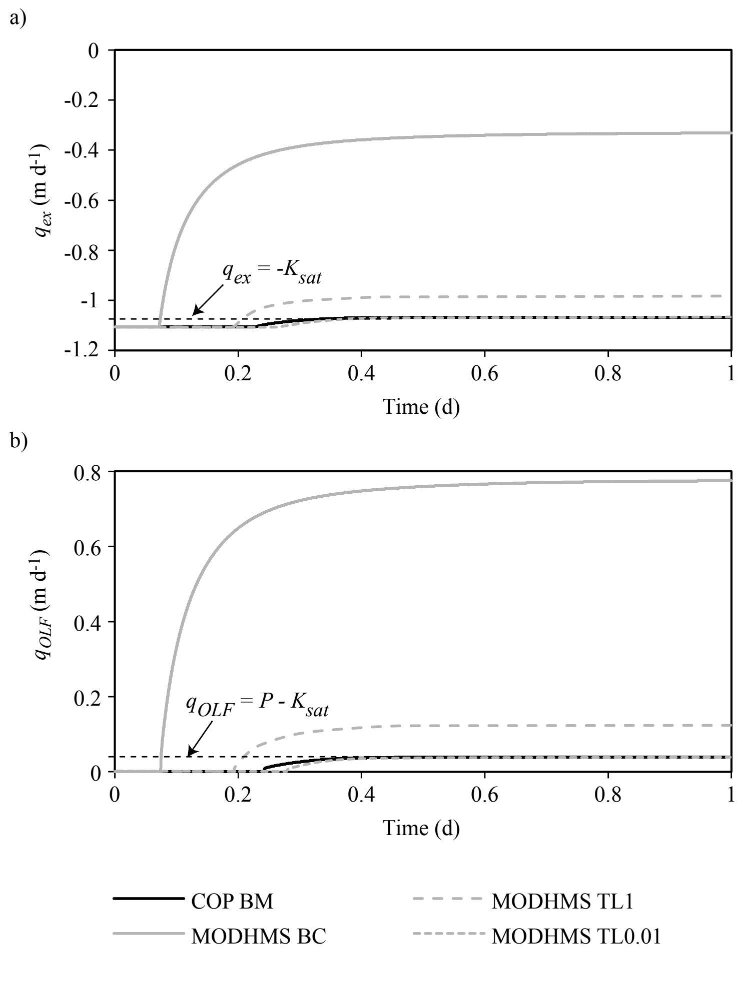

Figure 3.5 a) q_{ex} and b) q_{OLF} from the simulations that incorporate a single thin layer into the MODHMS BC simulation, compared to the COP BM simulation, for the first day of the 5-day simulation.

3.5 Discussion

The implementation of the FOEC approach requires careful consideration in block-centred codes. The inherent half-cell separation of the surface and uppermost subsurface nodes in block-centred codes causes a discrepancy between the saturation of the uppermost node (i.e. when $h_{ss} = z_{ss}$), and when h_{ss} intersects the land surface, which influences the initiation of overland flow. This issue must be considered when implementing the FOEC approach in block-centred codes that simulate coupled surface-subsurface flow. MODHMS accounts for this issue by: (1) formulating the FOEC approach such that it represents saturated flow through the top half of the uppermost subsurface cell (when $l_e = \Delta z/2$), and (2) by modifying the pressure-saturation relationship in the uppermost subsurface node so that saturation occurs concurrently with h_{ss} intersecting the land surface (i.e. at a pressure head of $\Delta z/2$; Figure 3.2). However, I demonstrate that such an approach may cause significant underestimation of steady-state q_{ex} and t_{OLF} given that the unsaturated hydraulic conductivity of the uppermost cell remains below K_{sat} until h_{ss} reaches the land surface, and the hydraulic gradient across the exchange interface falls below unity when $h_{ss} > z_{ss}$.

Chapter 3 shows that the introduction of a thin layer into the uppermost subsurface allows improved simulation of q_{ex} and t_{OLF} in a block-centred code. By bringing the uppermost subsurface node closer to the surface, and by subsequently increasing the value of α (i.e. via the suggested $l_e = \Delta z/2$), the block-centred approach essentially mimics the surface-subsurface nodal arrangement in mesh-centred codes. This minimises the effect of the gradient across the exchange interface falling below unity when $h_{ss} > z_{ss}$, and the unsaturated hydraulic conductivity in the uppermost cell remaining below K_{sat} until h_{ss} reaches the land surface. While it may seem intuitive that a thin layer will improve the simulation results in a block-centred code, this has not been discussed or quantified in the literature in the context of simulating integrated surface-subsurface interactions using the FOEC approach. This chapter has also shown that increasing the value of α independently of the model grid (Figure 3.4) allows for accurate capture of steady-state q_{ex}, but not t_{OLF} – further highlighting the need for a thin uppermost subsurface cell.

It is important to acknowledge that the addition of a thin layer does not provide a substitute for fine vertical grid resolution that is required throughout the subsurface for accurate simulation of unsaturated flow processes (e.g. Downer and Ogden, 2004). The use of a single thin layer merely allows for the block-centred solution to approximate that obtained using a mesh-centred model with an otherwise equivalent grid discretisation. Appropriate discretisation of underlying layers govern the accuracy of simulated unsaturated zone flow processes, such as propagation of wetting fronts, evapotranspiration, timing of recharge, and initiation of overland flow, etc. (e.g. Ross, 1990; Paniconi et al., 1991; van Dam and Feddes, 2000; Downer and Ogden, 2004; Kollet and Maxwell, 2006; Sulis et al., 2010). However, it was not the purpose of the current chapter to evaluate the grid dependency of unsaturated flow, but rather, the interdependency between FOEC parameters and uppermost cell thickness are characterised to provide guidance on the implementation of the FOEC approach in a block-centred code. Appropriate discretisation of underlying layers will be dependent on the scale and purpose of the study.

The requirement of a sufficiently fine thin layer at the surface applies also to more finely discretised models. Although the results are not shown here (for brevity), a simulation with a finely discretised column (i.e. 1 cm near the land surface increasing gradually up to 6.9 cm by a factor of 1.412 per cell) also required a very thin layer (0.01 cm) at the surface in order to achieve results similar to the mesh-centred approach. This finding illustrates that the benefits associated with the inclusion of a thin layer apply to both regional-scale (i.e. coarse) and local-scale (i.e. fine) grid discretisations. Importantly, the implementation of a single thin layer into the uppermost subsurface domain did not affect model run times significantly.

Although the rainfall conditions (rate and duration) used are unrealistic under natural conditions, they are used to illustrate the benefit of including the thin surface layer under Hortonian conditions. The issues regarding the formulation of the FOEC approach in the block-centred code and the pressure-saturation relationship in the uppermost cell are still present regardless of the material properties and the precipitation regime in the model. Moreover, the main findings are likely to apply also to simulation of other surface-subsurface interactions, such as saturation-excess overland flow, exfiltration, surface ponding conditions, etc. A brief analysis of non-Hortonian conditions (i.e. where rainfall rate is less than K_{sat}) also revealed that simulated q_{ex}, using a coarse uppermost cell thickness (i.e. 50 cm), was much smaller than expected (36% smaller than the COP method). The addition of a single thin layer improved the simulation of q_{ex} for this non-Hortonian scenario as well, and the simulated q_{ex} matched the COP results.

Other factors such as soil hydraulic properties (e.g. K_{sat} and van Genuchten parameters), rainfall rate, overland flow generation mechanism, horizontal grid dimensions, model dimensionality, etc, may also affect the thickness of the thin layer required to achieve accurate results with the block-centred code. It is suggested that future modelling studies should aim to undertake systematic sensitivity analyses that involve testing a series of at least three different thin uppermost layer thicknesses to ensure adequate convergence of the simulation results.

The challenges discussed in the current chapter involving the implementation of the FOEC approach in MODHMS extend to the application of any block-centred code that is capable of simulating integrated surface-subsurface flow. Alternative strategies for improving block-centred prediction of surface-subsurface interaction include implementing an additional subsurface node at the land surface (e.g. Kollet and Maxwell, 2006). With this arrangement, the implementation of the FOEC approach would be equivalent to the mesh-centred FOEC approach, with coincident surface and subsurface nodes (i.e. no dependence on the grid). As an example, the fully integrated code ParFlow adopts this grid structure (e.g. Kollet and Maxwell, 2006); however, it implements the COP approach and thus the single node at the land surface represents both the surface and uppermost subsurface node. Finally, Panday and Langevin (2012) presented a new package for MODFLOW showing how the concept of a “ghost node” can be used to better represent boundary features in block-centred finite-difference codes. However, this concept has only been applied to saturated conditions. It is possible that this method may also be adapted to aid in the simulation of surface-subsurface interactions in block-centred, variably saturated codes.

3.6 Conclusions

This work demonstrates some of the challenges in simulating the processes of infiltration and overland flow with the FOEC approach under Hortonian conditions in a block-centred code, where an inherent half-cell separation between the surface and uppermost subsurface nodes exists. This causes a discrepancy between saturation of the uppermost subsurface node, saturation of the uppermost subsurface cell, and the intersection of the subsurface head at the land surface, and this influences the simulation of both the exchange flux and time to initiate overland flow. MODHMS addresses this issue by: (1) using the FOEC approach to represent saturated flow through the top half of the uppermost subsurface cell (when $l_e = \Delta z/2$), and (2) modifying the pressure-saturation formulation in the uppermost layer so that saturation of the uppermost node occurs concurrently with the subsurface head reaching the land surface (in order for overland flow generation to occur when the subsurface head intersects the land surface). However, these methods still prevent the accurate simulation of infiltration and time to initiate overland flow.

With the conceptualisation of the FOEC approach that is adopted in MODHMS, the introduction of a single, thin layer at the land surface improves the predicted overland flow response. This occurs because the nodal arrangement is commensurate with that of a mesh-centred code, where the surface and uppermost subsurface node are coincident, thus ensuring that saturation of the uppermost subsurface node is concurrent with saturation of the uppermost subsurface cell and the head reaching the land surface. It is recommended that a sensitivity analysis be performed with at least three different thin layer thicknesses to evaluate the point at which the solution is not sensitive to changes in the uppermost layer thickness. The addition of a single thin layer does not provide a surrogate for fine vertical grid resolution throughout the subsurface, which is required for accurate simulation of unsaturated flow processes (Downer and Ogden, 2004). Rather, it allows accurate simulation of rainfall partitioning for a given grid discretisation. Chapter 3 has identified and quantified several challenges in implementing the FOEC approach in the simulation of surface-subsurface interactions, which are expected to occur in all block-centred codes. An awareness of both the issues and possible solutions outlined in this paper should be present in both the development and application of block-centred codes for fully integrated simulation of surface-subsurface interactions.

4. Fully integrated modelling of surface-subsurface solute transport and the effect of dispersion in tracer hydrograph separation

A version of this chapter is published as:

Liggett, J.E., Werner, A.D., Smerdon, B.D., Partington, D., Simmons, C.T., 2014 - Early View. Fully integrated modelling of surface-subsurface solute transport and the effect of dispersion in tracer hydrograph separation. Water Resour. Res., doi: 10.1002/2013WR015040

4.1 Introduction

Separating streamflow into its temporal and/or geographical origins can provide valuable information on catchment dynamics to aid in water resource planning. Tracer-based hydrograph separation has been widely used to identify the temporal streamflow components of event water from precipitation and pre-event water stored in the saturated or unsaturated zones (Genereux and Hooper, 1998; Jones et al., 2006). Applications of this method usually show that a large proportion of streamflow arising from a precipitation event consists of pre-event water, especially at early times (Buttle, 1994; McDonnell, 2003). The quick release of pre-event water after being stored long-term in a catchment has been called the 'rapid mobilization of old water paradox' by Kirchner (2003).

There have been a number of mechanisms proposed to explain the preponderance of large pre-event water contributions to streams, including capillary fringe groundwater ridging (e.g. Sklash and Farvolden, 1979; Abdul and Gillham, 1989), subsurface stormflow (e.g. Rodhe, 1981; Fiori and Russo, 2007), macropore flow (e.g. McDonnell, 1990; Park et al., 2011), and mixing between end-members (e.g. Chanat and Hornberger, 2003) due to such processes as bank storage and hydrodynamic dispersion (Jones et al., 2006; McCallum et al., 2010; Park et al., 2011). Investigating some of these mechanisms through numerical modelling, Jones et al. (2006) and Park et al. (2011) proposed that mixing from hydrodynamic dispersion, and in particular diffusion, can cause the large pre-event water contribution seen in tracer-based hydrograph separations. Hydrodynamic dispersion will be referred to herein simply as 'dispersion', which is comprised of the individual processes of (molecular) diffusion and mechanical dispersion. Jones et al. (2006) altered the dispersion parameters (dispersivity and diffusion coefficient) in both the surface and subsurface of their model, and compared the resulting pre-event water contribution from the tracer method to the hydraulic pre-event water contribution, as predicted by their integrated catchment model. They, and Sudicky et al. (2007), argued that dispersion results in an inflated value of pre-event water flux if the tracer-based results are interpreted as representative of hydraulically-driven flow to the stream. This is because the tracer flux arising from dispersion is not explicitly accounted for in the hydrograph separation (Jones et al., 2006). Following on from Jones et al. (2006), Park et al. (2011) used an analytical solution and numerical modelling to show that diffusion of event water from the surface into the subsurface can be quite large, and subsequently can cause an overestimation of pre-event contributions to stream flow. However, these studies do not discuss the differences between solute transport mechanisms occurring across the surface-subsurface interface versus those occurring in the subsurface (or surface) alone. As such, it is not clear whether dispersive processes within the subsurface or across the surface-subsurface interface induces stronger controls on pre-event tracer flux and the associated interpretation of the pre-event water contribution to streamflow.

The transfer of solutes between the surface and subsurface is an important topic in agriculture and watershed management, where the movement of pollutants from the soil zone to overland flow is a major concern (e.g. Sharpley et al., 2002). Shi et al. (2011) states that modelling surface-subsurface solute exchange is difficult due to an incomplete understanding of complex solute dynamics under rainfall-runoff conditions. Numerous conceptualizations of surface-subsurface solute transfer have been developed, and no single type has been shown to apply under all conditions (Sharpley et al., 2002; Shi et al., 2011; Barry et al., 2013). In developing a fully integrated hydrological code, VanderKwaak (1999) found that solute transport, and thus the tracer hydrograph separation result was sensitive to dispersion and the solute boundary condition applied at the surface-subsurface interface; however, he did not discuss the influence of subsurface dispersion parameters in his analysis.

This chapter demonstrates the effect of different conceptualizations for modelling solute transport across the surface-subsurface interface and implications for interpreting tracer-based hydrograph separation. I bring together the results of VanderKwaak (1999), Jones et al. (2006), and Park et al. (2011) by examining the process of dispersion both within the subsurface and across the surface-subsurface interface. The objectives are to: 1) quantify the relative effects of dispersion within the subsurface versus across the surface-subsurface interface on the pre-event tracer flux to stream and pre-event water interpretation, 2) demonstrate conditions when dispersion will impact tracer hydrograph separation results, and 3) discuss the implications of these findings for both modelling integrated surface-subsurface solute transport and the field application of tracer-based hydrograph separation methods. Simulations are performed using HydroGeoSphere (HGS) which is a fully integrated hydrological code that simultaneously solves surface and variably-saturated subsurface flow and transport (Therrien et al., 2009).

4.2 Background

The tracer-based hydrograph separation method is traditionally based on the combination of water and tracer mass balance equations. For a two-component hydrograph separation, the water and tracer balances, respectively, are:

$$Q_T = Q_p + Q_e \tag{4.1}$$

and

$$Q_T C_T = Q_p C_p + Q_e C_e \tag{4.2}$$

where Q [L^3T^{-1}] is the volumetric water flux in the stream and C [ML^{-3}] is the tracer concentration. The subscripts T, p, and e denote the total streamflow, pre-event and event components, respectively. Combining Equations 4.1 and 4.2, and rearranging yields:

$$Q_p = Q_T \frac{C_T - C_e}{C_p - C_e} \tag{4.3}$$

which is used to calculate the pre-event water contribution to stream flow. Alternately, Equations 4.1 and 4.2 can be combined to solve for the event water contribution to stream flow. In the field, Q_T and C_T are measured in the stream, and C_e and C_p are measured concentrations. In a numerical model, the tracer movement can be simulated taking into account both advective and dispersive components of solute transport, producing Q_T and C_T as a result.

Solute transport in a variably saturated porous matrix is often simulated using a form of the classical 3D advection-dispersion equation, where the dispersion is of the form described by Bear (1972) (Konikow, 2011). When modelling solute transport in the subsurface only, a boundary condition is required to represent land surface processes. However, in the case of a fully integrated code, solutes are transported between the surface and subsurface using functional relationships for the water and solute linkages between the two domains. In the field, the exchange of solutes between the surface and subsurface involves many different processes (Shi et al., 2011), and numerical codes vary in their conceptualisation and numerical implementation of surface-subsurface exchange relationships (Furman 2008; Shi et al., 2011; Chapter 3).

In HGS, the surface and subsurface domains are coupled by either a *shared-node* or a *dual-node* approach. For the *shared-node* approach, continuity of both hydraulic head and concentration between the surface and subsurface is assumed, and therefore, there is an instantaneous equilibrium between these domains (Therrien et al., 2009). Solute exchange between the surface and subsurface occurs via both advection and dispersion, with the dispersive flux governed by the subsurface transport parameters and equations. For the *dual-node* approach, surface-subsurface fluid exchange occurs in proportion to the head difference between coincident surface and subsurface nodes, and a first-order exchange coefficient (FOEC, or "conductance"). Some authors have conceptualised the FOEC approach as being representative of the geometry of an actual interface (e.g. Warren and Root, 1963; Gerke and van Genuchten, 1993), whilst others assert that the conductance is merely a lumped fitting/calibration parameter (e.g. Bencala, 1984; Kollet and Zlotnik, 2003; Mehl and Hill, 2010). Ebel et al. (2009) and Chapters 2 and 3 provide more broad discussions about the surface-subsurface interface in fully integrated codes. Regardless of the conceptualisation of the interface, appropriately chosen FOEC values (i.e. small values for the coupling length parameter in HGS) are required to preserve near-continuity of head and optimize model run times (Ebel et al., 2009; Chapter 2).

For solute transport using the dual-node approach, the mass flux between the surface and subsurface (F_{ex} [$ML^{-2}T^{-1}$], positive for solute movement from the subsurface to the surface), is a combination of the 1D advective (F_a [$ML^{-2}T^{-1}$]) and dispersive (F_d [$ML^{-2}T^{-1}$]) fluxes:

$$F_{ex} = F_a + F_d \tag{4.4}$$

where:

$$F_a = q_{ex}C \tag{4.5}$$

and:

$$F_d = -D\frac{\Delta C}{l_e} \tag{4.6}$$

For the advective term, q_{ex} [LT^{-1}] is the fluid exchange flux, negative for infiltration and positive for exfiltration, and C is either the concentration of solute at the surface node (C_s [ML^{-3}]) during infiltration or the concentration at the uppermost subsurface node (C_{ss} [ML^{-3}]) during exfiltration. For the dispersive term, ΔC is always C_s - C_{ss}, l_e is the coupling length [L] (also used in the determination of the fluid exchange flux, Chapters 2 and 3), and the dispersion coefficient (D [L^2T^{-1}]) is calculated based on Bear (1972) as:

$$D = \alpha_{ex}\left|q_{ex}\right| + n_e S_{ss}\tau D_d \tag{4.7}$$

In Equation 4.7, α_{ex} [L] is the dispersivity across the surface-subsurface interface (termed the "coupling dispersivity"), n_e [-] is the effective porosity of the porous media, S_{ss} [-] is the saturation of the uppermost node in the porous media, τ [-] is the tortuosity of the porous media, and D_d [L^2T^{-1}] is the diffusion coefficient. The first term on the right-hand side of Equation 4.7 represents the coefficient of mechanical dispersion (D_m [L^2T^{-1}]), while the second term is the effective diffusion coefficient (D^* [L^2T^{-1}]).

The implementation of solute transport across the surface-subsurface interface by Equations 4.4 and 4.7 provides flexibility where multiple levels of dispersion can be included (or excluded) in the solute exchange. This flexibility allows us to examine the influence of different solute transport processes on the internal dynamics of a catchment. First, dispersion can be neglected entirely, with mass flux between the surface and subsurface via advection only (Equation 4.5). Secondly, diffusion (α_{ex} = 0) and mechanical dispersion ($\alpha_{ex} > 0$) can be included in addition to advection. However, there is a lack of guidance on choosing an appropriate value of α_{ex}, and VanderKwaak (1999) described it as being useful as a calibration parameter.

4.3 Methods

Two hypothetical 2D hillslopes, shown in Figure 4.1, are used to examine the effects of advection, diffusion, and mechanical dispersion on the apparent pre-event water contribution to the streamflow. Previous studies have suggested that high water tables and associated groundwater ridging (i.e. due to capillary fringe interception with the land surface) may be responsible for contributing large amounts of pre-event water to streamflow (e.g. Sklash and Farvolden, 1979; Cloke et al., 2006; Park et al., 2011). Hence, two alternative hillslope geometries are considered, which provide contrasting interactions of the water table with the land surface. In one case, the

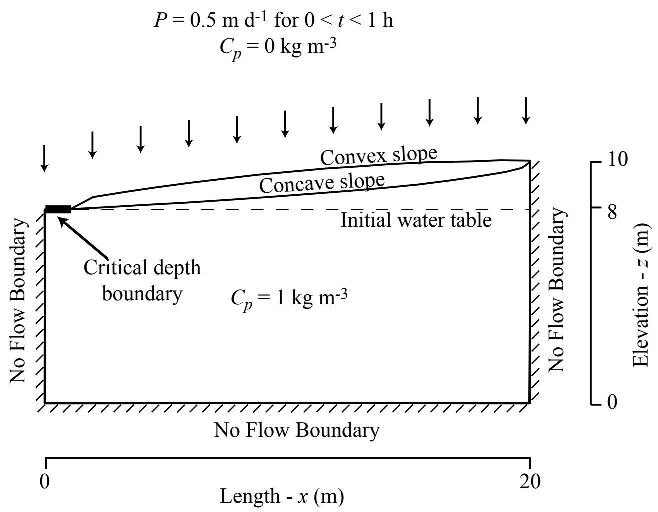

Figure 4.1 2D model dimensions, boundary conditions, and initial conditions for both hypothetical hillslopes (convex and concave). The domain is a unit width (i.e. 1m).

slope is concave (Figure 4.1), following the characteristic profile presented by Kirkby (1971) where m = 2 and n = 2 (Equation 24 in Kirkby, 1971). In the other case, the slope is convex (Figure 4.1), with m = 0 and n = 1, and the stream is incised by 0.5 m over a 1-m wide stream bank.

Both model domains are bounded by no-flow boundaries on the bottom and sides, and by a critical-depth boundary at the surface along a 1-m wide streambed that allows water to flow out of the model domain representing the total discharge to the stream (Figure 4.1). The surface-subsurface solute exchange under hillslope conditions as opposed to underneath surface water bodies is examined, hence, no downstream flow (i.e. in the y-direction) was considered. Additionally, the 1-m wide streambed was included to reduce boundary effects at the stream edge. The small domain relative to real-world systems is intended to represent near-stream processes.

The initial heads were determined by running each hillslope model to steady state under a constant precipitation rate of 1 mm yr^{-1}, which results in a water table ranging from an elevation of 8 m above the bottom of the model at the stream outlet to approximately 8.04 m at x = 20 m for both hillslopes. The soil is homogeneous and isotropic, and hydraulic properties are from Carsel and Parrish (1988), representing a sandy loam (Table 4.1). Other parameters used in the models are shown in Table 4.1. A value of 10^{-4} m is used for l_e throughout the entire model domain. This value was chosen based on the results of Ebel et al. (2009) and Chapter 2, which found that large values of l_e can inhibit surface-subsurface fluid flux and timing of initiation of overland flow, whereas small values of l_e promote continuity of pressure between the surface and subsurface.

Table 4.1 Model parameters

Parameter	All simulations			
Effective porosity (n_e)	0.41			
Saturated hydraulic conductivity	1.0608 m d^{-1}			
van Genuchten α	7.5 m^{-1}			
van Genuchten β	1.89			
Residual water content	0.159			
Specific Storage	1.0x10^{-4} m^{-1}			
Tortuosity (τ)	1			
Coupling length (l_e)	1x10^{-4} m			
Manning's n	0.05 s m$^{-1/3}$			
Microtopography (rill storage) height	1x10^{-4} m			
Longitudinal dispersivity (surface)	0.1 m			
	Subsurface dispersion simulations			
	Very low	**Low**	**Intermediate**	**High**
Longitudinal dispersivity (α_L)	0.1 m	0.1 m	1 m	10 m
Transverse dispersivity (α_T)	0.01 m	0.01 m	0.1 m	1.0 m
Coupling dispersivity (α_{ex})	0.01 m	0.01 m	0.1 m	1.0 m
Diffusion coefficient (D_d)	10^{-10} m^2 s^{-1}	10^{-9} m^2 s^{-1}	10^{-9} m^2 s^{-1}	10^{-9} m^2 s^{-1}

The pre-event water was represented by a tracer that is present in the subsurface with a unit concentration of 1 kg m^{-3} at the beginning of each scenario. Precipitation at the surface has a pre-event water tracer concentration of 0 kg m^{-3}. The model domains are very finely discretised to resolve sharp concentration gradients between event and pre-event water. Grid spacing is similar to Jones et al. (2006) and is 0.04 m along the length of the models, and between 0.019 and 0.025 m vertically (400 layers). The influence of the grid resolution on surface-subsurface solute transport is discussed further in Chapter 4.5.2.

Three different surface-subsurface transport conditions are applied to the models, each with four contrasting magnitudes of subsurface dispersion, for a total of twelve solute transport scenarios. Each of the twelve scenarios is performed using both hillslope geometries, resulting in 24 unique simulations. The first surface-subsurface transport condition (AO) considers only advective solute exchange between the surface and subsurface. The second condition (A+Diff) includes advection with diffusion (i.e. α_{ex} = 0 in Equation 4.7), and the third condition (A+Disp) includes advection with diffusion and mechanical dispersion. For each of the three surface-subsurface transport conditions, four simulations were performed with varying dispersion parameters in the porous medium (Table 4.1).

The values of longitudinal dispersivity (α_L [L], Table 4.1) were selected based on the results of Gelhar et al. (1992) for flowpaths corresponding to the length scale of the model domain. Values of transverse dispersivity (α_T [L]) are an order of magnitude smaller than α_L. There is no guidance on appropriate values of α_{ex}, and it is assigned a value an order of magnitude less than α_L in order to reflect the smaller length scale associated with the surface-subsurface interface. Additionally, preliminary modelling showed that this value promoted continuity of concentration between the surface and uppermost subsurface nodes, similar to the shared-node approach. Chapter 4.5.1

discusses the influence of α_{ex} on the simulation results. In all cases, the grid Péclet number (Anderson and Woessner, 2002) remains below 1 in order to reduce numerical oscillations in the simulations.

HGS was run in finite-difference mode using the dual-node approach for coupling the surface and subsurface. Adaptive time steps were used with a maximum time step of 0.05 d, which maintains a Courant number below 1. Each simulation is run for 4 d with precipitation applied to the land surface for the first hour, at a rate of 0.5 m d^{-1} (2.1 cm h^{-1}). This precipitation rate is less than the saturated hydraulic conductivity of the subsurface (i.e. Dunne conditions), meaning that no overland flow will occur unless by saturation excess. A set of 12 additional simulations under Hortonian conditions were also performed for the convex hillslope. These had a rainfall rate of 1.1 m d^{-1} and used each of the three surface-subsurface transport conditions and four subsurface dispersion parameters. Results of these simulations are discussed at the end of Chapter 4.5.1.

The tracer-based Q_p to the stream is an interpreted value, determined by applying Equation 4.3 with the simulated Q_T and C_T values (i.e. coming out of the model domain via the critical-depth nodes). There is an implicit assumption in this method that all tracer flux is via an (advective) fluid flux (McCallum et al., 2010). In this chapter, because C_e = 0 and C_p = 1, the simulated mass flux of pre-event tracer into the stream is equivalent to the tracer-based Q_p. In order to evaluate the tracer-based Q_p, the pre-event water, driven by hydraulic gradients in both the surface and subsurface (i.e. the hydraulic Q_p), must be quantified. Achieving this, even with modern fully integrated codes, is surprisingly difficult (Partington et al., 2011; Guay et al., 2013). For example, Renaud et al. (2007) argued that pre-event water that discharged to the hillslope was not accounted for in the method used by Jones et al. (2006) to determine the hydraulic pre-event water contribution to streamflow.

The hydraulic Q_p can be quantified using the hydraulic mixing cell (HMC) method, which explicitly tracks the delivery mechanism of water to the stream on a cell-by-cell basis in HGS (Partington et al., 2011, 2013). It also accounts for the time lags between rainfall and exfiltration on the hillslope, and arrival at the stream (Partington et al., 2011, 2013). The HMC method tracks water that enters the stream via: 1) direct rainfall, 2) overland flow from rainfall on the hillslope, 3) subsurface discharge (directly to the stream), and 4) overland flow from exfiltration to the hillslope (i.e. subsurface water indirectly discharged to the stream). The HMC method does not differentiate between water in the saturated and unsaturated zones; therefore, the term 'subsurface water' is used in this manuscript to represent all water within the porous media domain.

By summing the HMC components of subsurface discharge directly to the stream and the exfiltration to the hillslope that enters the stream, the total hydraulic Q_p is obtained However, the HMC method tracks the delivery mechanism to the stream, rather than the temporal (i.e. event and pre-event) contribution, so in this chapter I must assume that subsurface water only consists of pre-event water. This will produce a maximum hydraulic Q_p, because some subsurface water delivered to the stream is likely comprised of infiltrated event water, and this is not tracked by the HMC method.

4.4 Results

4.4.1 Hydraulic Response

The hour-long rainfall event produces different hydraulic responses and stream discharge hydrographs for each hillslope (Figure 4.2). For the convex hillslope, a

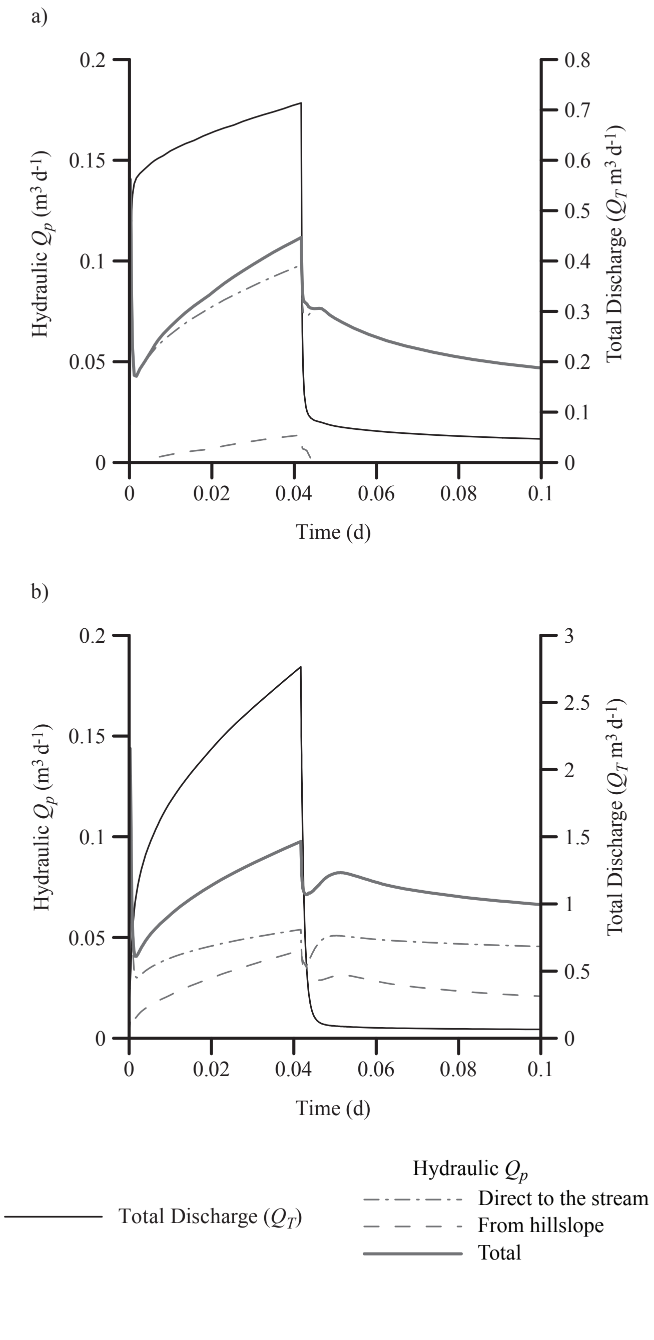

Figure 4.2 Q_T and hydraulic Q_p (HMC method) for the a) convex and b) concave hillslopes.

small groundwater ridge develops near the stream, but the water table remains relatively deep throughout the simulation and does not intersect the ground surface. Subsurface water discharges directly to the stream and exfiltrates along the stream bank only in the immediate vicinity of the stream (15 cm from the stream). For the concave hillslope, a much larger groundwater ridge develops and the water table reaches the surface across nearly 30% (6 m) of the hillslope. Exfiltration of subsurface water to the hillslope occurs up to 1.5 m away from the stream. The high water table leads to more saturation-excess overland flow relative to the convex hillslope, and consequently, discharge to the stream is greater (Figure 4.2). For the concave hillslope, the total discharge volume over the duration of the rainfall period is 0.87 m^3, compared to 0.027 m^3 for the convex hillslope.

For the convex hillslope, the (hydraulic) pre-event water contribution to the stream using the HMC method is 13% of the total discharge volume over the duration of the rainfall period. Most of the hydraulic pre-event water contribution is discharged directly to the stream, rather than exfiltrated to the hillslope (Figure 4.2a). The remaining stream discharge is comprised of rainfall onto the stream (78%) and overland flow from rainfall on saturated areas (9%). For the concave hillslope, the hydraulic pre-event water contribution to the stream is only 4% of the total discharge volume during the rainfall period. However, the hydraulic pre-event water contribution is more evenly split between discharge directly to the stream and exfiltration to the hillslope (Figure 4.2b). The remaining stream discharge in the concave hillslope is comprised mostly of rainfall entering the stream via overland flow (72%) rather than falling directly on the stream (24%). The hydraulic pre-event water contribution to the stream, determined from the HMC approach, does not change when solute transport parameters such as dispersivities are modified, as expected.

4.4.2 Dispersion at the surface-subsurface interface

Figure 4.3 shows the Q_p interpreted from the tracer hydrograph separation method for all 12 simulations and for each hillslope. These results show that with the AO condition, the tracer-based Q_p is very similar to the hydraulic Q_p (Figure 4.3), despite varying amounts of subsurface dispersion; however, including dispersion across the surface-subsurface interface results in a significantly higher tracer-based Q_p, compared to the hydraulic Q_p, for both hillslopes. As an example, for the convex hillslope with the AO transport condition and intermediate subsurface dispersion (Figure 4.3a), the tracer-based pre-event water contribution is 12% of the total volume discharged from the stream over the duration of the rainfall period, very similar to the hydraulic pre-event water discharge of 13%. However, the tracer-based pre-event water contribution is 38% and 65% of the total volume discharged during the rainfall period for the A+Diff and A+Disp conditions, respectively. The sensitivity of the simulations to changes in subsurface dispersion parameters is presented in Chapter 4.4.3.

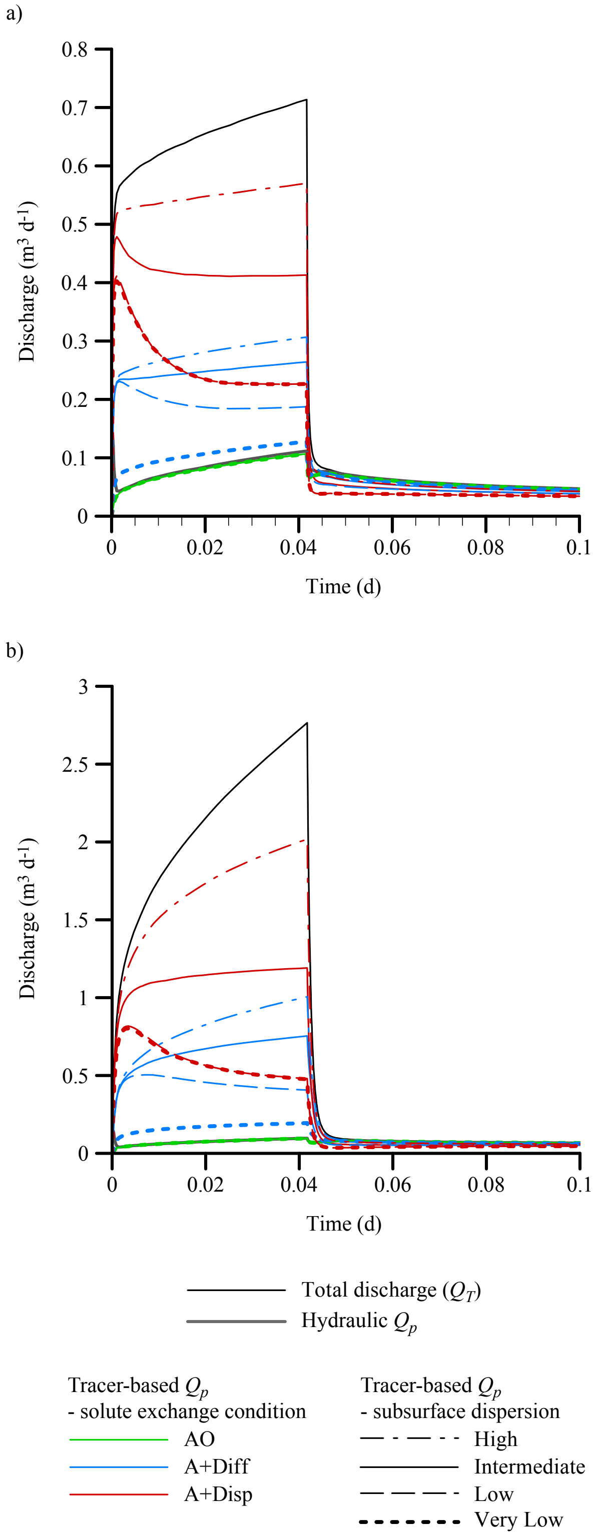

Figure 4.3 Tracer-based Q_p, hydraulic Q_p, and Q_T for each surface-subsurface transport condition and level of subsurface dispersion for both the a) convex and b) concave hillslopes. Note that the tracer-based Q_p under the AO condition (for all levels of subsurface dispersion) plot on top of one another as well as the hydraulic Q_p.

Figures 4.4a and 4.5a show the pre-event tracer F_{ex} along the lower portion of the hillslopes, where discharge occurs, at the end of the 1 h rainfall period for each surface-subsurface transport condition with intermediate subsurface dispersion. The subsurface hydraulic head and the water table are also shown for the corresponding portions of the hillslopes (Figures 4.4b and 4.5b), illustrating the groundwater ridges. For both hillslopes, pre-event tracer F_{ex} only occurs in the lower reaches of the hillslope, where the water table is at or near the surface (Figures 4.4 and 4.5). In the convex hillslope, this means that F_{ex} is restricted to the streambed and lower portion of the stream bank (Figure 4.4a), whereas in the concave hillslope, F_{ex} occurs much further up the hillslope, corresponding with the higher water table (Figure 4.5b).

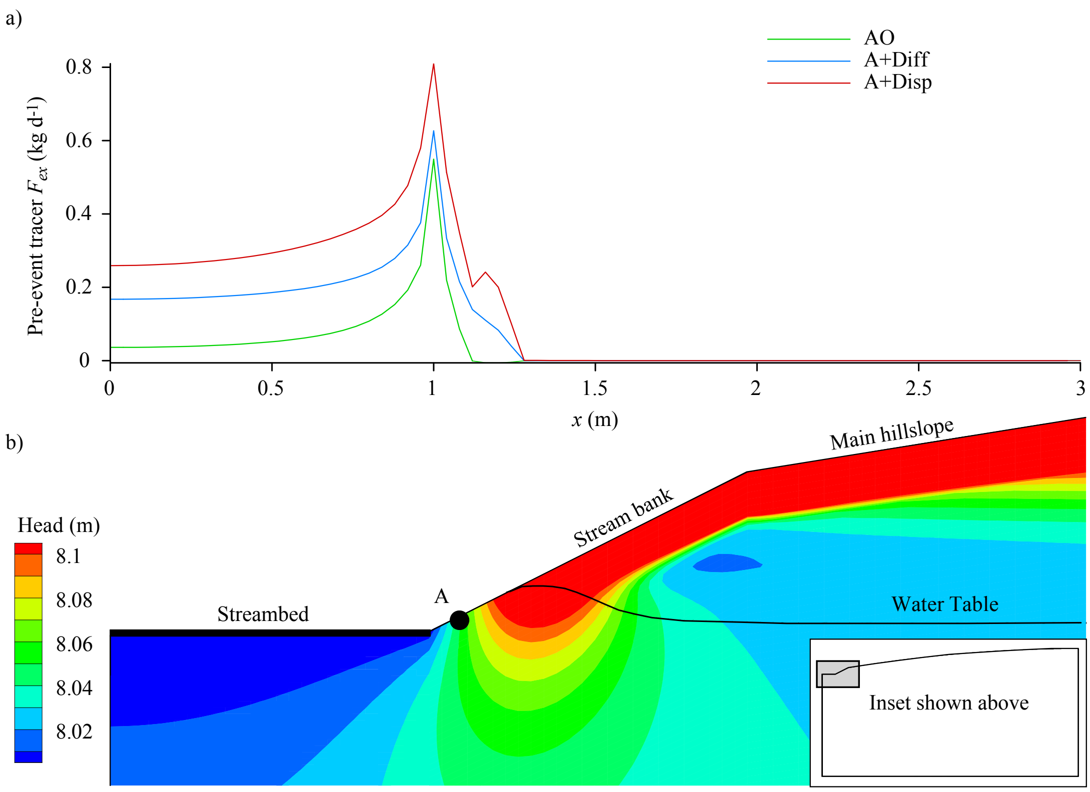

Figure 4.4 a) Pre-event tracer F_{ex} at the end of the rainfall period for each surface-subsurface transport condition along the bottom 3 m of the convex hillslope under intermediate subsurface dispersion, and b) corresponding subsurface head and water table. Note that the horizontal scale is the same for both a) and b), and there is no vertical exaggeration.

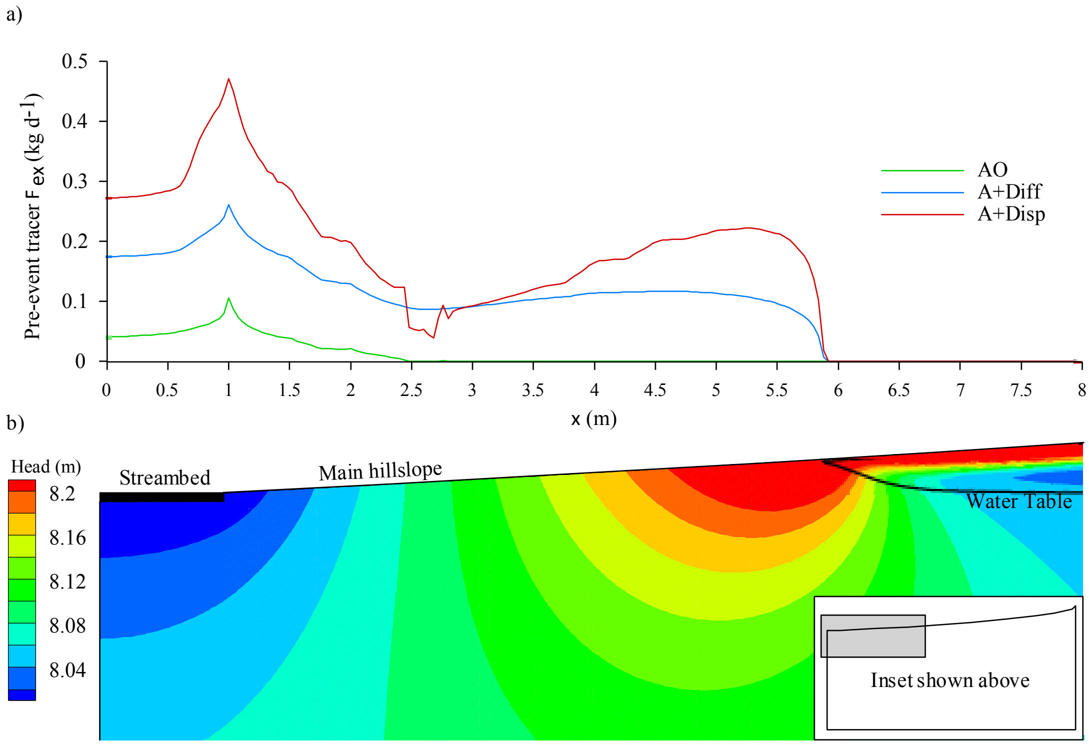

Figure 4.5 a) Pre-event tracer F_{ex} at the end of the rainfall period for each surface-subsurface transport condition along the bottom 8 m of the concave hillslope under intermediate subsurface dispersion, and b) corresponding subsurface head and water table. Note that the horizontal scale is the same for both a) and b), and there is no vertical exaggeration.

For both hillslopes, pre-event tracer F_{ex} is directly proportional to q_{ex} under the AO condition, and discharges to the surface only where exfiltration occurs, as expected (Figures 4.4a and 4.5a). The pre-event tracer F_{ex} increases when diffusion and mechanical dispersion are included across the surface-subsurface interface (Figures 4.4a and 4.5a). Additionally, tracer discharge is observed higher upslope than with the AO condition (Figures 4.4a and 4.5a), especially in the concave hillslope where tracer discharge occurs approximately 3.5 m further upslope of the AO tracer discharge. In these areas, tracer discharge occurs despite infiltration, because the pre-event tracer concentration gradient is from the subsurface to the surface, and the resulting dispersion is greater than infiltration/advection. The depression in F_{ex} for the A+Disp simulation at x = 2.5 m is at the transition between portions of the hillslope undergoing exfiltration and infiltration, where q_{ex} is near zero and diffusion is the only contributor to dispersion.

To further examine the dominant solute transport processes occurring during the simulations, Figure 4.6 shows the fluid and tracer fluxes with time across the surface-subsurface interface at Point A along the stream bank of the convex hillslope (see Figure 4.4b). Results are shown for each surface-subsurface transport condition and with intermediate subsurface dispersion. Four states of advective and dispersive fluxes are identified. At the beginning of the rainfall event (State I), water infiltrates into the unsaturated subsurface at a rate equal to that of precipitation (Figure 4.6a). For the AO condition, there is no net flux of pre-event tracer across the surface-subsurface interface (Figure 4.6d) because there is no pre-event tracer in the surface domain to be advected into the subsurface with infiltrating water. For the A+Diff and A+Disp conditions, pre-event tracer F_d occurs from the subsurface to the surface (Figure 4.6c) due to the direction of the concentration gradient, which is maintained throughout the rainfall event by dilution of exfiltrated subsurface water from precipitation and overland flow. However, pre-event tracer F_d to the surface is offset by F_a back into the subsurface, making F_{ex} almost equal to zero (Figures 4.6b,c,d). At about 0.004 d (State II) the subsurface saturates and infiltration begins to decrease (Figure 4.6a). Again, for the AO simulation there is very little pre-event tracer F_{ex} (Figure 4.6d). For the A+Diff and A+Disp conditions, F_{ex} is from the subsurface to surface (Figure 4.6d), due to the reduced infiltration rate and associated advective flux (Figure 4.6b, c).

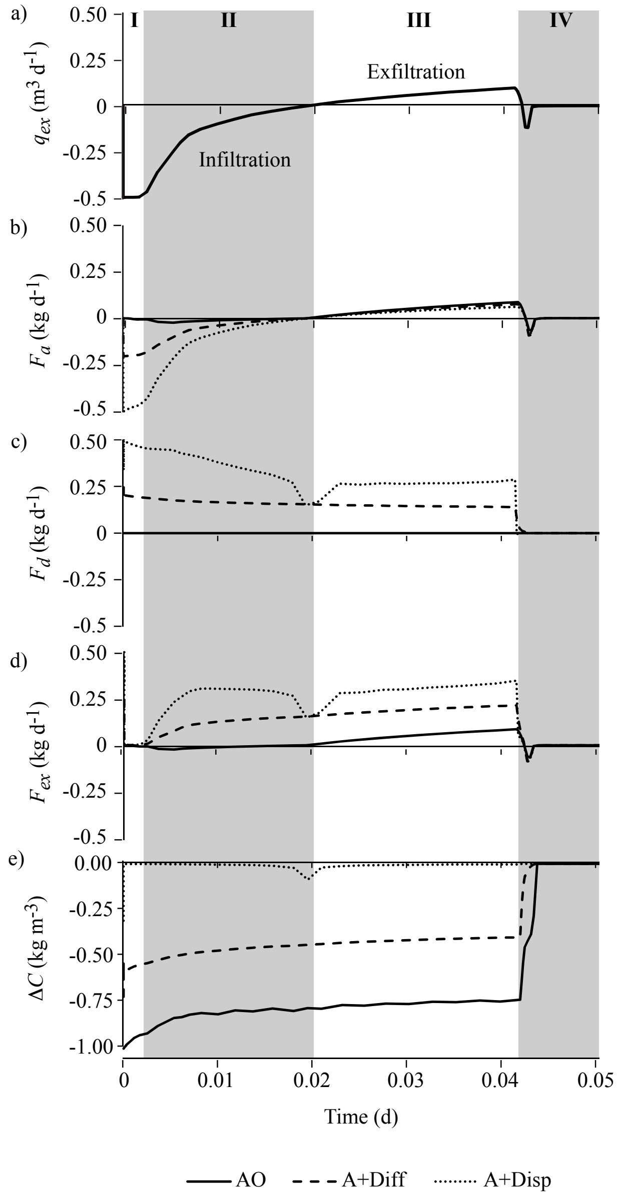

Figure 4.6 Surface-subsurface fluxes for each surface-subsurface transport condition, with intermediate subsurface dispersion, at Point A on the convex hillslope (Figure 4.4). a) fluid flux, b) advective pre-event tracer flux, c) dispersive pre-event tracer flux, d) net surface-subsurface pre-event tracer flux, and e) concentration difference between the surface and uppermost subsurface nodes.

At approximately 0.02 d, exfiltration begins (State III) and F_{ex} is increasingly from the subsurface to the surface for the AO condition (Figure 4.6b, d). At this time, F_d and F_a are both towards the surface under the A+Diff and A+Disp conditions (Figure 4.6b, c), and F_{ex} continues to increase (Figure 4.6d). The decrease in F_d for the

A+Disp condition at the transition between States II and III (where a shift from infiltration to exfiltration occurs) is due to the mechanical dispersion tending to zero (Equation 4.7), temporarily leaving diffusion as the only contributor to F_d. With the cessation of rainfall after 1 h (State IV), F_{ex} quickly reduces to near zero for all simulations as the system recovers. The groundwater ridge and subsurface head decline, the near surface becomes unsaturated, and there is little fluid exchange. The short period of infiltration immediately following the cessation of the rainfall is caused by the redistribution and infiltration of ponded water in the surface domain, a combination of precipitation and exfiltrated subsurface water, as the subsurface heads rapidly decline. The states shown in Figure 4.6 can occur across the extent of the model domain and are variable in time and space. For example, whilst Point A in Figure 4.4 undergoes all four states during the simulation period, the upper reaches of the hillslope only experience conditions reflective of States I and IV during the simulation. Similar states also apply if solute exchange is examined from the perspective of the event-water tracer, however the directions are reversed and the concentration gradient between the surface and subsurface is reduced over time as event water infiltrates into the subsurface.

The pre-event tracer F_d (Figure 4.6c) is driven by different mechanisms between the A+Diff and A+Disp transport conditions. Figure 4.6e shows the concentration difference across the surface-subsurface interface (i.e. ΔC in Equation 4.6). Firstly, under the AO transport condition there is a large ΔC throughout the rainfall event, as the pre-event tracer flux is driven by advection alone. With the addition of diffusion across the interface (i.e. A+Diff condition) F_d is driven by the large ΔC, resulting in a large amount of diffusion across the interface (Figure 4.6c). The increased mass flux from diffusion results in a lower ΔC than in the AO condition throughout the rainfall event (Figure 4.6e). Under the A+Disp transport condition, mechanical dispersion dominates the F_d, and there is near-continuity of concentration between the surface and uppermost subsurface nodes (i.e. a high D_m but a very low ΔC, Figure 4.6e).

4.4.3 Dispersion in the subsurface

Altering the dispersion parameters within the subsurface has very little effect on the tracer-based Q_p when dispersion across the surface-subsurface interface does not occur (i.e. the AO condition, Figure 4.3). Table 4.2 shows that the differences in pre-event water volume discharged to the stream, as interpreted from the tracer-based hydrograph separation during the rainfall period, are very small when the subsurface dispersion parameters are altered under the AO condition. This is the case for both hillslopes despite the differences in water table distributions, groundwater ridging, and mixing of event and pre-event water.

Table 4.2 Volumetric pre-event water delivered to the stream, as interpreted from the tracer-based hydrograph separation, during the rainfall period for the AO condition.

Subsurface dispersion	Convex Hillslope (L)	Concave Hillslope (L)
High	3.288	3.056
Intermediate	3.292	3.053
Low	3.292	3.045
Very low	3.295	3.045

The pre-event tracer concentrations in the concave hillslope are shown in Figure 4.7 for all 12 simulations, and at the end of the rainfall event. In the case of the AO condition, increasing the subsurface dispersion results in greater mixing of pre-event water in the lower portion of the hillslope, as expected, which can lead to either an increase and decrease in pre-event tracer concentration discharge to stream

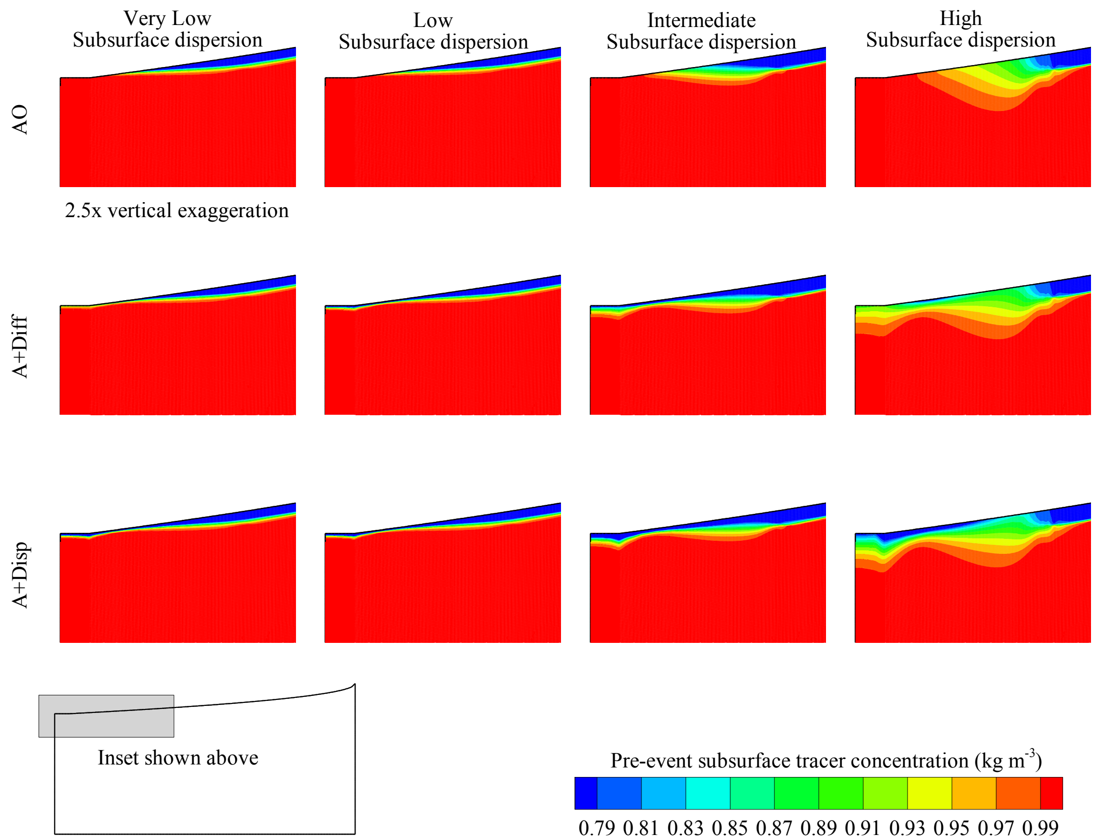

Figure 4.7 Pre-event water tracer concentrations near the stream for the concave hillslope at the end of the rainfall event.

depending on the location and time. However, the variation in subsurface pre-event tracer concentration due to increased subsurface dispersion (Figure 4.7) is subtle enough not to significantly alter F_{ex} (Table 4.2). Therefore, there is very little difference in the amount of pre-event tracer delivered to the stream. On the other hand, tracer-based Q_p is greatly affected by subsurface dispersion parameters when dispersion is considered across the surface-subsurface interface (i.e. A+Diff and A+Disp conditions, Figure 4.3). In the A+Diff and A+Disp simulations, increased mixing in the subsurface (Figure 4.7) increases F_{ex}, resulting in the decrease in pre-event tracer concentration seen in the near-surface in Figure 4.7.

Figures 4.3, 4.7, and Table 4.2 show very little difference in the results between the very low and low subsurface dispersion scenarios (where D_d is altered) under the AO condition. This result shows that diffusion within the subsurface is not significant for either hillslope. The reason for the large difference in the very low and low subsurface dispersion simulations under the A+Diff transport condition (Figure 4.3) is that, as described in Chapter 4.4.2, it is the large ΔC that drives the diffusion across the surface-subsurface interface under this transport condition. Therefore, since D_d is included in Equation 4.7, decreasing it results in the substantial decrease in diffusion across the interface (and thus F_{ex} and tracer-based Q_p) under the A+Diff transport condition seen in Figure 4.3. For the A+Disp transport condition, Figure 4.3 shows that reducing the D_d has practically no impact on the tracer-based Q_p because mechanical dispersion across the interface dominates over the diffusive flux (Figure 4.6c).

4.5 Discussion

4.5.1 Modelling surface-subsurface solute exchange

This work highlights the importance of carefully considering the solute transport mechanisms across the surface-subsurface interface when modelling and interpreting solute transport in catchments. The net effect of the solute transport mechanism across the surface-subsurface interface will be especially significant in the dynamic hydrologic environment near streams, where high concentration gradients, high water tables, and fluctuating flow fields are present. There is no consensus or guidance on which surface-subsurface solute transport condition is most appropriate for modelling the movement of solutes in an integrated manner, and it will likely depend on the conceptual model of the area of interest, purpose of the modelling, and time and scale of the problem. However, this work demonstrates a range of possibilities for diffusive and dispersive conditions at the surface-subsurface interface, and their effects on the simulation of solute transport and tracer-hydrograph interpretation.

Simulations under the AO condition produce the minimum amount of F_{ex} (Figures 4.4 to 4.6) and is similar to having a Cauchy solute boundary at the surface-subsurface interface, where mass enters either domain at a rate equal to the fluid flux at a given concentration. However, in a fully integrated code, the fluid flux varies throughout the simulation and concentration is dependent on the concentration of the source domain (e.g. the subsurface for exfiltration and the surface for infiltration), which can also vary in time and space. Simulations under the A+Disp condition (and large α_{ex}) produce the maximum amount of F_{ex} (Figures 4.4 to 4.6), promote continuity of concentration (as with the shared-node coupling approach), and are similar to imposing a constant concentration boundary at the interface. While constant concentration boundaries can result in unrealistic mass movement (Batu and van Genuchten 1990), with the fully integrated code the mass exchanged between domains at a particular time is limited by total mass conservation within the model. The A+Diff condition results in an intermediate amount of F_{ex} (Figures 4.4 to 4.6), driven by the discontinuity of concentration between the surface and uppermost subsurface nodes (i.e. high ΔC). Results from the A+Disp condition converge on the A+Diff case as a_{ex} approaches zero, as expected given Equation 4.7 and confirmed with both the hillslope and 1D column models (results not shown for brevity). Small values of l_e, whilst inducing a large concentration gradient, promote continuity of concentration (i.e. small ΔC) as solute moves between the surface and subsurface, which results from the relationship between F_d, C_s, C_{ss}, and l_e (Equation 4.6). As l_e is increased independently of any other parameters, results from the A+Diff and A+Disp conditions approach those from the AO condition. However, this promotes discontinuity of both solute concentration and hydraulic head, and may significantly change the flow solution if l_e is too high.

Modelling mechanical dispersion across the surface-subsurface interface presents a conceptual challenge with regards to the direction of F_d under conditions of exfiltration and infiltration. As shown in Figure 4.6c, including dispersion across the interface results in a large F_d of pre-event tracer that is always from the subsurface to the surface, despite the occurrence of infiltration in Stages I and II. This seems reasonable for the A+Diff condition, where diffusion is fundamentally driven by a concentration gradient; however, it seems odd that F_d is even larger for the A+Disp condition, given that q_{ex} is into the subsurface. Konikow (2011) recognises this issue as "upstream dispersion", which results because the classical advection-dispersion equation assumes mechanical dispersion, conceptually described as being due to velocity variations, is proportional to the concentration gradient. Additionally, the direction of velocity is not accounted for in the determination of D - the absolute value is used (e.g. Equation 4.7). The consequences of upstream dispersion have been recognised in modelling contaminant movement (e.g. Liu et al., 2004). In modelling integrated surface-subsurface solute transport the consequences of upstream dispersion can be prominent. Even with the shared-node approach in HGS, which eliminates the exchange interface and need for Equation 4.7, upstream dispersion still occurs (results not shown for brevity).

In practice, the surface-subsurface transport condition (i.e. AO, A+Diff, A+Disp) and solute coupling parameters (e.g. α_{ex}) are likely to be calibration parameters. For example, VanderKwaak (1999) found that adjustments to α_{ex} could replicate the results of the Abdul and Gillham (1984) lab experiment of capillary fringe groundwater ridging. Additionally, there may be the influence of other processes known to affect subsurface to surface solute exchange, such as ejection by raindrop impact, erosion, and adsorption/desorption (Shi et al., 2011) which α_{ex} may be able to account for. Future studies could also include the influence of scale, dimensionality (i.e. 2D versus 3D), multiple rainfall events, poorly mixed initial tracer concentrations, and heterogeneity in the subsurface. The additional set of simulations under Hortonian rainfall conditions had different quantities of Q_T, hydraulic and tracer-based Q_p, etc., reflecting the greater rainfall rate. However, these simulations showed similar responses to the surface-subsurface transport condition and subsurface dispersivities as described in this manuscript (e.g. greater tracer-based Q_p with A+Diff and A+Disp scenarios).

4.5.2 Tracer hydrograph interpretation

The results of Chapter 4 explicitly demonstrate the difference between advective-dispersive solute transport across the surface-subsurface interface compared to within the subsurface. Although the best approach to model solute transport across the surface-subsurface interface is not known, the results show that there is a possibility for dispersion within the subsurface to have little impact on the tracer-based Q_p, over the course of a single rainfall event (e.g. under the AO condition). Including dispersion across the surface-subsurface interface significantly alters the amount of pre-event tracer exiting the subsurface system. This large dispersive flux across the interface causes an increase in C_T in the stream, which is then interpreted as a large Q_p using Equation 4.3. While there may indeed be a dispersive component of pre-event water entering a stream, as pointed out by Renaud et al. (2007), attributing the dispersive flux entering a stream to an advective flux leads to an inflated interpretation of Q_p hydraulically contributed to a stream. This is because the assumption implicit in Equations 4.2 and 4.3 of mass flux via advection only is violated (Jones et al., 2006). Misinterpretation of Q_p may subsequently result in errors in determining near-stream hydraulic properties that rely on a Darcian value of subsurface flow.

While subsurface dispersion alone is probably unlikely to impact the tracer-based Q_p over a single rainfall event, it is expected to impact the hydrograph separation over longer timeframes and successive rainfall events by affecting the distribution of pre-event water concentrations in the subsurface and pre-event water end-member (i.e. C_p). For example, McCallum et al. (2010) modeled the subsurface mixing of stream water and regional groundwater due to bank storage. They found that the tracer-based hydrograph interpretation of 'groundwater' flux into the stream is affected by the location where the end-member concentration is measured: either from the stream at low flows (previously mixed groundwater and river water), or from the regional groundwater. Further study is needed into the role of subsurface dispersion on tracer-based Q_p in the case where the pre-event tracer is not well mixed prior to the rainfall event.

It can be difficult to separate modelling results that are a by-product of the numerical model itself from those that are representative of real-life physical processes, especially when using fully integrated models to help develop a conceptual understanding of a given study area. For example, diffusion can be an important mechanism for moving pesticides towards the surface from deeper soil layers (e.g. Walter et al., 2007), however its simulation can be highly influenced by such factors as the model grid (e.g. Weatherill et al., 2008, Konikow, 2011). Considering that a large amount of dispersion may occur at the surface-subsurface interface (Figure 4.6c) due to concentration gradients, the influence of the grid discretization was explored (Figure 4.8). A grid discretization two times smaller than that used in this chapter has relatively little impact on the total discharge and hydraulic contribution of pre-event water to the stream; however, a larger grid results in a larger tracer-based Q_p under the A+Diff and A+Disp conditions, especially at early times (Figure 4.8). Care must be taken to undertake a rigorous grid convergence analysis and have a sufficiently fine grid, especially near the land surface, when dispersion (diffusion and mechanical dispersion) is included in the surface-subsurface solute exchange, otherwise modeled solute transport and tracer-based hydrograph separation results may be affected.

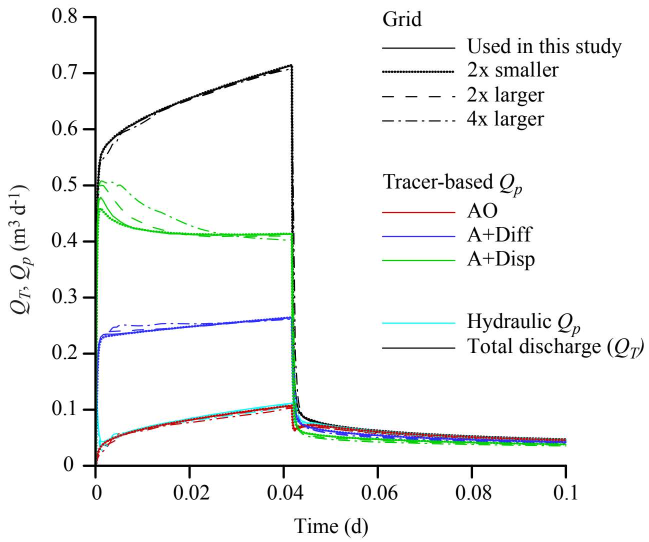

Figure 4.8 Sensitivity of Q_T and Q_p for each surface-subsurface condition with intermediate subsurface dispersion.

4.6 Conclusions

Chapter 4 expands on the results of Jones et al. (2006), Park et al. (2011), and VanderKwaak (1999) by separating the impacts of dispersion within the subsurface from dispersion across the surface-subsurface interface, and demonstrating the possible impact on interpretations of tracer hydrograph separations for two hypothetical 2D hillslopes. Dispersion across the surface-subsurface interface can significantly increases the delivery of pre-event tracer to the stream in absence of dispersion within the subsurface. This may lead to an inflated interpretation of pre-event water contribution hydraulically delivered to the stream when the tracer is assumed to have entered the stream via advection only, as per the classical tracer-based hydrograph separation method. While subsurface dispersion alone did not have an effect on tracer-based hydrograph separation over the duration of a single rainfall event, it will likely have an effect on the subsurface pre-event water concentration distribution over longer timeframes and successive rainfall events. This is likely to require careful selection of the pre-event end-member concentration.

Chapter 4 has shown the influence of modifying the representation of solute exchange across the surface-subsurface interface on the subsurface solute distribution, exchange mass flux, and tracer-based interpretation of pre-event water contribution to the stream, for a select range of situations. However, the best way to model surface-subsurface solute exchange, such that real-world processes are most accurately simulated, is still not clear. This work underscores the importance of having a well-understood conceptual model of catchment processes, including field data and the treatment of the surface-subsurface interface and its control of solute behavior. Given the sensitivity of model solute predictions to interface dispersion, which is currently practically immeasurable in field studies, it is recommend to include the parameterization of the interface as standard practice in sensitivity analyses of integrated catchment model performance.

5. Surface-subsurface solute transport in a fully integrated catchment model

5.1 Introduction

The coupling of surface and subsurface water flows in single, fully integrated models can provide significant advantages in hydrological investigations, especially where there are strong linkages between surface and subsurface flows (Guay et al., 2013). Whilst the application of models that fully couple surface and subsurface flow has increased in popularity (e.g. VanderKwaak and Loague, 2001; Werner et al., 2006; Jones et al., 2008; Mirus and Loague, 2013; Weill et al., 2013), coupled solute transport has received much less attention. Including solute transport in fully integrated models provides the opportunity to account for surface-subsurface interactions during simulations of contaminant transport (e.g. Sudicky et al., 2008), tracer hydrograph separation (e.g. Jones et al., 2006), and analysis of biogeochemical processes (e.g. Frei et al., 2012). However, published examples of coupled solute transport have hypothetical or relatively small and simple geometric domains (Weill et al., 2011, VanderKwaak, 1999; Jones et al., 2006; Park et al., 2011), simulate hypothetical contaminant releases without comparison to observed data (Sudicky et al., 2008), or do not consider coupled surface-subsurface solute fluxes (Frei et al., 2012). To the best of my knowledge, there have been no studies that directly compare observed solute measurements with results from a 3D, fully integrated, catchment-scale model.

Previous work has shown that flow across the surface-subsurface interface (i.e. between the land surface and porous media) in fully integrated models is sensitive to the method and model parameters used to couple the surface and subsurface (Delfs et al., 2009; Ebel et al., 2009; Chapter 2 and 3). In Chapter 4, a fully integrated 2D hillslope model was used to demonstrate that solute transport can be highly influenced by the type and amount of dispersion across the surface-subsurface interface. This in turn may affect the interpretation of stream flow generation processes from modelled solute transport results.

Chapter 5 aims to include both flow and solute transport in a fully integrated, 3D catchment model to examine relationships between the simulation of catchment dynamics and model transport parameters. Numerical modelling experiments are performed using the 3D, fully integrated, Lehstenbach catchment model (4.2 km^2), developed by Partington et al. (2013) in HydroGeoSphere (Therrien et al., 2009) (Figure 5.1). Note that the aim of this chapter is not to produce a calibrated, predictive model for the Lehstenbach catchment; rather, the chapter is designed to explore physical processes and model sensitivity using a model that is based on a real catchment with representative parameters.

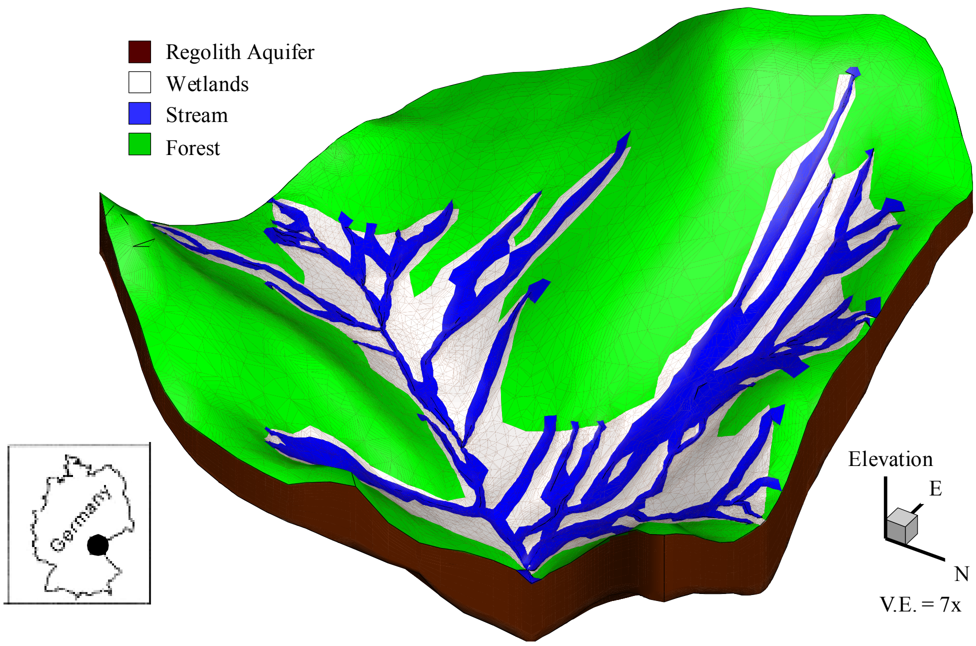

Figure 5.1 Lehstenbach catchment model domain.

Approximately 30% of the Lehstenbach catchment, located in southeast Germany, is covered in peat-forming wetlands (Figure 5.1) that contribute a majority of flow and solute flux to the stream during rainfall events (Lischeid et al., 2007; Frei et al., 2010; Strohmeier et al., 2013). Chapter 4 found that the solute transport results were highly sensitive to the method of solute transport across the surface subsurface interface, therefore three surface-subsurface transport conditions are simulated for a period during and following a single rainfall event in this chapter: advective solute exchange only (AO), advection plus diffusion (A+Diff), and advection plus full hydrodynamic dispersion (A+Disp). Chapter 4 also found that the simulations were more sensitive to changes in subsurface dispersivities when dispersion was included across the surface-subsurface interface. To further explore this sensitivity, the subsurface longitudinal and transverse dispersivities are varied by three orders of magnitude for each of the interface transport conditions in this chapter. The model results are compared to field observations of both flow and solute discharge from the catchment, and to streamflow generation mechanisms modelled with the hydraulic mixing cell (HMC) method (Partington et al., 2011 and 2013). The effects of the interface dispersion and subsurface dispersion on solute movement are examined with respect to the interpretation of catchment processes from the solute transport results.

5.2 Study Area

The Lehstenbach catchment (Figure 5.1) has been the site of biogeochemical and hydrological field studies since 1987 (e.g. Alewell and Ghere, 1999; Lischeid et al., 2002; Lischeid and Bittersohl, 2008; Knorr et al., 2009; Strohmeier et al., 2013). The ground surface elevation varies between 695 and 877 meters above sea level (m asl), and the average annual temperature and average annual rainfall are ~5°C and ~1150 mm yr^{-1}, respectively (Gerstberger et al., 2004). The catchment consists of forested upland areas, riparian wetlands, and a stream network. Much of the wetland areas, especially near the catchment outlet are dominated by vegetation-formed micro-topography consisting of hummocks and hollows.

The bedrock, a Variscan granite, is overlain by up to 40 m of weathered regolith that forms the major aquifer in the catchment (Partington et al., 2013). The regolith consists of heterogeneous layers of loamy sand, gravel, and boulders (Lischeid et al., 2002). The water table is typically greater than 10 meters deep in the forested upland areas, and very close to the surface in the wetlands (Lischeid et al., 2002). Previous field studies of the Lehstenbach catchment have indicated that the wetlands contribute most of the runoff and solute export to the stream during storm events, and saturation excess overland flow and shallow subsurface flow are the dominate mechanisms for generating runoff (Lischeid et al., 2007; Frei et al., 2010). A number of recent numerical modelling studies have confirmed the importance of the wetlands in the hydrology of the catchment (Partington et al., 2013) and the role of the wetland micro-topography in generating and controlling surface flows (Frei et al., 2010; Partington et al., 2013).

Peat-forming wetlands contain approximately 30% of the world's soil carbon, which is exported as dissolved organic carbon (DOC) to rivers and lakes and is critical for biogeochemical cycles (Pastor et al., 2003). The wetlands of the Lehstenbach catchment have high concentrations of DOC and have been investigated by a number of authors including Knorr (2013) and Strohmeier et al. (2013). In 2010 and 2011, DOC concentration was continuously measured at the catchment outlet (15 min intervals) and water samples were collected from different areas within the catchment (e.g. upland forest soil, wetland soil, deep groundwater) on 4 occasions (Strohmeier et al, 2013). They found that the DOC concentration is highest in the wetlands and decreases with depth (see Table 1 in Strohmeier et al., 2013). Additionally, Strohmeier et al. (2013) found that the signature of the DOC, from fluorescence excitation-emission matrices and a parallel factor analysis, was related to the origin of water within the catchment (e.g. deep groundwater, shallow groundwater in wetlands, overland flow from wetlands or forest). The DOC signature is different to the concentration of DOC (i.e. two samples may have the same concentration, but different signatures). At the catchment outlet, the DOC concentration and mass flux both increase with increasing discharge and the two main sources of DOC at the outlet (based on the DOC signatures) were from the riparian wetlands and the deeper groundwater (Strohmeier et al., 2013). As discharge increased, the proportion of DOC in the stream flow from the wetlands increased, whilst the proportion from the deeper groundwater decreased. Strohmeier et al. (2013) also noted counter-clockwise hysteresis loops in the relationship between DOC concentration and discharge at the outlet.

5.3 Model Set-Up and Numerical Experiments

The Lehstenbach catchment model, described in detail by Partington et al. (2013), is used for this chapter with some modifications. A summary of the model and its set-up in HydroGeoSphere (HGS, Therrien et al., 2009) are described below. The surface topography was discretised into triangular elements with nodal spacing of 10 m near the streams, up to 30 m in the riparian wetlands, and increasing to 100 m in the upland areas. In the fully integrated model, surface water and streams are generated interactively in topographically low areas; however, as the streams in the catchment are narrower than the 10 m grid. Consequently, nodes corresponding to the field location of streams were lowered by 1 m to compensate for the smoothing of the grid (Partington et al., 2013).

The catchment is conceptualised as two major geological units: the main regolith aquifer, and the organic peat soils within the upper 1 m of the wetlands that are separated from the main regolith aquifer by a basal clay layer (Partington et al., 2013). In the wetlands, the saturated hydraulic conductivity decreases exponentially with depth, in 0.1 m increments from 20 to $8.6x10^{-3}$ m d^{-1}, to represent the transmissivity feedback mechanism that Bishop et al. (2004) and Jacks and Norrström (2004) described for peat-forming wetlands (Partington et al., 2013). In the current chapter, the first modification to the Lehstenbach model is to refine the vertical grid discretisation in the near surface from 10 cm to 1 cm to better simulate the movement of water and solutes at the surface-subsurface interface. The fine vertical discretisation in the near surface is not only required to improve the simulation of infiltration (Downer and Ogden, 2004; Vogel and Ippisch, 2008; Carrera-Hernández et al., 2012), but also to resolve sharp concentration gradients that exist between the subsurface water and overland flow in the surface (Chapter 4). In the current chapter, the vertical grid in the upper 1 m ranges from 1 cm at the surface to a maximum of 10 cm at a depth of 30 cm. Below the uppermost meter, and into the main regolith aquifer, the grid discretisation is the same as in Partington et al. (2013) with 10 sub-layers ranging from 2 to 5 m in thickness (total model thickness 20-40 m). In the wetland area of the surface domain, three values of sub-grid rill/depression storage (0.1, 0.5 and 1.0 m) were spatially distributed to account for the effects of micro-topography. The rill storage is 0.5 m in the forested areas.

Manning's *n* values were 1.9×10^{-6} d $m^{-1/3}$ in the forest areas and 8.1×10^{-5} d $m^{-1/3}$ in the wetland areas.

Partington et al. (2013) used the Lehstenbach model to investigate the 2000/2001 hydrological year, and they specified daily rainfall rates. However, this chapter examines the hydrological response and DOC export from a single rainfall event using hourly precipitation rates. As such, two more modifications from the Partington et al. (2013) model were made to adequately represent the observed hydrological response for the simulation period. In the areas classified as streams (Figure 5.1), the rill storage in the surface was increased from 0.0001 m to 0.03 m, and the Manning's *n* value was increased from 4×10^{-7} to 2×10^{-5} d $m^{-1/3}$. These modifications were made because the areas demarcated as streams in the model are much larger than the actual stream areas, owing to the discretisation of the grid as described in Partington et al. (2013), and effectively contain the stream and some riparian wetlands. Increasing the rill storage and Manning's *n* increases the surface storage capacity and overcomes the resolution of discretisation of the grid as described in Partington et al. (2013) to better represent the proportion of riparian wetland compared to actual stream area.

The simulation period for this chapter is from May 31st to June 4th, 2011. This period began with a large rainfall event (41 mm) that lasted approximately one day and also has high frequency measurements of discharge (30 min) and DOC concentrations (15 min) at the catchment outlet, as described by Strohmeier et al. (2013). Initial head conditions were generated by running the model to steady state (~100 000 d) with a rainfall rate of 0.3835 mm d^{-1}, such that the stream discharge was approximately equal to the observed stream discharge prior to the rainfall event. For the simulation period, hourly precipitation rates were applied as specified fluid fluxes to the surface of the model domain. Estimates of potential evapotranspiration (PET) were not available for the simulation period, therefore daily PET rates were applied based on the same days of the year from the 2000/2001 model. Actual evapotranspiration and interception are calculated within HGS following the methods of Kristensen and Jensen (1975) and Wigmosta et al. (1994).

Because of the significant short-term variation of DOC in relation to discharge, and its link to different source compartments within the catchment (Strohmeier et al., 2013), DOC is assumed to be a conservative solute and tracer in this modelling study. It is expected that over the short term, such as the simulated rainfall event, the DOC does not undergo significant biogeochemical reactions within the catchment. The DOC was simulated as two separate solutes to represent and track the two main sources of DOC within the catchment, which were identified by differing signatures in Strohmeier et al. (2013). The first is a shallow wetland component (wDOC) and the second is a deep groundwater and forest component (dDOC). In the wetlands, the initial concentration of wDOC was 0.045 kg m^{-3} from the surface to 0.5 m below ground, and 0.005 kg/m^{-3} from 0.5 to 1 m below ground. Below 1 m, there is no wDOC and an initial concentration of dDOC of 0.001 kg m^{-3}. In the forests, there was an initial concentration of dDOC of 0.001 kg m^{-3} throughout the entire subsurface. Both DOC components were simulated by applying the initial solute concentrations into the model domain at the beginning of each simulation, which allows the DOC to be mobilised through the catchment as a pulse over the course of the rainfall event. Initial concentrations in the model were based on the sampling results of Strohmeier et al. (2013). In the model, the total mass flux of DOC at the catchment outlet is obtained by adding the mass flux of the wDOC and dDOC components.

Twelve simulations were performed for this chapter, with different transport conditions across the surface-subsurface interface and subsurface dispersivities between the simulations. In the same manner as in Chapter 4, three types of transport across the surface-subsurface interface are considered in this chapter. The first condition simulates surface-subsurface solute transport by advection only (AO). The second condition includes diffusion in addition to advection (A+Diff), and the third also includes mechanical dispersion (A+Disp). Throughout the rest of this chapter, "dispersion" will refer to full hydrodynamic dispersion, a combination of the processes of (molecular) diffusion and mechanical dispersion.

The coupling dispersivity influences the amount of mechanical dispersion occurring across the surface-subsurface interface, where flow and solute transport occur in 1D, vertically between the surface and uppermost subsurface node (See Figure 3.1a for nodal arrangement). There is no guidance on appropriate values for the coupling dispersivity parameter. As such, both low and high coupling dispersivities are tested under the A+Disp condition. For the low interface dispersion condition (A+DispL), a coupling dispersivity of 0.001 m is used, following Gelhar et al. (1992) for dispersion along a small length scale associated with the surface-subsurface interface (i.e. the coupling length). For the high interface dispersion condition (A+DispH) the coupling dispersivity is arbitrarily equal to the transverse dispersivity of the porous media. In preliminary modelling, this condition promoted solute flux across the interface, resulting in a small concentration gradient across the interface and near-equal concentrations for the surface and uppermost subsurface nodes. Results were similar to the shared-node approach in HGS, where a single node represents both the surface and uppermost subsurface nodes.

For each of the four surface-subsurface interface conditions (i.e. AO, A+Diff, A+DispL, A+DispH), three simulations were performed with low, intermediate, and high values of subsurface dispersivity. Longitudinal dispersivities in the porous media were 1, 10, and 100 m for the low, intermediate, and high simulations respectively. Transverse dispersivities (and likewise coupling dispersivities) were an order of magnitude smaller than the longitudinal dispersivities. These dispersivities were chosen to fit within the range for flowpaths on the order of tens to hundreds of meters (Gelhar et al., 1992), fitting with the catchment size. In the surface domain, the longitudinal and transverse dispersivities were both set to 100 m for all simulations in order to minimise numerical oscillations associated with high surface flow velocities. A diffusion coefficient of $1.9x10^{-10}$ m^2 s^{-1} was used for all simulations and for both wDOC and dDOC components. This value is within the range for major natural solutes and for values for carbon-14 (e.g. Sudicky and Frind, 1981; Walker and Cook, 1991; Sanford, 1997).

The simulations were completed in HGS using the control-volume finite-difference mode, and dual-node approach for coupling the surface and subsurface. The coupling length was set to 0.1 m in all areas except the streams. This value of coupling length (0.1 m) was equal to (or smaller than) the rill storage in all areas, a condition suggested in Chapter 2 to ensure adequate coupling between the surface and subsurface. In the streams, the coupling length was set equal to the rill storage of $1x10^{-4}$ m. A sensitivity analysis of model results to coupling length was performed as suggested in Chapter 2, and these values of coupling length were found to be suitably converged for the purposes of the modelling exercise. Adaptive time steps were used throughout the simulation with a maximum time step of 0.1 d.

The HMC method (Partington et al., 2011, 2013) was included in the simulations in order to track in-stream and overland flow generation mechanisms. This method works by advectively tracking the volumetric fractions of water within each surface cell, originating from each of the flow generation mechanisms. The flow generation mechanisms measured are: overland flow from the forest area (FOR), direct rainfall to the wetlands (RF-WL), groundwater discharge to wetlands (GW-WL), direct rainfall to the stream (RF-ST), and groundwater discharge to the stream (GW-ST).

5.4 Results

Figure 5.2a shows the modelled and observed discharge at the catchment outlet for the simulation period. The modelled discharge is similar to the observed response despite only slight modifications to the model to better represent the event-scale response (i.e. stream rill storage increased from 0.0001 m to 0.03 m, and the stream Manning's *n* increased from 4×10^{-7} to 2×10^{-5} d m$^{-1/3}$). The observed response has a peak discharge of 9 625 m^3 d^{-1} occurring at 1.25 d, whereas the modelled response has a peak of 13 362 m^3 d^{-1} occurring at 1.32 d. Figure 5.2b shows the streamflow generation components computed by the HMC method. Similar to the results of Partington et al. (2013), most of the stream flow over the rainfall event is derived from RF-ST. RF-WL is the next largest contributor to stream flow and occurs due to saturation excess overland flow in the wetlands. GW-ST forms the third-highest stream flow component, and GW-WL is quite insignificant (Figure 5.2). Partington et al. (2013) identified that the high RF-ST component is due to the larger stream

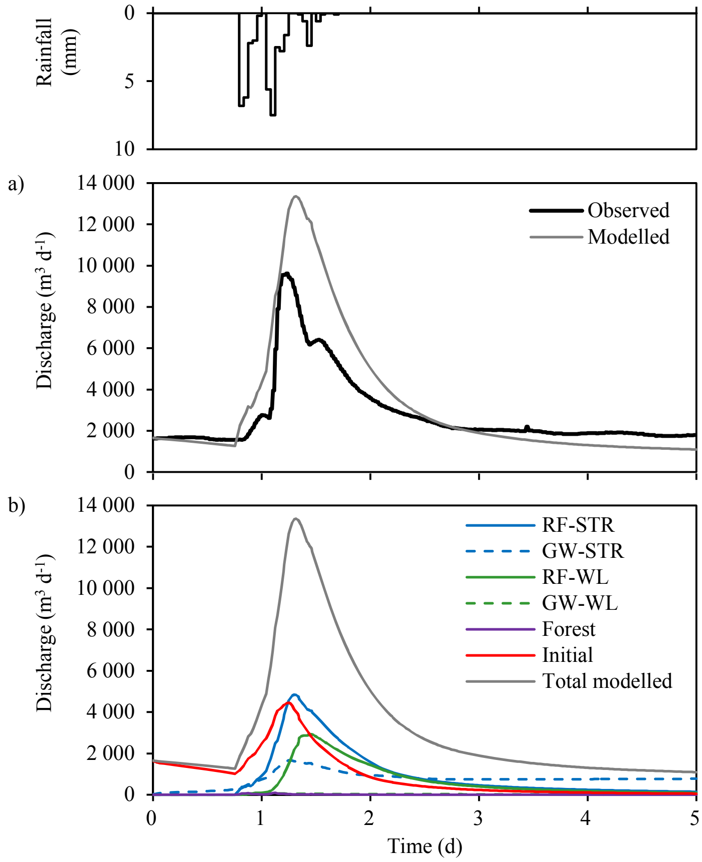

Figure 5.2 a) observed vs. modelled discharge, and b) HMC components at the catchment outlet.

area within the model, due to the model grid size. The large "initial" HMC fraction is water that was present in the surface domain at the beginning of the simulation.

Figure 5.3 shows the spatially distributed, surface-subsurface fluid exchange flux at three times during the simulation period. Immediately prior to the rainfall event (Figure 5.3a), groundwater is discharging to only the lower reaches of the stream, and there is a minimal amount of infiltration across the rest of the domain. At the peak of the rainfall event (Figure 5.3b), most of the catchment is undergoing infiltration and there is a much higher discharge of subsurface water to the stream. As the system equilibrates after the rainfall event (Figure 5.3c), infiltration decreases, but groundwater discharge to the stream is still relatively high.

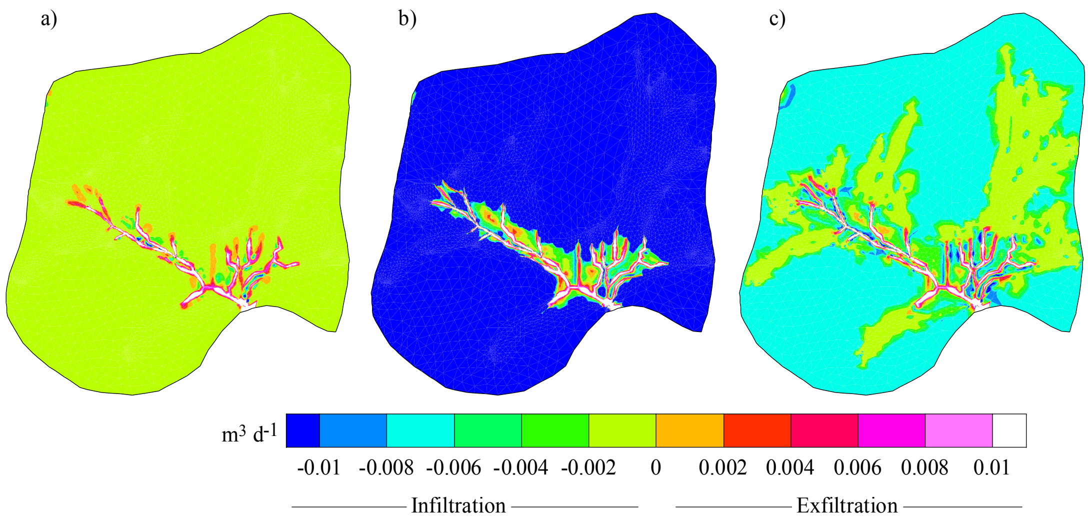

Figure 5.3 Surface-subsurface exchange flux a) before the rainfall event (0.7 d), b) at the peak of the event (1.1 d), and c) after the cessation of rainfall (2.6 d).

Figure 5.4 shows the total DOC mass flux (wDOC + dDOC components) at the catchment outlet for each surface-subsurface transport condition and intermediate subsurface dispersion, compared to the observed response over the course of the rainfall event. The simulations that include dispersion across the surface-subsurface interface (i.e. A+Diff, A+DispL, A+DispH) compare well with the observed DOC mass fluxes; however, the AO simulation has a significantly lower mass flux than observed (Figure 5.4). A smaller coupling dispersivity (A+DispL) produces results closer to the A+Diff simulation, as predicted by the coupling equations for HGS given in Chapter 4. Figure 5.5 shows that the wDOC component of the total DOC flux increases with discharge (Figure 5.5a) whilst the dDOC component decreases (Figure 5.5b). This trend in the modelling results is generally the same for the different surface-subsurface transport conditions and is consistent with the field results of Strohmeier et al. (2013).

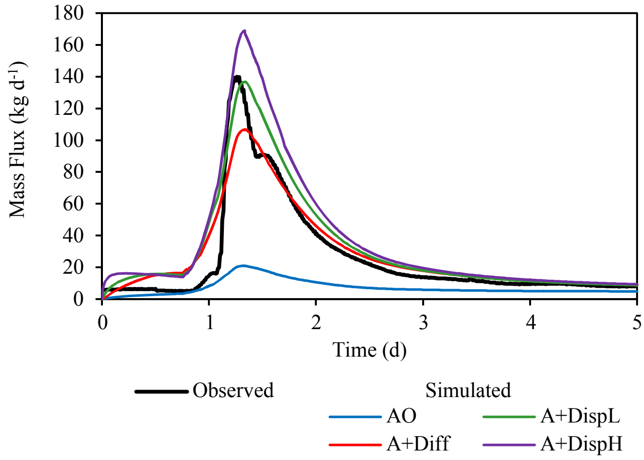

Figure 5.4 Total DOC mass flux at the catchment outlet with each interface transport condition and intermediate subsurface dispersion.

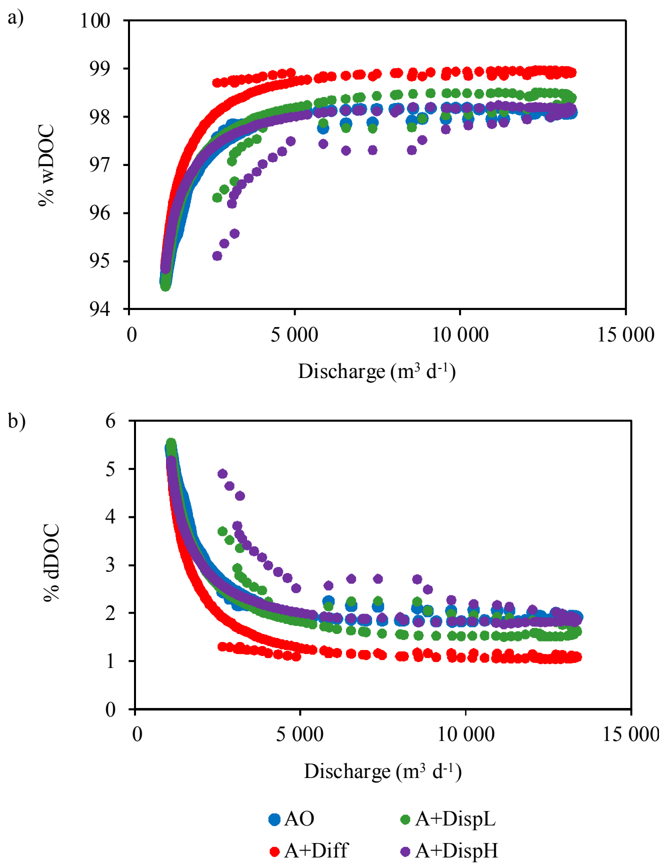

Figure 5.5 Percent of total DOC at the catchment outlet for the a) wDOC and b) dDOC components for each surface-subsurface interface condition and intermediate subsurface dispersion.

Figure 5.6 shows the spatially distributed mass flux of total DOC between the surface and subsurface, as well as the surface concentrations of wDOC and dDOC components, at the peak of the rainfall event (t = 1.1d) for each surface-subsurface transport condition and adopting intermediate subsurface dispersion. Under the AO transport condition, very little DOC moves between the surface and subsurface and most exfiltrates to the stream, where water is also exfiltrating (Figures 5.3 and 5.6). With the A+Diff and A+Disp transport conditions, the dominant mass flux is from the subsurface to the surface, regardless of the direction of fluid exchange flux. This is due to the direction and magnitude of the concentration gradients which drive mass flux towards the surface, in some cases exceeding the advective component of mass flux (i.e. causing subsurface-to-surface mass discharge despite water flowing in the opposite direction). The direction of the concentration gradients are maintained by dilution of the surface water by rainfall. Discharge of DOC to the surface increases as dispersion across the surface-subsurface interface is increased (i.e. A+Diff to A+DispL and A+DispH), as does the concentration of both the wDOC and dDOC components across the surface domain (Figure 5.6). Higher concentrations of wDOC are found mostly in the stream area under the A+Diff and A+DispL simulations, however in the A+DispH simulation higher concentrations of wDOC are found throughout the entire wetland area (Figure 5.6).

Altering the subsurface dispersivity values has a significant impact on the mass flux of DOC at the catchment outlet (Figure 5.7), creating a large envelope of results. Unlike the results in Jones et al. (2006), Park et al. (2011), and Chapter 4, increasing subsurface dispersion resulted in decreasing mass flux at the catchment outlet. This occurs because most of the DOC resides in the near surface of the wetlands, and increased subsurface dispersion allows for more mixing of DOC into the deeper

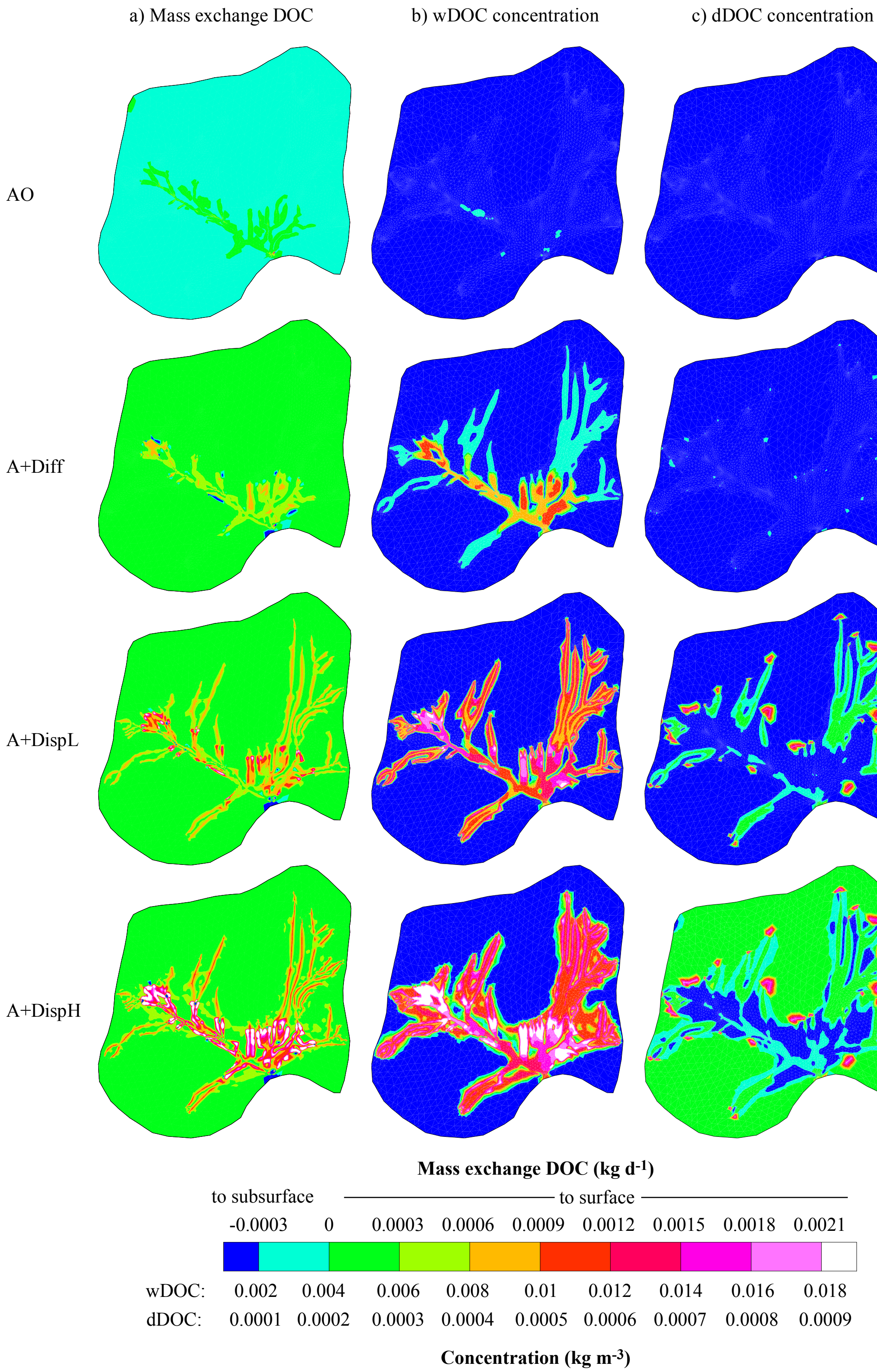

Figure 5.6 a) the total DOC surface-subsurface mass exchange and surface concentrationfor the b) wDOC and c) dDOC coponenents for each of the surface-subsurface transport conditions, with intermediate subsurface dispersion, and at the peak of the rainfall event (1.1 d).

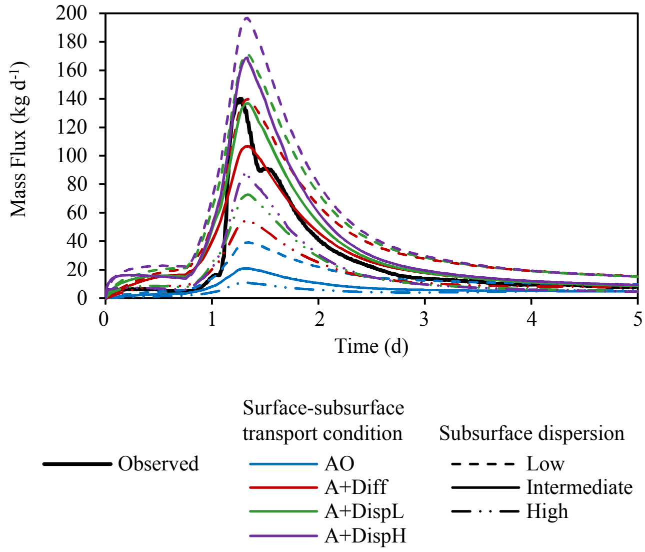

Figure 5.7 Influence of subsurface dispersion on mass flux of total DOC at the catchment outlet.

subsurface rather than the being discharged to the surface as a well-defined pulse. In contradiction to the results in Chapter 4, changes to the subsurface dispersivity impacted the mass flux at the outlet under the AO condition, although the differences in the results were smaller than when subsurface dispersivity was varied under the A+Diff and A+Disp conditions. The sensitivity of the solute response to subsurface dispersion parameters under the AO transport condition is likely due to longer flowpaths than in the 2D hillslopes in Chapter 4, and more mixing in the subsurface due to transient and dynamic flow fields. Consequently, the solute transport in the subsurface is more greatly affected by changes in the subsurface dispersion parameters than in Chapter 4. This leads to differences in surface-subsurface solute exchange and ultimately differences in mass flux at the catchment outlet.

Some of the simulations in Figure 5.7 show a very similar DOC mass flux at the catchment outlet despite different surface-subsurface solute exchange conditions and subsurface dispersivities. Figure 5.8 shows that despite very similar responses of

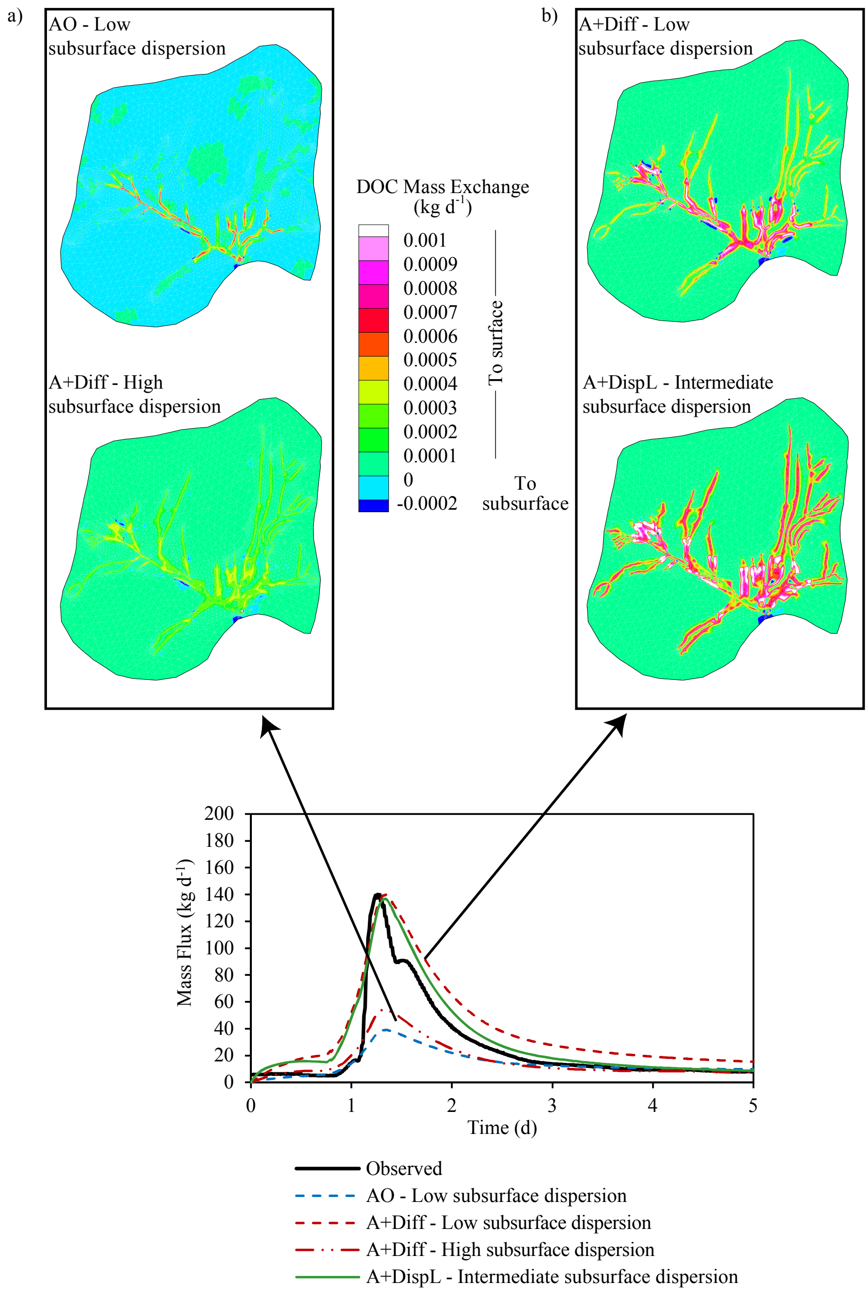

Figure 5.8 Total DOC mass exchange across the surface subsurface interface at the peak of the rainfall event (t = 1.1 d).

mass flux out of the catchment, the distributed responses of surface-subsurface mass exchange are quite different. In Figure 5.8a, the AO simulation with low subsurface dispersivity shows most of the DOC discharging directly into the stream, with very little mass exchange throughout the rest of the catchment, at the peak of the rainfall event. This is contrary to the A+Diff simulation with high subsurface dispersivity, where less DOC discharges directly to the stream but DOC discharge occurs over a much larger part of the stream network and wetlands at the peak of the rainfall event. Figure 5.8b shows a greater amount of DOC discharging to the surface, over a larger portion of the stream network, under the A+DispL scenario with intermediate subsurface dispersion rather than the A+Diff scenario with low subsurface dispersion. Despite the spatial differences in surface-subsurface mass flux, both of the scenarios in Figure 5.8b produce mass flux results closest to that observed at the catchment outlet.

Figure 5.9 shows the concentration versus discharge graphs for each of the surface-subsurface solute conditions with intermediate subsurface dispersion, compared to the observed results during the simulation period. Similar to Strohmeier et al. (2013),

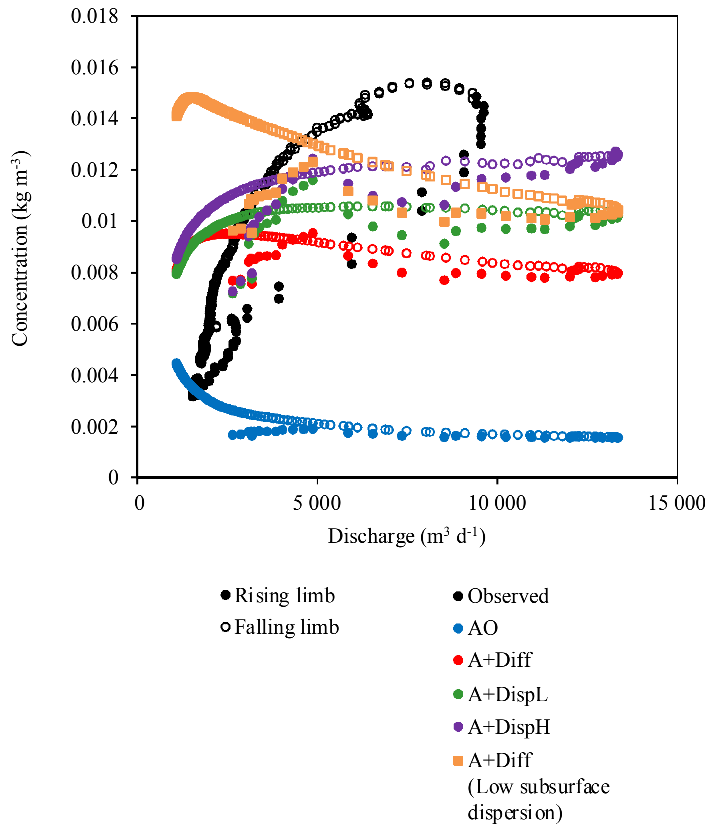

Figure 5.9 Total DOC concentration vs. discharge for each of the surface-subsurface solute transport conditions and intermediate subsurface dispersion. The A+Diff simulation with low subsurface dispersion is also shown.

the fully integrated simulations produced counter-clockwise hysteresis loops (Figure 5.9), with lower DOC concentrations on the rising limb of the hydrograph and higher DOC concentrations on the falling limb. However, the modelled DOC loops were not as open as the observed data, and did not have the same slope. Also shown on Figure 5.9 are the results for the A+Diff transport condition with low subsurface dispersion, which produces a similar mass flux at the catchment outlet as the A+DispL condition with intermediate subsurface dispersion (e.g. Figures 5.7 and 5.8b). Like the spatial distribution of solute exchange flux (Figure 5.8), the concentration-discharge relationship for these two simulations is different, despite very similar mass fluxes at the catchment outlet.

5.5 Discussion

The addition of solutes into the fully integrated Lehstenbach model is useful for understanding both the performance of this particular model, as well as the simulation of integrated surface-subsurface solute transport in general. With regards to evaluating the model performance, the increased wDOC component with discharge (Figure 5.5) indicates that more DOC (and therefore water) is discharged to the stream from the shallow wetlands than from the deeper groundwater during a rainfall event. This model behaviour follows the observed results of Strohmeier et al. (2013) and gives confidence that the model is capturing this particular aspect of catchment functioning.

Also similar to the observed results is the counter-clockwise hysteretic behaviour of the DOC concentration relationship with discharge (Figure 5.9), although the model does not accurately capture the shape of the observed loop. Strohmeier et al. (2013)

discussed a possible mechanism for the counter-clockwise hysteresis loops involving the extensive microtopography in the wetland area of the catchment. During the rising limb of the hydrograph there is relatively little connection of the surface water flow network in the hummocks and hollows of the wetlands, and overland flow is diluted by rainfall. During the falling limb, no dilution of rainfall occurs, the water table is high, the surface water network is established, and there is a higher concentration of DOC entering the stream. The model results from Figure 5.9 show the possibility that the influence of the microtopography in the wetlands is not captured very well in the model, despite the variable rill storage used throughout the wetlands. Incorporating the effects of microtopography in integrated models is an active area of research (e.g. Frei et al., 2010). Frei and Fleckenstein (2014) demonstrated how highly spatially distributed rill storage values, in an otherwise planar numerical model, could account for the hydrological effects of microtopography without significantly increased run times. It is possible that smaller grid sizes, with even more variable rill storage values, would better capture the local, microtopography-driven flow systems, and the connection and disconnection of surface flow network in the model. Such an improvement in the simulation of internal (and lateral) flow processes within the catchment may improve the simulation of the DOC behaviour at the catchment outlet (i.e. the DOC hysteresis loops).

With regards to the general aspects of modelling integrated surface-subsurface solute transport, this work shows that the simulations of solute transport in a fully integrated model are very sensitive to the type of dispersion across the surface-subsurface interface (Figures 5.4, 5.6, and 5.9). At present, there is no consensus in the literature on which method of interface dispersion is most suitable for simulating coupled surface-subsurface transport in fully integrated codes. Additionally, model results are highly non-unique, as various combinations of interface and subsurface dispersion can produce similar mass flux responses at the catchment outlet (Figure 5.7). Two combinations (of the simulations performed in this chapter) provided results closest to the observed mass flux at the catchment outlet. These were the A+DispL transport condition simulation with intermediate subsurface dispersion, and the A+Diff transport condition simulation with low subsurface dispersion (Figures 5.7 and 5.8b). However, the types of dispersion affect the solute transport simulations differently, and although the mass flux at the catchment outlet may be similar, dispersion within the subsurface and across the surface-subsurface can produce quite different distributed solute responses (Figure 5.8) and concentration-discharge relationships (Figure 5.9).

Loague and VanderKwaak (2004) discussed that an advantage of fully integrated codes was the ability to include solute transport to help evaluate the simulation of water flow. Whilst modelling the transport of solutes has been shown to be useful in evaluating the flow component of other types of models (e.g. groundwater-only or lumped rainfall-runoff, Reilly et al., 1994; Castro and Goblet, 2003; Birkel et al., 2010), care must be taken when evaluating the model performance and interpreting catchment processes from fully integrated models using solute transport. For example, modelled solute transport may not match observations due to the non-uniqueness of the solute solution as opposed to errors in the flow solution. Therefore, it is important that appropriate spatial and temporal resolutions of solute measurements (and fluid fluxes) are obtained from the field in order to constrain the non-uniqueness of the solute transport solution in the fully integrated model.

The availability of measured field data by Strohmeier et al. (2013) for the Lehstenbach catchment was essential in beginning to constrain the non-uniqueness of the model in this chapter. Field sampling provided some bounds on the initial concentrations and depths of the various DOC compartments and the observed mass flux at the catchment outlet allowed for comparison of the wide range of solute transport results from the various combinations of surface-subsurface transport condition and subsurface dispersion. Many other authors (e.g. Seibert and McDonnell, 2002; Dunn et al., 2008; McMillian et al., 2011) have defended the importance of the inclusion of field data and catchment process knowledge in conceptualising, building, and evaluating the performance of numerical models. Additionally, the combination of different solutes (or tracers, such as heat) with different transport properties may also help constrain the model non-uniqueness.

Partington et al. (2013) outlined some of the limitations of the Lehstenbach model, including the grid size in the vicinity of the streams, the fact that only discharge at the catchment outlet was available for calibration, and the spatiotemporal resolution of rainfall and evapotranspiration. Whilst some modifications were made to the model to better represent the simulated rainfall event (e.g. hourly rainfall, modifications to stream Manning's *n* and rill storage), the purpose here was not to (re-)calibrate the Lehstenbach model, but to use it to perform the numerical experiments to provide an illustration of the effects of different types of dispersion on modelled results. As such, the model does not necessarily reflect all of the processes occurring in the Lehstenbach catchment. Additionally, an exhaustive study of the sensitivity of the transport simulations to other factors such as initial concentrations, diffusion coefficient, or horizontal grid size was not performed.

5.6 Conclusions

Whilst the simulation of fully integrated, surface-subsurface flow in hydrological models is gaining popularity, coupled solute transport has received much less attention. This work demonstrates the inclusion of solute transport in a 3D, fully integrated, catchment-scale model over the course of a rainfall event. The model generally captured the observed mass flux from the catchment, the increasing wetland component of DOC with increasing discharge, and the counter-clockwise direction of the concentration-discharge hysteretic relationship. Different combinations of surface-subsurface dispersion and subsurface dispersivities can produce similar solute responses at the catchment outlet, but show different amounts of mass flux across the surface-subsurface interface.

Chapter 5 demonstrates that care must be taken when interpreting the results of fully coupled surface-subsurface solute transport simulation, because the combination of the surface-subsurface transport condition and subsurface dispersion results in a non-unique solution. It is important that a number of metrics be included in evaluating the modelled solute transport response, including the internal catchment response in addition to the response at the catchment outlet. This will help improve the representation of internal catchment dynamics. Field measurements of both the integrated and distributed response of the catchment are vital to constraining the simulation of fully integrated surface-subsurface solute transport. This chapter also highlights the need to continue both field and modelling investigations of surface-subsurface solute transport in order to better represent solute movement in fully integrated models.

6. Thesis summary and conclusions

The aim of this thesis was to examine the implementation of surface-subsurface coupling approaches in fully integrated codes, and to evaluate their controls on simulating integrated flow and solute transport. Chapter 2 shows that both the continuity of pressure (COP) and the first-order exchange coefficient (FOEC) coupling approaches can be useful in simulating surface-subsurface flow. The FOEC approach can be used to reduce the computational burden that can occur with the COP approach, whilst maintaining accuracy if the FOEC is high enough (i.e. coupling length [l_e] is low enough in HGS). The FOEC solution approaches the COP solution as l_e decreases, but the convergence pattern varies with hydrological scenario, soil type and rill storage height. Lower l_e values are required for infiltration under Hortonian conditions, in lower permeability soils, and to capture the initiation of overland flow. A threshold value of l_e is found to be equal to rill storage, above which inaccurate simulations can occur, especially under Hortonian conditions. These findings highlight the importance of using a value of l_e that accommodates all surface-subsurface interaction types, soil types and rill storage values within a model. This may require different values of l_e spatially within the model domain when applied to whole-catchment models with spatially distributed properties.

Chapter 3 highlights the challenges of implementing the FOEC approach in a block-centred code (MODHMS). The half-cell separation between the surface and uppermost subsurface nodes causes a discrepancy between saturation of the uppermost subsurface node, saturation of the uppermost subsurface cell, and the intersection of the subsurface head at the land surface. With the conceptualisation of the FOEC approach in MODHMS, defining the FOEC based on the uppermost grid size inhibits accurate prediction of infiltration and the time to initiate overland flow under Hortonian conditions. Increasing the FOEC independently of the grid allows for accurate simulation of infiltration, but not timing of overland flow. The addition of a thin layer at the surface improves model accuracy substantially because the uppermost subsurface node is much closer to the land surface, ensuring that saturation of the uppermost subsurface node is concurrent with saturation of the uppermost subsurface cell and the head reaching the land surface.

Modelling surface-subsurface solute transport in a fully integrated code remains a significant conceptual challenge. Chapters 4 and 5 show that solute transport is highly affected by the surface-subsurface solute transport condition, and considering this condition is just as important as considering the subsurface dispersion when modelling integrated solute transport. In Chapter 4, the 2D models of hypothetical hillslopes show that the surface-subsurface transport condition influences the relationship between subsurface dispersion and the interpretation of pre-event water to the stream. Additionally, the transport condition at the interface affects the solute response differently then dispersion within the subsurface, as demonstrated in Chapter 5, and although mass flux results at the catchment outlet might be similar, the distributed solute transport processes are different. As the solute transport results are highly non-unique, care must be taken in interpreting catchment processes, and field data are vital to constraining the model results.

Unfortunately, there is no guidance in the literature about which solute transport condition at the surface-subsurface interface may be most appropriate for modelling solute transport in such an integrated fashion. In Chapter 4, the advective solute exchange only transport condition agreed well with the hydraulic contribution to stream flow, however, some dispersion was required across the surface-subsurface interface in order to represent the field-measured solute response at the catchment outlet in Chapter 5.

A major advantage of fully integrated hydrological codes is their apparent ability to "seamlessly" couple surface and subsurface flow and solute transport, and eliminate the need for a boundary condition at the land surface, which is otherwise required in uncoupled or iteratively coupled codes. The results of this thesis show that despite the lack of an explicit boundary condition at the surface-subsurface interface, the coupling approach and associated parameters can highly influence both the integrated and distributed response of flow and solute transport. As such, it is important that the coupling approach is carefully considered, parameters thoughtfully chosen, and sensitivity analyses be performed to ensure robust model performance. The inclusion of solute transport into a fully integrated model can be of great benefit to evaluating model performance and understanding catchment dynamics. However, the utility of modelling integrated solute transport in the absence of field data, with which to constrain the model results, seems limited at this time.

6.1 Recommendation for future work

Recommendations for future work from this thesis are as follows:

- Improving the representation of surface-subsurface flow in block-centred codes that use the FOEC approach (e.g. MODHMS). Possibilities for achieving this include the addition of a subsurface node at the land surface or of a "ghost node" above the land surface.

- Performing field experiments, combined with numerical modelling, which focus specifically on the surface-subsurface interface and near-surface hydrology and solute transport in order to gain more insight into which solute transport condition, if any, is most representative of natural field conditions.

- More detailed investigation into the non-uniqueness of the solute transport solution in fully integrated codes and the use of multiple tracers to constrain the model results in fully integrated surface-subsurface models.

- Extending intercode comparisons of fully integrated codes, such as the recent study by Maxwell et al. (2014), to include solute transport. It is important that more metrics than just the outflow hydrograph are considered, as Chapters 2 and 5 both showed that there can be differences in distributed flow and solute transport for very similar outflow hydrographs.

The continued testing of fully integrated surface-subsurface hydrological codes to ensure their representativeness of real-life processes is an important step in the continued success of fully integrated surface-subsurface hydrological modelling.

References

Abdul, A.S., Gillham, R.W., 1984. Laboratory studies of the effects of the capillary fringe on streamflow generation. Water Resour. Res. 20, 691–698. doi: 10.1029/WR020i006p00691

Abdul, A.S., Gillham, R.W., 1989. Field studies of the effects of the capillary fringe on streamflow generation. J. Hydrol. 112, 1–18. doi: 10.1016/0022-1694(89)90177-7

Alewell, C., Gehre, M., 1999. Patterns of stable S isotopes in a forested catchment as indicators for biological S turnover. Biogeochemistry 47, 319–333. doi: 10.1007/BF00992912

Anderson, M.P., Woessner, W.W., 2002. Applied groundwater modelling: simulation of flow and advective transport. Academic Press, San Diego, CA, USA.

Barenblatt, G.I., Zheltov, I.P., Kochina, I.N., 1960. Basic concepts in the theory of seepage of homogeneous liquids in fissured rocks [strata]. J. of Appl. Math. Mech., 24(5), 1286-1303.

Barr, A., Barron, O., 2009. Application of a coupled surface water–groundwater model to evaluate environmental conditions in the Southern River catchment. CSIRO: Water for a Healthy Country National Research Flagship. 84 pp.

Barry, D.A., Sander, G.C., Jomaa, S., Yeghiazarian, L., Steenhuis, T.S., Selker, J.S., 2013. Solute and sediment transport at laboratory and field scale: contributions of J.-Y. Parlange. Water Resour. Res. 49, 1–27. doi: 10.1002/wrcr.20510

Batu, V., van Genuchten, M.T., 1990. First- and third-type boundary conditions in solute transport modeling. Water Resour. Res. 26, 339–350. doi: 10.1029/WR026i002p00339

Bear, J., 1972. Dynamics of fluids in porous media. American Elsevier Publishing Company, New York.

Bencala, K.E., 1984. Interactions of solutes and streambed sediment 2. A dynamic analysis of coupled hydrologic and chemical processes that determine solute transport. Water Resour. Res. 20, 1804–1814. doi: 10.1029/WR020i012p01804

Beven, K.J., 1985. Distributed models. In Hydrologic forecasting, Anderson, M.G, Burt, T.P. (eds). John Wiley and Sons, New York, 405–435.

Birkel, C., Dunn, S.M., Tetzlaff, D., Soulsby, C., 2010. Assessing the value of high-resolution isotope tracer data in the stepwise development of a lumped conceptual rainfall–runoff model. Hydrol. Process. 24, 2335–2348. doi: 10.1002/hyp.7763

Bishop, K., Seibert, J., Köhler, S., Laudon, H., 2004. Resolving the double paradox of rapidly mobilized old water with highly variable responses in runoff chemistry. Hydrol. Process. 18, 185–189. doi: 10.1002/hyp.5209

Brookfield, A.E., Sudicky, E.A., Park, Y.-J., Conant Jr., B., 2009. Thermal transport modelling in a fully integrated surface/subsurface framework. Hydrol. Process. 23, 2150-2164. doi: 10.1002/hyp.7282

Buttle, J.M., 1994. Isotope hydrograph separations and rapid delivery of pre-event water from drainage basins. Prog. Phys. Geogr. 18, 16–41. doi: 10.1177/030913339401800102

Cardenas, M.B., 2008. The effect of river bend morphology on flow and timescales of surface water-groundwater exchange across pointbars. J. Hydrol. 362, 134–141. doi:10.1016/j.jhydrol.2008.08.018

Carrera-Hernández, J.J., Smerdon, B.D., Mendoza, C. A., 2012. Estimating groundwater recharge through unsaturated flow modelling: Sensitivity to boundary conditions and vertical discretization. J. Hydrol. 452-453, 90–101. doi: 10.1016/j.jhydrol.2012.05.039

Carsel, R.F., Parrish, R.S., 1988. Developing joint probability distributions of soil water retention characteristics. Water Resour. Res. 24(5), 755-769. doi: 10.1029/WR024i005p00755

Castro, M.C., Goblet, P., 2003. Calibration of regional groundwater flow models: Working toward a better understanding of site-specific systems. Water Resour. Res. 39(6), 1172. doi: 10.1029/2002WR001653

Chanat, J.G., Hornberger, G.M., 2003. Modeling catchment-scale mixing in the near-stream zone—Implications for chemical and isotopic hydrograph separation. Geophys. Res. Lett. 30, 1091. doi: 10.1029/2002GL016265

Cloke, H.L., Anderson, M.G., McDonnell, J.J., Renaud, J.-P., 2006. Using numerical modelling to evaluate the capillary fringe groundwater ridging hypothesis of streamflow generation. J. Hydrol. 316, 141–162. doi: 10.1016/j.jhydrol.2005.04.017

Delfs, J.O., Park, C.H., Kolditz, O., 2009. A sensitivity analysis of Hortonian flow. Adv. in Water Resour. 32(9), 1386-1395. doi: 10.1016/j.advwatres.2009.06.005

Donn, M.J., Barron, O.V., Barr, A.D., 2012. Identification of phosphorus export from low-runoff yielding areas using combined application of high frequency water quality data and MODHMS modelling. Sci. Total Environ. 426, 264 – 271. doi: 10.1016/j.scitotenv.2012.03.021

Doppler, T., Franssen, H.-J.H., Kaiser, H.-P., Kuhlman, U., Stauffer, F., 2007. Field evidence of a dynamic leakage coefficient for modelling river-aquifer interactions. J. Hydrol. 347(1-2), 177-187. doi:10.1016/j.jhydrol.2007.09.017

Downer, C.W., Ogden, F.L., 2004. Appropriate vertical discretization of Richards' equation for two-dimensional watershed-scale modeling. Hydrol. Process. 18, 1-22. doi: 10.1002/hyp.1306

Dunkerley, D., 2008. Rain event properties in nature and in rainfall simulation experiments: a comparative review with recommendations for increasingly systematic study and reporting. Hydrol. Process. 44, 4415-4435. doi: 10.1002/hyp.7045

Dunn, S. M., Freer, J., Weiler, M., Kirkby, M. J., Seibert, J., Quinn, P. F., Lischeid, G., Tetzlaff, D. and Soulsby, C., 2008. Conceptualization in catchment modelling: simply learning? Hydrol. Process. 22, 2389–2393. doi: 10.1002/hyp.7070

Dunne, T., 1978. Field studies of hillslope flow processes. In: Kirkby, M.J. (Ed.), Hillslope Hydrology. John Wiley & Sons, Chichester, New York, pp. 389.

Dunne, T., Zhang, W., Aubry, B.F., 1991. Effects of rainfall, vegetation, and microtopography on infiltration and runoff. Water Resour. Res. 27(9), 2271-2285. doi: 10.1029/91WR01585

Ebel, B.A., Loague, K., Borja, R.I., 2010. Impacts of hysteresis on variably saturated hydrologic response and slope failure. Environ. Earth Sci. 61, 1215-1225. doi: 10.1007/s12665-009-0445-2

Ebel, B.A., Mirus, B.B., Heppner, C.S., VanderKwaak, J.E., Loague, K., 2009. First-order exchange coefficient coupling for simulating surface water-groundwater interactions: Parameter sensitivity and consistency with a physics-based approach. Hydrol. Process. 23(13), 1949-1959. doi: 10.1002/hyp.7279

Fiori, A., Russo, D., 2007. Numerical analyses of subsurface flow in a steep hillslope under rainfall: The role of the spatial heterogeneity of the formation hydraulic properties. Water Resour. Res. 43, W07445. doi: 10.1029/2006WR005365

Fleckenstein, J.H., Krause, S., Hannah, D.M., Boano, F., 2010. Groundwater-surface water interactions: New methods and models to improve understanding of processes and dynamics. Adv. Water Resour. 33, 1291–1295. doi: 10.1016/j.advwatres.2010.09.011

Freeze, R.A., Harlan, R.L., 1969. Blueprint for a physically-based digitally-simulated hydrologic response model. J. Hydrol. 9, 237-258. doi: 10.1016/0022-1694(69)90020-1

Frei, S., Fleckenstein, J.H., Kollet, S.J., Maxwell, R.M., 2009. Patterns and dynamics of river-aquifer exchange with variably-saturated flow using a fully coupled model. J. Hydrol. 375, 383-393. doi: 10.1016/j.hydrol.2009.06.038

Frei, S.G., Lischeid, G., Fleckenstein, J.H., 2010. Effects of micro-topography on surface-subsurface exchange and runoff generation in a virtual riparian wetland – A modeling study. Adv. in Water Resour. 33(11), 1388–1401. doi: 10.1016/j.advwatres.2010.07.006

Frei, S., Knorr, K.H., Peiffer, S., Fleckenstein, J.H., 2012. Surface micro-topography causes hot spots of biogeochemical activity in wetland systems: A virtual modeling experiment. J. Geophys. Res. 117, G00N12. doi: 10.1029/2012JG002012

Frei, S., Fleckenstein, J.H., 2014. Representing effects of micro-topography on runoff generation and sub-surface flow patterns by using superficial rill/depression storage height variations. Environ. Model. Softw. 52, 5–18. doi: 10.1016/j.envsoft.2013.10.007

Furman, A., 2008. Modeling coupled surface-subsurface flow processes: A review. Vadose Zone J. 7(2), 741-756. doi:10.2136/vzj2007.0065

Gaukroger, A.M., Werner, A.D., 2011. On the Panday and Huyakorn surface-subsurface hydrology test case: analysis of internal flow dynamics, Hydrol. Process. 25(13), 2085-2093. doi: 10.1002/hyp.7959

Gelhar, L.W., Welty, C., Rehfeldt, K.R., 1992. A critical review of data on field-scale dispersion in aquifers. Water Resour. Res. 28, 1955–1974. doi: 10.1029/92WR00607

Genereux, D.P., Hooper, R.P., 1998. Oxygen and hydrogen isotopes in rainfall-runoff studies, in: Kendall, C., McDonnell, J.J. (Eds.), Isotope Tracers in Catchment Hydrology. Elsevier, New York, pp. 319–346.

Gerke, H.H., van Genuchten, M.T., 1993. Evaluation of a first-order water transfer term for variably saturated dual-porosity flow models. Water Resour. Res. 29(4), 1225-1238. doi: 10.1029/92WR02467

Gerstberger, P., Foken, T., Kalbitz, K., 2004. The Lehstenbach and Steinkreuz catchments in NE Bavaria, Germany. In: Matzner, E. (Ed.), Biogeochemistry of Forested Catchments in a Changing Environment. A German Case Study. Ecological Studies, vol. 172. Springer, Heidelberg, pp. 399–436.

Goderniaux, P., Brouyére, S., Fowler, H.J., Blenkinsop, S., Therrien, R., Orban, P., Dassargues, A., 2009. Large scale surface–subsurface hydrological model to assess climate change impacts on groundwater reserves. J. Hydrol. 373, 122-138. doi: 10.1016/j.jhydrol.2009.04.017

Guay, C., Nastev, M., Paniconi, C., Sulis, M., 2013. Comparison of two modeling approaches for groundwater-surface water interactions. Hydrol. Process. 27, 2258–2270. doi: 10.1002/hyp.9323

Hantush, M.S., 1965. Wells near streams with semipervious beds. J. Geophys. Res. 70(2), 2829-2838. doi: 10.1029/JZ070i012p02829

Hillel, D., 1980. Infiltration and surface runoff, Applications of Soil Physics. Academic Press, pp. 44.

Horton, R.E., 1933. The role of infiltration in the hydrologic cycle. Eos. Trans. Am. Geophys. Union 14, 446-460.

Huang, G., Yeh, G.T., 2009. Comparative study of coupling approaches for surface water and subsurface interactions. J. Hydraul. Eng. 14(5), 453-462. doi: 10.1061/_ASCE_HE.1943-5584.0000017

Hunt, B., 1999. Unsteady stream depletion from ground water pumping. Ground Water 37(1), 98-102. doi: 10.1111/j.1745-6584.1999.tb00962.x

HydroGeoLogic Inc., 2006. MODHMS software (version 3.0) documentation. Volume I: Groundwater flow modules, Volume II: Transport modules, Volume III: Surface water flow modules, Herndon, USA.

Jacks, G., Norrström, A.C., 2004. Hydrochemistry and hydrology of forest riparian wetlands. For. Ecol. Manage. 196(2–3), 187–197. doi:10.1016/j.foreco.2004.01.055

Jones, J.P., Sudicky, E.A., Brookfield, A.E., Park, Y.-J., 2006. An assessment of the tracer-based approach to quantifying groundwater contributions to streamflow. Water Resour. Res. 42, W02407. doi: 10.1029/2005WR004130

Jones, J.P., Sudicky, E.A., McLaren, R.G., 2008. Application of a fully-integrated surface-subsurface flow model at the watershed-scale: A case study. Water Resour. Res. 44(3), W03407. doi: 10.1029/2006WR005603

Keese, K.E., Scanlon, B.R., Reedy, R.C., 2005. Assessing controls on diffuse groundwater recharge using unsaturated flow modelling. Water Resour. Res. 41(6), W06010. doi: 10.1029/2004WR003841

Kirchner, J.W., 2003. A double paradox in catchment hydrology and geochemistry. Hydrol. Process. 17, 871–874. doi: 10.1029/2005WR004130

Kirkby, M.J., 1971. Hillslope process-response models based on the continuity equation, in: Brunsden, D. (Ed.), Slopes Form and Process. Institute of British Geographers, Special Publication no. 3, pp. 15–30.

Knorr, K.-H., Lischeid, G., Blodau, C., 2009. Dynamics of redox processes in a minerotrophic fen exposed to a water table manipulation. Geoderma 153(3-4), 379-392. doi: 10.1016/j.geoderma.2009.08.023

Knorr, K.-H., 2013. DOC-dynamics in a small headwater catchment as driven by redox fluctuations and hydrological flow paths – are DOC exports mediated by iron reduction/oxidation cycles? Biogeosciences 10, 891–904. doi: 10.5194/bg-10-891-2013

Kollet, S.J., Maxwell, R.M., 2006. Integrated surface-groundwater flow modeling: A free-surface overland flow boundary condition in a parallel groundwater flow model. Adv. in Water Resour. 29(7), 945-958. doi: 10.1016/j.advwatres.2005.08.006

Kollet, S.J., Maxwell, R.M., 2008. Influence of groundwater dynamics on land surface processes using an integrated, distributed watershed model. Water Resour. Res. 44, W02402. doi: 10.1029/2007WR006004

Kollet, S.J., Maxwell, R.M., Woodward, C.S., Smith, S., Vanderborght, J., Vereecken, H., Simmer, C., 2010. Proof of concept of regional scale hydrologic simulations at hydrologic resolution utilizing massively parallel computer resources. Water Resour. Res. 46(4), W04201. doi: 10.1029/2009wr008730

Kollet, S.J., Zlotnik, V.A., 2003. Stream depletion predictions using pumping test data from a heterogeneous stream-aquifer system (a case study from the Great Plains, USA). J. Hydrol. 281(1-2), 96-114. doi: 10.1016/S0022-1694(03)00203-8

Konikow, L.F., 2011. The secret to successful solute-transport modeling. Ground Water 49, 144–59. doi: 10.1111/j.1745-6584.2010.00764.x

Kristensen, K., Jensen, S., 1975. A model for estimating actual evapo- transpiration from potential evapotranspiration, Nord. Hydrol. 6(3), 170–188. doi:10.2166/nh.1975.011

Kumar, M., Duffy, C.J., Salvage, K.M., 2009. A second order accurate, finite volume-based, integrated hydrologic modelling (FIHM) framework for simulation of surface and subsurface flow. Vadose Zone J. 8(4), 873-890. doi: 10.2136/vzj2009.0014

Lemieux, J-M., Sudicky, E.A., Peltier, W.R., Tarasov, L.. 2008. Dynamics of groundwater recharge and seepage over the Canadian landscape during the Wisconsinian glaciation. J. Geophys. Res. 113, F01011. doi: 10.1029/2007JF000838

Li, Q., Unger, A.J.A., Sudicky, E.A., Kassenaar, D., Wexler, E.J., Shikaze, S., 2008. Simulating the multi-seasonal response of a large-scale watershed with a 3D physically-based hydrologic model. J. Hydrol. 357, 317–336. doi: 10.1016/j.jhydrol.2008.05.024

Lischeid, G, Bittersohl, J., 2008. Tracing biogeochemical processes in stream water and groundwater using non-linear statistics. J. Hydrol. 357, 11-28. doi: 10.1016/j.jhydrol.2008.03.013

Lischeid, G., Kolb, A., Alewell, C., 2002. Apparent translatory flow in groundwater recharge and runoff generation. J. Hydrol. 265, 195–211. doi: 10.1016/S0022-1694(02)00108-7

Lischeid, G., Kolb, A., Alewell, C., Paul, S., 2007. Impact of redox and transport processes in a riparian wetland on stream water quality in the Fichtelgebirge region, southern Germany. Hydrol. Process. 21, 123-132. doi: 10.1002/hyp.6227

Liu, G., Zheng, C., Gorelick, S.M., 2004. Limits of applicability of the advection-dispersion model in aquifers containing connected high-conductivity channels. Water Resour. Res. 40, W08308. doi: 10.1029/2003WR002735

Loague, K., Heppner, C.S., Mirus, B.B., Ebel, B.A., Ran, Q., Carr, A.E., BeVille, S.H., VanderKwaak, J.E., 2006. Physics-based hydrologic-response simulation: foundation for hydroecology and hydrogeomorphology. Hydrol. Process. 20, 1231-1237. doi: 10.1002/hyp.6179

Loague, K., Vanderkwaak, J.E., 2002. Simulating hydrological response for the R-5 catchment: Comparison of two models and the impact of the roads. Hydrol. Process. 16(5), 1015-1032. doi: 10.1002/hyp.316

Loague, K., VanderKwaak, J.E., 2004. Physics-based hydrologic response simulation: Platinum bridge, 1958 Edsel, or useful tool. Hydrol. Process. 18(15), 2949-2956. doi: 10.1002/hyp.5737

Maneta, M.P., Torres, M.O., Wallender, W.W., Vosti, S., Howitt, R., Rodrigues, L., Bassoi, L.H., and Panday, S., 2009. A spatially distributed hydroeconomic model to assess the effects of drought on land use, farm profits, -and agricultural employment. Water Resour. Res. (45), W11412. doi:10.1029/2008WR007534

Markstrom, S.L., Niswonger, R.G., Regan, R.S., Prudic, D.E., and Barlow, P.M., 2008. GSFLOW—Coupled ground-water and surface-water flow model based on the integration of the Precipitation-Runoff Modeling System (PRMS) and the Modular Ground-Water Flow Model (MODFLOW-2005). U.S. Geological Survey Techniques and Methods 6-D1, 240 pp.

Maxwell, R.M., Kollet, S.J., 2008a. Interdependence of groundwater dynamics and land-energy feedbacks under climate change. Nat. Geosci. 1, 665–669. doi:10.1038/ngeo315

Maxwell, R.M., Kollet, S.J., 2008b. Quantifying the effects of three-dimensional subsurface heterogeneity on Hortonian runoff processes using a coupled numerical, stochastic approach. Adv. in Water Resour. 31(5), 807-817. doi: 10.1016/j.advwatres.2008.01.020

McCallum, J.L., Cook, P.G., Brunner, P., Berhane, D., 2010. Solute dynamics during bank storage flows and implications for chemical base flow separation. Water Resour. Res. 46, W07541. doi: 10.1029/2009WR008539

McDonnell, J.J., 1990. A rationale for old water discharge through macropores in a steep, humid catchment. Water Resour. Res. 26, 2821–2832. doi: 10.1029/WR026i011p02821

McDonnell, J.J., 2003. Where does water go when it rains? Moving beyond the variable source area concept of rainfall-runoff response. Hydrol. Process. 17, 1869–1875. doi: 10.1002/hyp.5132

McDonald, M.G., Harbaugh, A.W., 1988. A modular three-dimensional finite-difference ground-water flow model, US Geological Survey Techniques of Water-Resources Investigations, Book 6 [Chapter A1].

McMillan, H.K., Clark, M.P., Bowden, W.B., Duncan, M., Woods, R.A., 2011. Hydrological field data from a modeller's perspective: Part 1. Diagnostic tests for model structure. Hydrol. Process. 25, 511–522. doi: 10.1002/hyp.7841

Mehl, S., Hill, M.C., 2010. Grid-size dependence of Cauchy boundary conditions used to simulate stream-aquifer interactions. Adv. in Water Resour. 33(4), 430-442. doi:10.1016/j.advwatres.2010.01.008

Mirus, B.B., Loague, K., 2013. How runoff begins (and ends): Characterizing hydrologic response at the catchment scale. Water Resour. Res. 49, 2987–3006. doi: 10.1002/wrcr.20218

Mirus, B.B., Ebel, B.A., Heppner, C.S., Loague, K., 2011. Assessing the detail needed to capture rainfall-runoff dynamics with physics-based hydrologic response simulation. Water Resour. Res. 47, W00H10. doi:10.1029/2010WR009906

Mirus, B.B., Loague, K., VanderKwaak, J.E., Kampf, S.K., Burges, S.J., 2009. A hypothetical reality of Tarrawarra-like hydrologic response. Hydrol. Process. 23(7), 1093-1103. doi: 10.1002/hyp.7241

Morita, M., Yen, B.C., 2000. Numerical methods for conjunctive two-dimensional surface and three-dimensional sub-surface flows. Int. J. Numer. Methods Fluids 32(8), 921-957. doi: 10.1002/(SICI)1097-0363(20000430)32:8<921::AID-FLD993>3.0.CO;2-3

Morita, M., Yen, B.C., 2002. Modeling of conjunctive two-dimensional surface-three-dimensional subsurface flows. J. Hydraul. Eng. 128(2), 184-200. doi: 10.1061/(ASCE)0733-9429(2002)128:2(184)

Panday, S., Huyakorn, P.S., 2004. A fully-coupled spatially distributed model for evaluating surface/subsurface flow. Adv. in Water Resour. 27, 361–382. doi:10.1016/j.advwatres.2004.02.016

Panday, S., Langevin, C.D, 2012. Improving sub-grid scale accuracy of boundary features in regional finite-difference models. Adv. in Water Resour. 41, 65–75. doi: 10.1016/j.advwatres.2012.02.011

Paniconi, C., Aldama, A.A., Wood, E.F., 1991. Numerical evaluation of iterative and noniterative methods for the solution of the nonlinear Richards equation. Water Resour. Res. 27(6), 1147-1163. doi: 10.1029/91WR00334

Park, Y.-J., Sudicky, E.A., Brookfield, A.E., Jones, J.P., 2011. Hydrologic response of catchments to precipitation: quantification of mechanical carriers and origins of water. Water Resour. Res. 47, W12515. doi: 10.1029/2011WR010075

Partington, D., Brunner, P., Simmons, C.T., Therrien, R., Werner, A.D., Dandy, G.C., Maier, H.R., 2011. A hydraulic mixing-cell method to quantify the groundwater component of streamflow within spatially distributed fully integrated surface water–groundwater flow models. Environ. Model. Softw. 26, 886–898. doi: 10.1016/j.envsoft.2011.02.007

Partington, D., Brunner, P., Frei, S., Simmons, C.T., Werner, A.D., Therrien, R., Maier, H.R., Dandy, G.C., Fleckenstein, J.H., 2013. Interpreting streamflow generation mechanisms from integrated surface-subsurface flow models of a riparian wetland and catchment. Water Resour. Res. 49. doi: 10.1002/wrcr.20405

Pastor, J., Solin, J., Bridgham, S. D., Updegraff, K., Harth, C., Weishampel, P. and Dewey, B., 2003. Global warming and the export of dissolved organic carbon from boreal peatlands. Oikos 100, 380–386. doi:10.1034/j.1600-0706.2003.11774.x

Penman, H., L., 1961. Weather, plant and soil factors in hydrology. Weather 16, 207–219. doi: 10.1002/j.1477-8696.1961.tb01934.x

Prickett, T.A., Lonnquist, C.G., 1971. Selected digital computer techniques for groundwater resources evaluation. Illinois State Water Survey, Bull. No. 55.

Renaud, J.-P., Cloke, H.L., Weiler, M., 2007. Comment on "An assessment of the tracer-based approach to quantifying groundwater contributions to streamflow" by J. P. Jones et al. Water Resour. Res. 43, W09601. doi: 10.1029/2006WR005157

Reilly, T. E., Plummer, L.N., Phillips, P.J., Busenberg, E., 1994. The use of simulation and multiple environmental tracers to quantify groundwater flow in a shallow aquifer, Water Resour. Res. 30(2), 421–433. doi:10.1029/93WR02655

Rodhe, A., 1981. Spring flood: meltwater or groundwater? Nord. Hydrol. 12, 21–30. doi: 10.2166/nh.1981.002

Ross, P.J., 1990. Efficient numerical methods for infiltration using Richards' equation. Water Resour. Res. 26, 279-290.

Rushton, K., 2007. Representation in regional models of saturated river-aquifer interaction for gaining/losing rivers. J. Hydrol. 334, 262-281. doi: 10.1016/j.jhydrol.2006.10.008

Sanford, W.E., 1997, Correcting for diffusion in carbon-14 dating of ground water. Ground water 35(2), 357-361. doi: 10.1111/j.1745-6584.1997.tb00093.x

Schoups, G., Hopmans, J.W., Young, C.A., Vrugt, J.A., Wallender, W.W., Tanji, K.K., Panday, S., 2005. Sustainability of irrigated agriculture in the San Joaquin Valley, California. Proc. Nat. Acad. Sci. USA, 102, 15352-15356.

Sebben, M.L., Werner, A.D., Liggett, J.E., Partington, D., Simmons, C.T., 2013. On the testing of fully integrated surface-subsurface hydrological models. Hydrol. Process. 27(8), 1276-1285. doi: 10.1002/hyp.9630

Seibert, J., McDonnell, J.J., 2002. On the dialog between experimentalist and modeler in catchment hydrology: Use of soft data for multicriteria model calibration. Water Resour. Res. 38(11), 1241. doi:10.1029/2001WR000978

Sharpley, A.N., Kleinman, P.J.A., McDowell, R.W., Gitau, M., Bryant, R.B., 2002. Modeling phosphorus transport in agricultural watersheds : Processes and possibilities. J. Soil Water Conserv. 57, 425–439.

Shi, X., Wu, L., Chenc, W., Wang, Q., 2011. Solute Transfer from the Soil Surface to Overland Flow: A Review. Soil Sci. Soc. Am. J. 75, 1214–1225. doi: 10.2136/sssaj2010.0433

Sklash, M.G., Farvolden, R.N., 1979. The role of groundwater in storm runoff. J. Hydrol. 43, 45–65. doi: 10.1016/0022-1694(79)90164-1

Smerdon, B.D., Mendoza, C.A., Devito, K.J., 2007. Simulations of fully coupled lake groundwater exchange in a subhumid climate with an integrated hydrologic model. Water Resour. Res. 43: W01416. doi: 10.1029/2006WR005137

Smerdon, B.D., Mendoza, C.A., Devito, K.J., 2008. Influence of subhumid climate and water table depth on groundwater recharge in shallow outwash aquifers. Water Resour. Res. 44, W08427. doi:10.1029/2007WR005950

Sophocleous, M., 2002. Interactions between groundwater and surface water: The state of the science. Hydrogeol. J. 10, 52–67. doi: 10.1007/s10040-001-0170-8

Strohmeier, S., Knorr, K.-H., Reichert, M., Frei, S., Fleckenstein, J.H., Peiffer, S., Matzner, E., 2013. Concentrations and fluxes of dissolved organic carbon in runoff from a forested catchment: insights from high frequency measurements. Biogeosciences 10, 905–916. doi: 10.5194/bg-10-905-2013

Sudicky, E.A., Frind, E.O., 1981. Carbon-14 dating of groundwater in confined aquifers: Implications of aquitard diffusion. Water Resour. Res. 17(4), 1060-1064. doi: 10.1029/WR017i004p01060

Sudicky, E.A., Jones, J.P., Brookfield, A.E., Park, Y.-J., 2007. Reply to comment by J.-P. Renaud et al. on "An assessment of the tracer-based approach to quantifying groundwater contributions to streamflow". Water Resour. Res. 43, W09602. doi: 10.1029/2006WR005416

Sudicky, E.A., Jones, J.P., Young-Jin, P., Brookfield, A.E., Colautti, D., 2008. Simulating complex flow and transport dynamics in an integrated surface-subsurface modeling framework. Geosci. J. 12, 107–122. doi: 10.1007/s12303-008-0013-x

Sulis, M., Meyerhoff, S.B., Paniconi, C., Maxwell, R.M., Putti, M. and Kollet, S.J. 2010. A comparison of the two physics-based numerical models for simulating surface water-groundwater interactions. Adv. in Water Resour. 33: 456-67. doi:10.1016/j.advwatres.2010.01.010

Therrien, R., McLaren, R.G., Sudicky, E.A., Panday, S.M., 2009. HydroGeoSphere: a three-dimensional numerical model describing fully-integrated subsurface and surface flow and solute transport, Groundwater Simulations Group, University of Waterloo, Waterloo.

Therrien, R., Sudicky, E.A., 1996. Three-dimensional analysis of variably saturated flow and transport in discretely fractured porous media. J. Contam. Hydrol. 23, 1–44. doi: 10.1016/0169-7722(95)00088-7

Theis, C. V., 1941. The effect of a well on the flow of a nearby stream. Trans. Am. Geophys. Union. 22(3), 734-738.

van Dam, J.C., Feddes, R.A., 2000. Numerical simulation of infiltration, evaporation and shallow groundwater levels with the Richards equation. J. Hydrol. 233(1), 72-85. doi: 10.1016/S0022-1694(00)00227-4 van Genuchten, M.T., 1980. Closed-form equation for predicting the hydraulic conductivity of unsaturated soils. Soil Sci. Soc. Am. J. 44(5), 892-898. doi: 10.2136/sssaj1980.03615995004400050002x

van Genuchten, M.T., Wierenga, P.J., 1976. Mass transfer studies in sorbing porous media: analytical solution. Soil Sci. Soc. Am. J. 40, 473–480. doi: 10.2136/sssaj1976.03615995004000040011x

VanderKwaak, J.E., 1999. Numerical simulation of flow and chemical transport in integrated surface-subsurface hydrologic systems, University of Waterloo, Waterloo, ON, Canada, 242 pp.

VanderKwaak, J.E., Loague, K., 2001. Hydrologic-response simulations for the R-5 catchment with a comprehensive physics-based model. Water Resour. Res. 37(4), 999-1013. doi: 10.1029/2000WR900272

Vogel, H.J., Ippisch, O., 2008. Estimation of a critical spatial discretization limit for solving Richard's Equation at large scales. Vadose Zone J. 7, 112-114. doi: 10.2136/vzj2006.0182.

Walker, G. R., Cook, P. G., 1991. The importance of considering diffusion when using carbon-14 to estimate groundwater recharge to an unconfined aquifer. J. Hydrol. 128, 41-48. doi: 10.1016/0022-1694(91)90130-A

Walter, M.T., Gao, B., Parlange, J.-Y., 2007. Modeling soil solute release into runoff with infiltration. J. Hydrol. 347, 430–437. doi: 10.1016/j.jhydrol.2007.09.033

Warren, J.E., Root, P.J., 1963. The behaviour of naturally fractured reservoirs. Soc. Petrol. Eng. 3, 245-255. doi: 10.2118/426-PA

Weatherill, D., Graf, T., Simmons, C.T., Cook, P.G., Therrien, R., Reynolds, D.A., 2008. Discretizing the fracture-matrix interface to simulate solute transport. Ground Water 46, 606–615. doi:10.1111/j.1745-6584.2007.00430.x

Weill, S., Mazzia, A., Putti, M., Paniconi, C., 2011. Coupling water flow and solute transport into a physically-based surface–subsurface hydrological model. Adv. Water Resour. 34, 128–136. doi: 10.1016/j.advwatres.2010.10.001

Weill, S., Altissimo, M., Cassiani, G., Deiana, R., Marani, M., Putti, M., 2013. Saturated area dynamics and streamflow generation from coupled surface–subsurface simulations and field observations. Adv. Water Resour. 59, 196–208. doi: 10.1016/j.advwatres.2013.06.007, Werner, A.D., Gallagher, M.R., Weeks, S.W., 2006. Regional-scale, fully coupled modelling of stream–aquifer interaction in a tropical catchment. J. Hydrol. 328, 497-510. doi:10.1016/j.jhydrol.2005.12.034.

Wigmosta, M. S., Vail, L. W., Lettenmaier, D. P., 1994. A distributed hydrology vegetation model for complex terrain, Water Resour. Res. 30(6), 1665–1679. doi: 10.1029/94WR00436

Winter, T.C., Harvey, J.W., Franke, O.L., Alley, W.M., Survey, U.S.G., 1998. Ground water and surface water A single resource, U.S. Geological Survey Circular. U. S. Geological Survey, Denver, CO, USA.